AFIT/DS/ENP/94J-2

NUCLEAR CLOUD RISE AND GROWTH

DISSERTATION

Vincent J. Jodoin, Captain, USAF

AFIT/DS/ENP/94J-2

Approved for public release; distribution unlimited

AFIT/DS/ENP/94J-2

NUCLEAR CLOUD RISE AND GROWTH

DISSERTATION

Presented to the faculty of the Graduate School of Engineering

of the Air Force Institute of Technology

Air University

In Partial Fulfillment of the

Requirements for the Degree of

Doctor of Philosophy

Vincent J. Jodoin, B.S.N.E., M.S.E.E., M.S.N.E., P.E.

Captain, USAF

June 1994

AFIT/DS/ENP/94J-2

NUCLEAR CLOUD RISE AND GROWTH

Vincent J. Jodoin, B.S.N.E., M.S.E.E., M.S.N.E., P.E.

Captain, USAF

Approved:

Charles J. Bridgman, Chairman — 24 May '94

Richard S. Hartley, Lt Col, USAF — 24 May '94

George John — 24 May '94

Mark E. Oxley — 24 May 94

Accepted:

Robert A. Calico, JR. — 6 June '94

Dean, Graduate School of Engineering

Preface

After being selected for the doctoral program at AFIT, my first task was to choose a dissertation topic and a research advisor. Before I even arrived in Ohio I had already asked Dr. Bridgman if he would take me on as his student, in addition to his many duties as Associate Dean for Research. He agreed to lead me in a couple of special studies in his research specialty: nuclear fallout modeling. After my coursework and exams were completed, we agreed that nuclear cloud rise modeling was an area we both wanted to learn more about.

I would like to thank Dr. Bridgman for taking the time to guide me in the area of nuclear fallout modeling. His skill as a teacher was known to me from my time as a master's student a few years earlier. His reputation as an excellent researcher became evident as I began speaking with others in the nuclear weapons effects community. His search for unbiased truth was driven home in our weekly meetings. His lifetime commitment to education was seen in his commitment to my success and those around me. Finally, his ability to joke with me while keeping me motivated toward the goal of graduating was summed up by his favorite line to me: "I got *my* degree!"

I would also like to thank Dr. Oxley and Lt. Col. Hartley whom I enjoyed as teachers as well as committee members. I am also honored for having Dr. John serve as my Dean's Representative for my dissertation. I am also thankful for the other "nukes" in the department, both students and teachers, which helped me out during my years at AFIT.

The research using DELFIC and especially the particle rise modeling would not have been accomplished without the advice and feedback of Dr. McGahan at SAIC. I greatly

appreciate the many hours that he and Dr. Cockayne spent with me, both listening and teaching. I was very fortunate to have access to Dr. Cockayne who has, in my experience, the best command of both theory and experiments related to nuclear weapons effects. I would like to thank LTC Byers of DNA who arranged access to the TASS results and provided computer time for plotting the results. I am grateful to Tom Dunn and Dr. Bacon for helping me understand the megabytes of data involved and the workings of the TASS code.

My wife Carol and my three beautiful daughters, Jenna, Danielle, and Christina, deserve a lot of the credit for my success. Their encouraging words and ability to listen to my troubles helped me get through some rough periods without losing hope. I thank them for their sacrifice of family time and a "normal" job schedule, especially near the end of my research. Most of all I thank my Creator God who gave me the desire and ability to do the work. Out of all my studies, nothing compares to the fulfillment and worth of what I've learned over the past few years about Him and his love.

Vincent J. Jodoin

Table of Contents

List of Figures

List of Tables

List of Notation

Symbols

a = radius of the sphere (m)
$A(\psi)$= arbitrary function of ψ
$\bar{c}_p(T)$= mass weighted mean of the specific heats of air and water vapor (J/kg K)
$c_{pa}(T)$= specific heat of entrained air (dry air) (J/kg K)
C_D = coefficient of drag
d = particle diameter (m)
E = turbulent kinetic energy density (J/kg)
F = rate of soil mass leaving the cloud (kg/s)
F_D = drag force (kg m/s^2)
F_g = gravity force (kg m/s^2)
F_p = force on the particle (kg m/s^2)
g = acceleration due to gravity (9.8 m/s^2)
H_c = cloud vertical thickness (m)
k_2 = eddy viscous drag parameter
k_3 = a constant
k_6 = a constant
KDI = 15 + ln (W in kilotons) is the number of vertical layers
L = latent heat of vaporization of water or ice (J/kg)
m = total cloud mass (air, vapor, water, and soil) (kg)
$\left.\frac{dm}{dt}\right|_{ent}$ = rate of change of mass due to entrainment (kg/s)
N = number of shots in data set (54)
p = pressure at cloud center altitude (Pa)
r = radius coordinate for spherical coordinate system (m)
r_p = particle radius (m)
R = the radial distance from the axis of symmetry (m)
R_a = gas constant of air (287 J/kg K)
R_c = horizontal radius of the cloud (m)
s = cloud soil mixing ratio (ratio of soil mass to dry air mass)
S = surface area of the cloud (m^2)
t_i = initial time before bubble rise (s)
t_{st} = stabilization time (s)
T = cloud temperature (K)
T_e = ambient temperature (K)

$T^* = T\frac{1+x/\xi}{1+x}$ is cloud virtual temperature (K)

$T_e^* = T_e\frac{1+x_e/\xi}{1+x_e}$ is ambient virtual temperature (K)

u = rate of cloud rise (m/s)
U = velocity of the moving body of fluid (m/s)
U_Z = the vertical velocity (m/s)
U_R = the radial velocity (m/s)

$v = Max(u, \sqrt{2E})$ is the characteristic velocity (m/s)
v_s = wind velocity difference between the top and base of the cloud (m/s)
V = cloud volume = m/ρ (m^3)
V_R = particle radial velocity (m/s)
V_Z = particle vertical velocity (m/s)
w = cloud condensed water mixing ratio
x = cloud water vapor mixing ratio (ratio of water vapor mass to dry air mass)
x_e = ambient water vapor mixing ratio
z = cloud center height (m)
z_{calc}=calculated cloud top height (m)
z_{obs}=observed cloud top height (m)
Z_1 = the vertical distance from the midplane of the real vortex (m)
Z_2 = the vertical distance from the midplane of the imaginary vortex (m)

$\beta' = \frac{1+x}{1+x+w}$ is ratio of cloud gas density to total cloud density

$\varepsilon = \frac{k_3(2E)^{3/2}}{H_c}$ is turbulent kinetic energy dissipation rate per unit mass (J/kg s)

μ = entrainment parameter
ρ_e = ambient air density (kg/m^3)
ρ = cloud density (kg/m^3)
ρ_m = particle (mass) density (kg/m^3)
ρ_a = air (or cloud) density (kg/m^3)
θ = angle from axis of motion in spherical coordinate system
ψ = streamfunction of the flow
ξ = 18/29 is ratio of the molecular weight of water vapor to that of dry air

Acronyms

Cloud Rise Module (CRM)
Cloud Rise/Transport Interface Module (CRTIM)
Defense Atomic Support Agency (DASA) now DNA
Defense Land Fallout Interpretive Code (DELFIC)
Defense Nuclear Agency (DNA)
Department of Defense (DoD)
Diffusive Transport Module (DTM)
Fractional Mean Deviation (FMD)
Fractional Root Mean Square (FRMS) Error
Height of Burst (HOB)
K-division DNA Fallout Code (KDFOC)
Kiloton (kt)
Multiphase Adaptive Zoning (MAZ)
Megaton (MT)
Naval Radiological Defense Laboratory (NRDL)
Ordinary Differential Equation (ODE)
Output Processor Module (OPM)
Science Applications International Corporation (SAIC)
Single Burst Nuclear Cloud Database (SBNCD)
Scaled Heights of Bursts (SHOB)
Terminal Area Simulation System (TASS)
Vortex Dust Model (VORDUM)
Weapon Test (WT) reports

Abstract

Nuclear cloud rise and growth to stabilization is investigated. The Cloud Rise Module of the Defense Land Fallout Interpretive Code (DELFIC) is reviewed and improved. Both the modeling of bubble rise dynamics and particle rise dynamics are addressed. Improvements are made in predicting the stabilized particulate cloud for nuclear fallout purposes. The results are compared to US atmospheric nuclear weapons tests and to the output of MAZ/TASS hydrocode simulations.

The improvements to the bubble rise dynamics include using a single term entrainment equation and constants for the entrainment and eddy viscous drag parameters. The validation showed a slight improvement was obtained with the improved model in predicting the cloud top values for 54 US near-surface bursts.

The improvement to the particle rise model consisted of replacing the 1-D particle rise with a 2-D analytical flow field model. The model was based on Hill's spherical vortex. This improvement provided a radial distribution to the radioactive dust cloud. The larger fallout particles (>200 microns) achieved a higher altitude due to simulating the circulation within the cloud. Dose rate contours for some cases will be altered due to this change in vertical distribution from the 1-D model.

NUCLEAR CLOUD RISE AND GROWTH

I. Introduction

Background

Nuclear cloud rise and growth is typically modeled in two parts: 1) nuclear cloud rise and growth to "stabilization" and 2) diffusive growth and transport in the atmosphere after stabilization. The second part requires a definition of the stabilized cloud from the first part.

This report describes efforts to improve the cloud rise and growth to stabilization prediction capabilities of bubble, or single-cell, cloud rise models. A single-cell model assumes constant properties throughout the cloud (e.g. temperature) as opposed to hydrocodes which use a multicell approach that produces spatially varying properties. An example of bubble or cloud rise models is the Cloud Rise Module (CRM) of the Defense Land Fallout Interpretive Code (DELFIC). The Defense Nuclear Agency (DNA) is currently updating DELFIC, the Department of Defense's (DoD's) primary research reference fallout code, which was last published in 1979. Being a research code, DELFIC contains as much physics as practical while reducing the number of empiricisms. As a reference code, DELFIC is used by many other operational codes which either mimic or directly use DELFIC results for systems studies. Science Applications International Corporation (SAIC), in particular Dr. Joseph McGahan, is directing the update of DELFIC. The focus

of this study is only on improving the CRM of DELFIC, and it does not address improvements in the cloud transport model.

Brief Physical Description. When a nuclear weapon detonates near the earth's surface, the fireball contacts the soil on the ground and generates a large cloud of dust which rises and grows in the atmosphere. After an initial ballistic phase, the fireball begins to rise buoyantly like a bubble in water. The incompressible phase starts once the pressure inside the cloud comes close to equilibrium with ambient atmospheric pressure. The upward motion of the cloud distorts the initial spherical shape and sets up a toroidal vortex motion within the cloud (See Figure 1 on page 3). The cloud entrains ambient air and water vapor as it rises. The transfer of potential energy within the cloud to kinetic energy of rise, followed by transfer to turbulence, influences the rise and growth of the cloud, and ultimately the location of the dust within the cloud. Modeling the distribution of the dust within the cloud is important because it contains the residual radioactivity of the weapon "fallout". The position of the dust is a function of time during both cloud rise and transport to the ground and it determines the radiation hazard on the ground.

Motivation for the Research. The CRM's definition of the stabilized radioactive dust cloud in DELFIC is problematic for two reasons. The first reason is the errors that exist in the CRM's bubble rise equations. These errors include both theoretical and programming errors. The second reason is the simplistic way in which the CRM models the particulate cloud in one dimension. This modeling may be the reason for the discrepancy between DELFIC results and the data from hydrocodes.

Huebsch's Recommendations on Bubble Rise Modeling. Huebsch was the original author of the CRM (22). Huebsch's 1975 critique of Norment's 1970 version of the

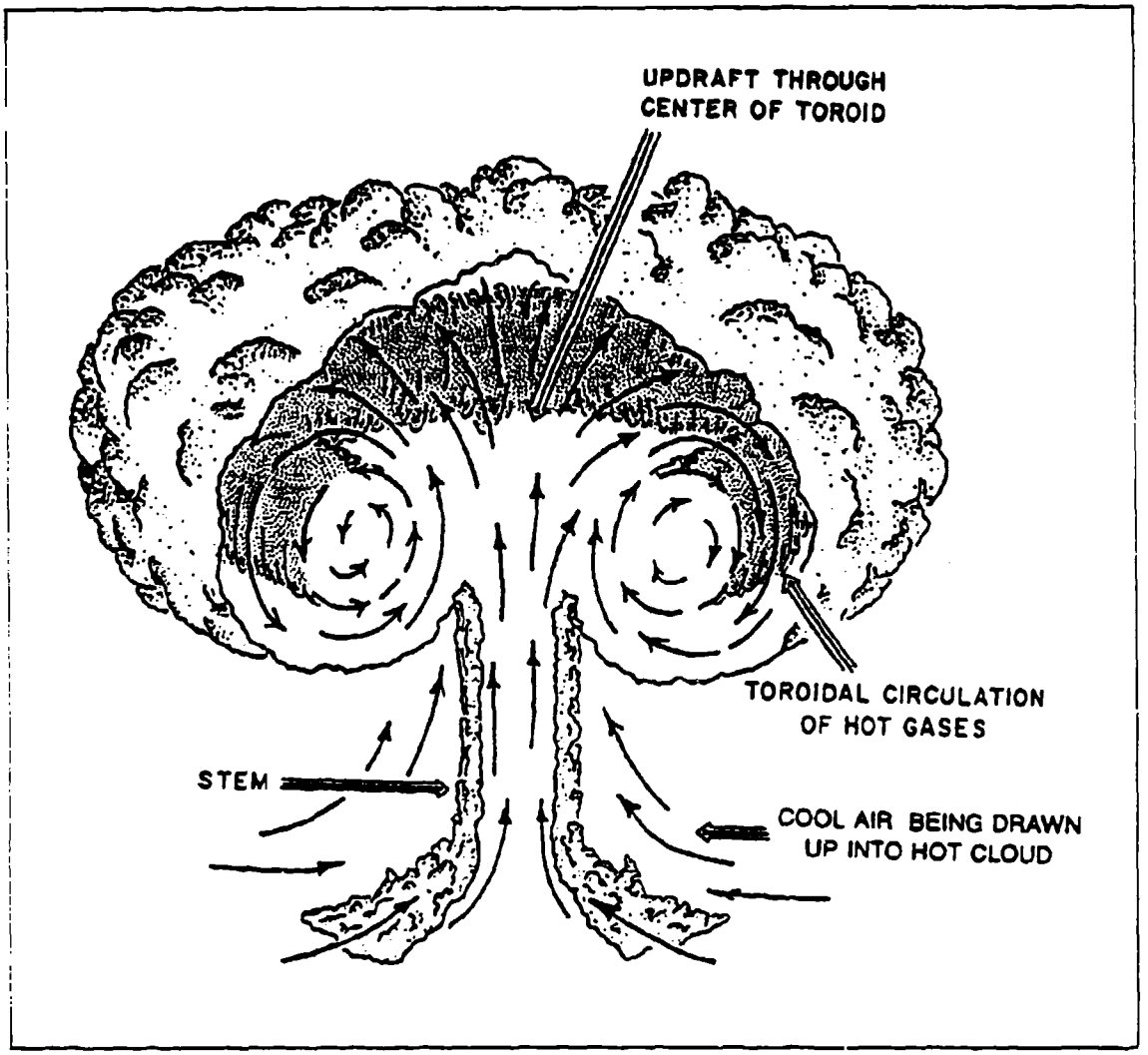

Figure 1: Toroidal circulation within the radioactive cloud from a nuclear explosion (13:29)

CRM stated that the bubble rise model produced physically unrealistic results or results that disagreed with the experimental data (24:iii). Upon closer examination of the model, Huebsch proposed the errors were due to the formulation of the equations for the cloud's mass, velocity, temperature, and dimensions. He found that some of the terms in the equations contained theoretical errors.

Huebsch presented an amended set of bubble rise equations which removed both the theoretical errors and output discrepancies. He made further recommendations on how to improve the CRM of DELFIC. He also presented one way in which stabilized cloud models could be categorized, described later in this report (See Table 1 on page 11).

In response to Huebsch's critique, Norment published a validation study of a modified CRM (46). Norment did change the momentum (or velocity) equation, as Huebsch had recommended, but not the entrainment equation. He adjusted some of his empirical parameters as another method of reaching better agreement with experimental data. He pointed out which parameters, using his set of equations, most influenced changes in the results. Huebsch recommended keeping only a single term of the entrainment equation based on current theory. Norment argued against such a move, desiring rather to have results matching test data than equations matching current theory. A model which does not violate current theory *and* matches the test data is needed in research level codes.

McGahan's Recommendations on Particle Rise Modeling. McGahan suggested using vortex theory and a two-dimensional representation of the particles' spatial distribution to replace the limited 1-D modeling in the CRM (34). Vortex theory could be used to provide a two-dimensional flow-field in the rising cloud. By tracing the flow of particles during the cloud's rise, the position, velocity, and acceleration of particles could be tracked up to stabilization. While experimental results to validate particle rise history are not available, results of a two-dimensional (many cell) hydrodynamics code are available for comparison.

A goal of this research is to refine the vertical distribution of all particles, especially the larger particles modeled in DELFIC. Recent studies have shown that DELFIC cur-

rently stabilizes the larger particles at much lower altitudes than the hydrocodes predict (33). Vortex theory combined with bubble rise theory would be a better method of calculating the stabilized radioactive dust cloud in the research level code used by the nuclear effects community. Accounting for the spatially and temporally varying flow field (vortex theory) will provide a better way of tracking the particles. This approach will predict a vertical variation which should be different than the current prediction of DELFIC's CRM. In addition, it will definitely provide a radial distribution of particles that is not currently available in DELFIC's CRM. Not only will this tracking give a better definition of the particle distribution with time, but also give a dynamic representation of the particles.

Problem

The problem statement is simply: To determine the best available theory for cloud rise and growth using a single bubble model, and to analyze the effect of using vortex theory for particle distribution within the rising cloud.

Scope

This research includes two main sections: bubble rise modeling and particle rise modeling. The bubble rise modeling focuses on *correcting* the current versions of DELFIC's CRM, *improving* the model based on Huebsch's recommendations, and *validating* the corrected and improved versions' results to atmospheric nuclear test observations. The second section, particle-rise modeling, requires a more substantial change to the procedure in which the positions of nuclear cloud particulates are computed. A comparison can then be made to current DELFIC procedures for computing particle positions and also to the output of a hydrodynamics code.

The CRM *corrections* were straight forward and consisted of checking the subroutines line-by-line for consistency with the code's documentation. Each line of the CRM was reviewed and the logic flow checked. The *improvements* consisted of reverting to a single-term entrainment equation and changing two parameters to constants (the entrainment and eddy viscous drag coefficients). The best values for these constants were then determined.

The improvements and corrections were *validated* against experimental measurements using the observed cloud tops of US atmospheric nuclear weapons tests. The observed cloud bases were also examined. The comparison presented is a relative (or fractional) error of calculation to observation. A set of 54 US atmospheric nuclear tests was used for the comparison. The yields (in equivalent tons of TNT) ranged from 7.8 tons to 15 megatons (MT). The shots in the validation set included a wide range for the height of burst (HOB). They included a slightly buried burst, a surface burst, some near surface bursts, and some pure air bursts. For all cases, actual measured values of atmospheric properties (temperature, pressure, humidity, and winds) at the time of the shot were inputted to the codes.

The improvements in the particle rise modeling of the radioactive dust cloud required entirely new methods for tracking trace particles in two dimensions. An initial 2-D grid of trace particles were used to describe the initially uniform distribution of mass in the cloud. This replaced a 1-D stack of disks which were loaded uniformly in the vertical dimension. Each trace particle was tracked up through the rise history of the cloud with both vertical and radial velocity components to determine a 2-D distribution of mass in the stabilized cloud. This replaced the rise of disks with only a vertical component of velocity. A study

was made of how the initial soil loading is distributed within the cloud before it starts its rise. Also noted was the effect of the vortex flow with particle size.

Particle positions within the cloud have not been experimentally measured but have been calculated by hydrocodes. Contour plots of the cloud's density were chosen as the best method for comparing two-dimensional descriptions of the radioactive dust cloud with two-dimensional hydrocode output. When comparing the stabilized particulate cloud to current one-dimensional CRM output, the vertical distribution of the mass was chosen for comparison. A study of the radial distribution of particles in the cloud using two-dimensional flow in DELFIC was performed and implications of the distribution on fall-out contours is discussed.

The test cases chosen for particle rise modeling included the DELFIC 1979 documentation test case (48:34-50) and a range of cases from the Single Burst Nuclear Cloud Database generated by the hydrocodes (9:15). These cases ranged in scaled heights of bursts (SHOB = HOB/yield$^{1/3}$) from 0 to 120 ft./kt$^{1/3}$ and yields from 20 to 800 kilotons.

Assumptions

As with any design study, this work required certain assumptions and limitations. It was accepted that certain studies previously performed in determining some initial conditions and model parameters of the CRM need not be repeated in this study. Since the changes made to the entrainment equation were substantial, the model parameters directly associated with it were varied. Although some initial conditions and other model parameters were investigated, none were altered.

The test data used for comparison (cloud tops) were known more precisely than other values for US atmospheric tests, such as cloud bases and radii. No assumption is made as to the error in the observed cloud top values. Likewise, the actual atmospheric soundings (temperature, pressure, humidity, and wind) obtained were assumed to be the best input for the test shots even though some error exists in their values because of instrumentation (1;10;39), timing, and location of the measurements.

One may not assume that the hydrocode data represents the radioactive cloud. The hydrocodes do not distinguish between radioactive and nonradioactive dust. DELFIC, on the other hand, is solely concerned with radioactive dust. Care must then be taken when comparing DELFIC's particulate cloud to the hydrocode results because of this distinction. The hydrocode data used for comparison was not produced as part of this study, but rather is part of a database maintained by DNA for those in the nuclear effects community.

General Approach

The sequence of major steps accomplished as part of this research will now be reviewed in chronological order. To begin, the 1979 version of DELFIC was modeled in Mathematica (63), a higher-level programming language. The theoretical/empirical equations of the CRM were programmed in Mathematica and solved numerically. This gave a baseline from which to depart. Once the equations were programmed identically to the stated theory of DELFIC, the results were compared to DELFIC's FORTRAN output. This identified FORTRAN programming errors that were known to exist (38:53-57) and uncovered others that had yet to be found. It also showed, qualitatively, how those programming errors affected the output of the CRM.

The next major step was to analyze the recommendations of Huebsch that were discarded by Norment. The purpose of this step was to correct the equations being used so that they no longer violated current theory. The theory that best reduced the number of empiricisms, yet still reproduced the test data, was determined. A check was then made against the original test data previously used to validate the CRM. Once this phase was accomplished the first half of the project was complete.

The work on the two-dimensional particle rise modeling started with a review of vortex theory. In particular, it included theory about the flow in and around a rising bubble. The theoretical equations were coded in Mathematica for symbolic, numeric, and visual manipulation and for a better physical understanding. Once the theory was understood, a review of its application to dust cloud modeling was undertaken. Next, additional FORTRAN subroutines were written to implement the theory into DELFIC's CRM. While Mathematica is a very useful tool to benchmark a program written in FORTRAN or similar languages, the cost for these advantages is longer execution time. It is currently too slow for use in an operational code on today's computers.

The new method of particle rise was then used to produce a database similar to that of the hydrocode output. The two sets of results were then compared using contour plots of the dust densities at various times. The vortex modified code was then compared to the one-dimensional particle rise of the current CRM. The comparison was made of the vertical distribution of mass in the stabilized cloud since the current CRM does not define a radial distribution. Finally, the radial distribution of the two-dimensional model was reviewed and implications of the vertical distribution on fallout contours were found.

Sequence of Presentation

The research is now presented in more detail. Chapter II begins with an overview of the bubble rise theory in DELFIC. It details the equations which were corrected, improved, and validated to give the rise characteristics of the nuclear cloud using an entraining bubble assumption. Chapter III then reviews how the rise characteristics can be used with vortex theory to solve the flow field in and about the cloud. This flow field is used to trace the history of particles which end up defining the stabilized nuclear particulate cloud. Chapter IV examines the results of both the bubble-rise and the particle-rise test runs. The implications of these results are discussed in Chapter V.

II. Bubble Rise Dynamics

The purpose of this chapter is to explain the theory of bubble rise dynamics and state the work done by the author in this general area. The chapter is divided into three main sections. The first section is a short overview of one way in which cloud rise models can be classified. The next section is much larger and explains the level of effort used in this work. The final section is a breakdown of the steps taken to correct, improve, and then validate this part of the cloud rise model.

Levels of Effort

There are three main levels of effort for a cloud rise model, as detailed by Huebsch (24:18-19) (See Table 1 on page 11). A first level effort is one that obtains the stabilized cloud results through empirical fits. It develops time histories of cloud height, dimensions, and temperature as functions of yield and height of burst. The effort is not responsive to atmospheric inputs. The empirical fits could be derived from atmospheric test observations or from the output of a second or third level effort. The K-division DNA Fallout Code (KDFOC) is an example of fallout codes which use this approach to model the stabilized cloud (15).

Table 1: Levels of Effort

Level	Variables	Method
1	Height, dimensions, and temperature	Empirical fits
2	Above plus turbulence, mass, and partitions of mass	One zone cloud
3	Above plus pressure and density	Multiple cell cloud

A second level effort is one that uses a bubble, or single zone, cloud model assumption to solve conservation equations for the stabilized cloud properties. The bubble contains global properties for the entire cloud (e.g. a single temperature everywhere in the cloud). This effort calculates the time histories of the cloud's height, dimensions, temperature, turbulent kinetic energy, and fractions of mass in the form of air, water vapor, condensed water, and soil. The model has yield and height of burst (HOB) as inputs. It is also responsive to atmospheric conditions. That is, the cloud rise depends on the pressure, temperature, water content, and other variables derived from them, of the atmosphere through which the cloud is rising. This level of effort uses the continuity equations to obtain a coupled set of nonlinear ordinary differential equations, with time as the only independent variable. This set is then solved to give the time histories mentioned.

A third level effort is a full hydrodynamics code solution to the cloud variables. Local horizontal and vertical variations within the cloud are modeled in a multicell representation of the cloud. This could be a 2-D or 3-D level hydrocode which also provides information such as pressure and density of the individual cells. The independent variables include both time and position coordinates. Ambient atmospheric properties are, of course, included in the calculation.

Existing hydrocodes include MAZ and TASS. These are typically run on supercomputers. The MAZ/TASS tandem solves the cloud dynamic equations for the compressible (<1 min.) and incompressible (1 min. to 1 hr.) phases of the cloud's history, respectively. These codes have additional parameters which must be determined/chosen, which are unique to this higher level of modeling.

Theory Used in the CRM of DELFIC

The DoD research reference fallout code, DELFIC, contains three main modules: the Cloud Rise Module (CRM), the Diffusive Transport Module (DTM), and the Output Processor Module (OPM) (See Figure 2 on page 14). The CRM has two main functions. The first is to calculate the solution of the bubble rise history of a single zone cloud, as described previously for a second level effort. The second function is to simulate the particle rise to describe the stabilized particle cloud, which is needed as input for the DTM. This second function will be described in more detail in "Particle Rise Dynamics" on page 40.

History of DELFIC's Cloud Rise Module. The original transport models of the 1950s used an empirically computed stabilized cloud as input for their fallout calculations (61:11;18). These empirical fits provided the dimensions and height of the cloud once it stopped rising. An assumed distribution of radioactive mass within the cloud was then made that produced adequate agreement with measured fallout on the ground.

In the late 1950s, it was agreed by the nuclear effects community that using physics in modeling the cloud rise and growth (instead of empiricism) was the major area missing in the current models. In the early 1960s Huebsch developed a model for surface bursts over water for the Naval Radiological Defense Laboratory (NRDL) that included a physical modeling of the cloud rise and particle growth, instead of using an empirical stabilized cloud (20). He then modified his model to include a soil burden for land surface bursts and implemented it in the original version of the DoD research reference fallout code DELFIC (22). Huebsch's model was the original CRM of DELFIC and was published as Volume III of seven volumes in 1967 (22;41;42;43;55;59;62).

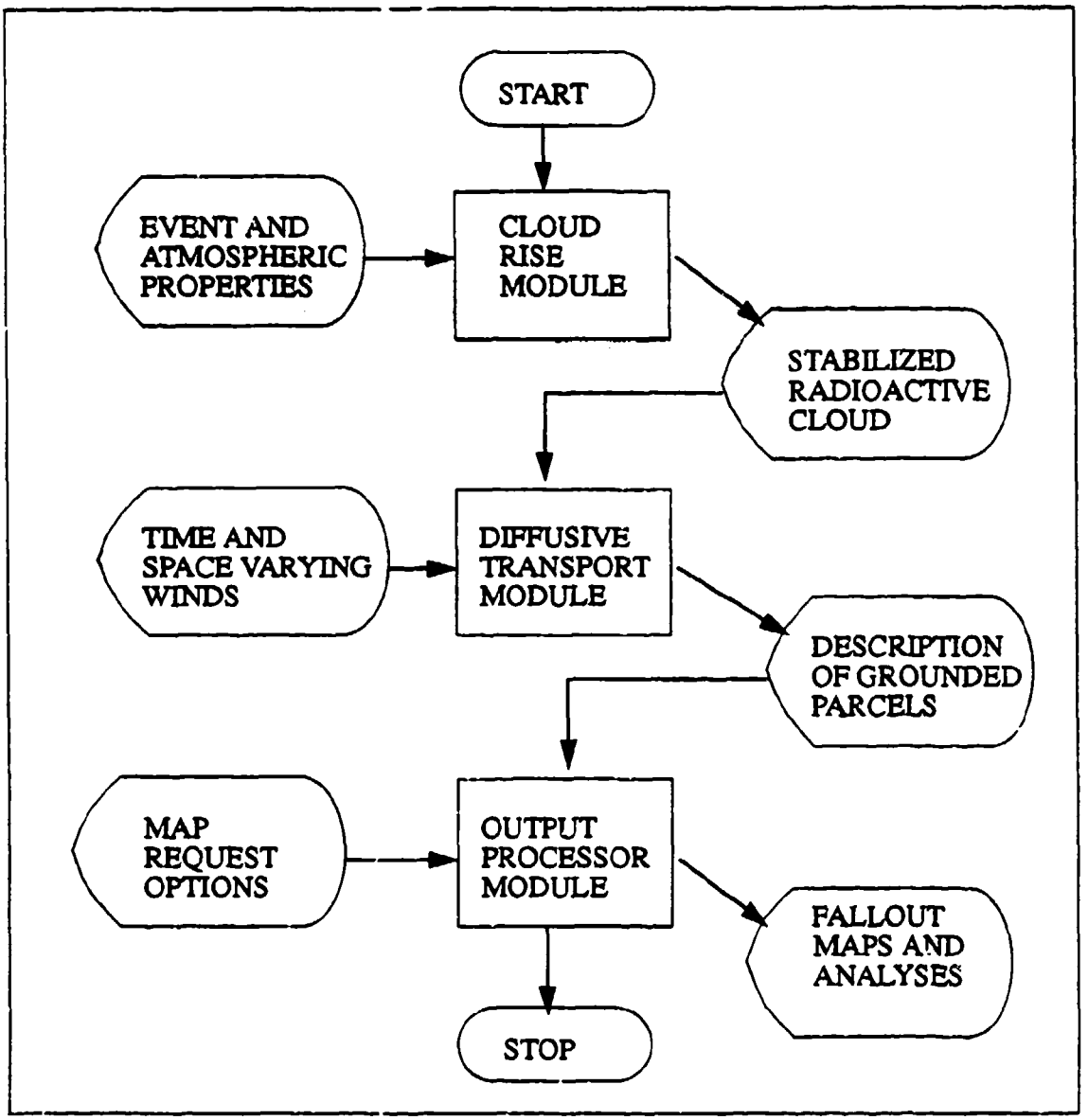

Figure 2: Top Level Flow Chart of DELFIC

The CRM has seen many revisions since 1967 (See Table 2 on page 15). In 1970, Norment (45) revised the CRM and among other changes, completely removed the particle growth capability. In 1975 Huebsch (24) critiqued the 1970 CRM-Revised of Norment.

Huebsch showed that the 1970 equations violated the conservation of energy. Huebsch's recommendations were addressed in Norment's 1977 validation of CRM-Revised (46).

Table 2: History of DELFIC's Cloud Rise Module

Author	Date	Title
Huebsch	1964	Development of a Water-Surface-Burst Fallout Model: The Rise and Expansion of the Atomic Cloud.
Huebsch	1967	The Department of Defense Land Fallout Prediction System. Volume III. Cloud Rise.
Norment	1970	The Department of Defense Land Fallout Prediction System. Volume III. Cloud Rise. Revised.
Huebsch	1975	Analysis and Revision of the Cloud Rise Module of the Department of Defense Land Fallout Prediction System (DELFIC).
Norment	1977	Validation and Refinement of the DELFIC Cloud Rise Module.
Norment	1979	DELFIC: Department of Defense Fallout Prediction System. Volume I - Fundamentals.

In the 1977 version of the CRM, Norment revised the equations and model assumptions so they no longer violated the conservation of energy. One change occurring in this revision was the removal of the virtual mass factor on the momentum (velocity) equation. The effect of removing this factor is negligible for the times of interest in DELFIC. However, the virtual mass factor is needed when considering bubbles starting from rest to limit their acceleration to twice that of gravity (32:4).

Finally, in 1979, Norment published the last well-documented revision of DELFIC (47;48). Other modifications to DELFIC, including conversion from FORTRAN IV to FORTRAN 77, have been accomplished since then (31). These other modifications, how-

ever, have not been well documented or produce questionable results, and therefore the 1979 version was selected as the baseline for this effort (34).

Initial Conditions. The CRM's computations are started at some time other than the time of detonation. In the CRM, initial conditions are calculated as a set of empirical fits to nuclear test data (functions of yield and HOB). This provides the initial size, mass, height, temperature, and velocity at the initial time for the cloud rise calculations. The selection of the initial time, approximately 1 to 20 seconds after detonation, occurs before the majority of the cloud's rise, but after pressure equilibrium with the atmosphere has been achieved. This allows an incompressible model assumption. By the initialization time, the cloud has cooled sufficiently to assume radiative losses of energy are negligible. The initial time also is needed for the entraining bubble assumption, since the very early-time rise of the fireball lacks entrainment of ambient air (20:14).

A thorough review of the initial conditions was completed to determine if any should be altered in this study. Most were found to be based on observation, with only a few based on conjecture. The two initial conditions that contained the most uncertainty concerning their origin were the initial mass and temperature of the soil in the cloud. Over the many revisions of DELFIC, however, the value for the soil's temperature has been adjusted to ensure reasonableness in its value for all yields (28). The initial soil mass has not been revised since the original DELFIC, but was found to differ only slightly from the more modern fit by Carpenter (5). The difference was minor when compared to the CRM assumption that the cloud obtains immediate loading of the entire soil mass at initial time. Therefore, none of the initial conditions were changed from the way they were calculated in the 1979 version of DELFIC.

Ordinary Differential Equations. Starting with the initial conditions, the CRM uses the conservation equations of mass, momentum, turbulent kinetic energy, and heat to solve for eight basic variables (see Table 3 on page 17). The derivations of these equations are contained in Huebsch's 1964 document, and revised by Norment in his later publications (45;46). The equations are transformed into eight first-order nonlinear ordinary differential equations (ODEs) in the basic variables. These variables are vertical velocity, height, temperature, turbulent kinetic energy, mass, and fraction of mass in the soil, vapor, and condensed water phases. Given these variables, all other variables of interest can be determined. All variables solved for are global, in that the cloud model is a single bubble with uniform properties throughout.

Table 3: Basic Variables Solved for in the Cloud Rise Module ODEs

Symbol	Variable	Balance Equation
u	vertical velocity of rise	momentum
z	vertical height of the cloud center	
T	temperature of the cloud	heat
E	turbulent kinetic energy density	turbulent kinetic energy
m	total mass of the cloud (air, soil, water, & vapor)	mass
s	ratio of condensed soil in cloud mass to that of air	
x	ratio of water vapor in cloud mass to that of air	
w	ratio of condensed water in cloud mass to that of air	

A short derivation for some of the ODEs follows. This derivation assumes that no condensed water is present in the cloud. A more complete derivation may be found in the works of Huebsch (20;21;22).

Velocity Equation. The bubble's velocity equation is derived by equating its rate of change of momentum to the sum of its buoyancy force and its eddy viscous drag force

$$\left\{\begin{matrix}\text{rate of change} \\ \text{of momentum}\end{matrix}\right\} = \left\{\begin{matrix}\text{buoyancy} \\ \text{force}\end{matrix}\right\} + \left\{\begin{matrix}\text{eddy viscous} \\ \text{drag force}\end{matrix}\right\} \quad (1)$$

$$\frac{d}{dt}(mu) = V(\rho_e - \rho)\, g - \frac{2k_2 vu}{H_c \frac{\rho}{\rho_e}} m \quad (2)$$

where

v = $Max\,(u, \sqrt{2E})$ is the characteristic velocity (m/s)

m = total cloud mass (air, vapor, water, and soil) (kg)

u = rate of cloud rise (m/s)

V = cloud volume = m/ρ (m^3)

ρ_e = ambient air density (kg/m^3)

ρ = cloud density (kg/m^3)

g = acceleration due to gravity (9.8 m/s^2)

k_2 = eddy viscous drag parameter

E = turbulent kinetic energy density (J/kg)

H_c = cloud vertical thickness (m)

Then using the gas law for air and water vapor one can rewrite the buoyancy term using the following relation

$$\frac{\rho_e}{\rho} = \frac{T^*}{T_e^*}\beta' \tag{3}$$

where

$T^* = T\frac{1+x/\xi}{1+x}$ is cloud virtual temperature (K)

$T_e^* = T_e\frac{1+x_e/\xi}{1+x_e}$ is ambient virtual temperature (K)

$\beta' = \frac{1+x}{1+x+w}$ is ratio of cloud gas density to total cloud density

T = cloud temperature (K)

T_e = ambient temperature (K)

x = cloud water vapor mixing ratio (ratio of water vapor mass to dry air mass)

x_e = ambient water vapor mixing ratio

$\xi = 18/29$ is ratio of the molecular weight of water vapor to that of dry air

w = cloud condensed water mixing ratio

Then one can rearrange terms to give the differential equation for the time rate of change of cloud velocity. The first term on the right in Eqn (4) is the buoyancy term while the second term includes the eddy viscous and entrainment drag effects

$$\frac{du}{dt} = \left(\frac{T^*}{T_e^*}\beta' - 1\right)g - \left(\frac{2k_2 v}{H_c}\frac{T^*}{T_e^*}\beta' + \frac{1}{m}\frac{dm}{dt}\right)u \tag{4}$$

Energy Equation. The time rate of change of turbulent kinetic energy per unit mass, E, is obtained by balancing the sources and sinks of kinetic energy in the cloud during a small time interval dt

$$dE = \left\{\begin{matrix}\text{source by eddy}\\ \text{viscous drag}\end{matrix}\right\} + \left\{\begin{matrix}\text{source by inelastic}\\ \text{collision}\\ \text{entrainment}\end{matrix}\right\} - \left\{\begin{matrix}\text{diluted by}\\ \text{entrainment}\end{matrix}\right\} - \left\{\begin{matrix}\text{dissipated}\\ \text{to heat}\end{matrix}\right\} \tag{5}$$

$$\frac{dE}{dt} = 2k_2\frac{T^*}{T_e^*}\beta'\frac{u^2 v}{H_c} + \frac{u^2}{2}\frac{1}{m}\frac{dm}{dt}\bigg|_{ent} - E\frac{1}{m}\frac{dm}{dt}\bigg|_{ent} - \varepsilon \tag{6}$$

where

$\left.\frac{dm}{dt}\right|_{ent}$ = rate of change of mass due to entrainment (kg/s)

$\varepsilon = \frac{k_3 (2E)^{3/2}}{H_c}$ is turbulent kinetic energy dissipation rate per unit mass (J/kg s)

k_3 = a constant

Temperature Equation. The temperature equation can be obtained by the conservation of energy(heat) during a time interval dt.

$$\left\{\begin{array}{c}\text{heat used to warm}\\ \text{entrained air dm}\end{array}\right\} + \left\{\begin{array}{c}\text{heat absorbed in}\\ \text{adiabatic expansion dp}\end{array}\right\} = \left\{\begin{array}{c}\text{heat gained from}\\ \text{turbulent energy dissipation}\end{array}\right\} \quad (7)$$

$$\left(\int_{T_e}^{T} c_{pa}(\tilde{T})\, d\tilde{T}\right) dm + m\left(\bar{c}_p(T)\, dT - R_a T^* \beta' \frac{dp}{p}\right) = \varepsilon m \beta' dt \quad (8)$$

where

$c_{pa}(T)$= specific heat of entrained air (dry air) (J/kg K)

$\bar{c}_p(T)$= mass weighted mean of the specific heats of air and water vapor (J/kg K)

R_a = gas constant of air (287 J/kg K)

p = pressure at cloud center altitude (Pa)

Then using the hydrostatic equation

$$\frac{dp}{dz} = -g\frac{p}{R_a T^*} \quad (9)$$

one can transform the expansion term, divide through by dt, and rearrange terms to get the time rate of change of cloud temperature. The first term inside the brackets on the right below accounts for adiabatic expansion, the second accounts for entrained air, while the third is for turbulent kinetic energy dissipation to heat.

$$\frac{dT}{dt} = -\frac{\beta'}{\bar{c}_p(T)}\left[\frac{T^*}{T_e^*}gu + \left(\int_{T_e}^{T} c_{pa}(\tilde{T})\,d\tilde{T}\right)\frac{1}{\beta' m}\frac{dm}{dt}\bigg|_{ent} - \varepsilon\right] \tag{10}$$

Mass Equation. The equation for the rate of change of mass due to entrainment as derived by Norment is shown below.

$$\frac{dm}{dt}\bigg|_{ent} = \frac{\dfrac{\beta' m}{T}\left(\dfrac{S}{V}\mu v + \dfrac{\beta'}{T^*\bar{c}_p}\left[\dfrac{T^*}{T_e^*}gu - \varepsilon\right] - \dfrac{gu}{R_a T_e^*}\right)}{1 - \dfrac{\beta'}{T^*\bar{c}_p}\displaystyle\int_{T_e} c_{pa}(\tilde{T})\,d\tilde{T}} \tag{11}$$

where

S = surface area of the cloud (m^2)

μ = entrainment parameter

This version of the entrainment equation is much different than the original version and that suggested by Huebsch in Eqn (12)

$$\frac{dm}{dt}\bigg|_{ent} = m\frac{S}{V}\mu v \tag{12}$$

Norment's Eqn (11) has two extra terms inside the parentheses on the right representing temperature effects and hydrostatic expansion. These terms and the leading multiplier on the right arise due to Norment's assumptions in his derivation (45). Some of Norment's assumptions are no longer consistent with the current CRM, and Eqn (12) is therefore the

preferred form of the equation. Huebsch has stated that either form of the entrainment equation can be used without violating the other conservation equations.

Dry Equations. The above four equations are then combined with four equations that define the change in mixing ratios of water vapor, condensed water, and soil, and the definition of velocity. The entire set of eight ODEs used in the current CRM are listed as Eqns (4), (6), (10), (11), (13), (14), (15), and (16).

$$\frac{dx}{dt} = -\frac{1+x+s}{1+x_e}(x-x_e)\frac{1}{m}\frac{dm}{dt}\bigg|_{ent} \tag{13}$$

where s denotes the cloud soil mixing ratio (ratio of soil mass to dry air mass).

$$\frac{dw}{dt} = -\frac{1}{\beta'}\left(\frac{1+x}{1+x_e}\right)(w+x-x_e)\frac{1}{m}\frac{dm}{dt}\bigg|_{ent} - \frac{dx}{dt} \tag{14}$$

$$\frac{ds}{dt} = -\frac{1}{\beta'}\frac{1+x}{1+x_e}s\frac{1}{m}\frac{dm}{dt}\bigg|_{ent} - \frac{1+x+s+w}{m}\left(\frac{s}{s+w}\right)F \tag{15}$$

where F denotes the rate of soil mass leaving the cloud (kg/s).

$$\frac{dz}{dt} = u \tag{16}$$

where z denotes the cloud center height (m).

Wet Equations. Some of the equations listed above have to be altered to include the effects of latent heat. Since the equations were derived from conservation relationships, extra terms are needed for the source of energy released when the water vapor in the cloud condenses. This occurs when the saturation temperature for the pressure of the cloud has been reached. The release of latent heat can be significant in some cases (20:10) ("Appendix B: Latent Heat" on page 129). The derivation of this set of equations can be found elsewhere, and it suffices to list just those equations that need altering (20;21;22).

$$\left.\frac{dm}{dt}\right|_{ent} = \frac{\beta' m}{1 - \frac{1}{T^*}\left[\frac{\beta'}{1 + \frac{L^2 x \xi}{c_p R_a T^2}}\right]\left[T - T_e + \frac{L(x - x_e)}{c_p}\right]} \times \left\{\frac{S}{V}\mu v + \left[\frac{\beta'/T^*}{1 + \frac{L^2 x \xi}{c_p R_a T^2}}\right]\left[\frac{guT^*}{T_e^* c_p}\left(1 + \frac{Lx}{R_a T}\right) - \frac{\varepsilon}{c_p}\right] - \frac{gu}{R_a T_e^*}\right\} \quad (17)$$

where L denotes the latent heat of vaporization of water or ice (J/kg).

$$\frac{dT}{dt} = -\frac{\beta'}{1 + \frac{L^2 x \xi}{c_p R_a T^2}}\left[\left((T - T_e) + \frac{L(x - x_e)}{c_p}\right)\frac{1}{m\beta'}\left.\frac{dm}{dt}\right|_{ent} + \frac{T^*}{T_e^*}\frac{g}{c_p}u\left(1 + \frac{Lx}{R_a T}\right) - \frac{\varepsilon}{c_p}\right] \quad (18)$$

$$\frac{1}{x}\frac{dx}{dt} = (1 + x/\xi)\frac{L\xi}{R_a T^2}\frac{dT}{dt} + (1 + x/\xi)\frac{g}{R_a T_e^*}u \qquad (19)$$

Solution of the ODE's. The model uses the set of eight ODEs and solves them numerically using a fourth-order Runge-Kutta-Gili method (4:363). By using 3 time domains from initial time to stabilization time (t_i to t_i + 1 sec, t_i + 1 sec to t_i + 100 sec, and t_i + 100 sec to t_{st}) with 3 different time steps (1/32, 1/4, and 2 1/2 sec), the CRM solves the set of ODEs for each phase of the solution. A somewhat different set of variables (base, top, radius, base-rate, top-rate, and radial-rate, T, and ρ) is calculated, printed, and stored in an array at various times during the cloud rise to fully define the history of rise (See Table 4 on page 26). The set of variables stored is used to run the later subroutines that distribute the particles in the vertical dimension. Plots of the basic variables, as generated from a typical run are shown (See Figure 3 on page 27).

Model Parameters. In the above equations there exist two parameters that were altered in this work to be consistent with the literature and to best match observed cloud tops: parameters for entrainment (μ) and eddy viscous drag (k_2). These parameters are both currently functions of yield, W, (See Figure 4 on page 28). The original version of the CRM had these two parameters as constants: μ=0.2 and k_2=0.1. These were both changed by Norment to become functions of yield in his 1970 revision. He then changed them again in his 1977 validation to the functions plotted in Figure 4 on page 28. The increase in the slope of μ past 15 MT is questionable since there were no atmospheric tests above this yield to validate against.

Table 4: DELFIC's CRM Bubble Rise History for 1979 Test Case (50 kt, 0 ft HOB)

Time (sec)	Base (m)	Top (m)	Radius (m)	Base Rate (m/s)	Top Rate (m/s)	Radial Rate (m/s)	Temperature (K)	Density (kg/m^3)
4.357E+00	2.149E+02	7.263E+02	3.866E+02	6.412E+01	8.645E+01	1.688E+01	2.629E+03	1.284E-01
4.545E+00	2.269E+02	7.425E+02	3.897E+02	6.725E+01	9.061E+01	1.766E+01	2.545E+03	1.323E-01
4.982E+00	2.563E+02	7.821E+02	3.975E+02	6.874E+01	9.259E+01	1.803E+01	2.233E+03	1.503E-01
5.857E+00	3.165E+02	8.631E+02	4.132E+02	6.171E+01	9.454E+01	2.482E+01	1.620E+03	2.054E-01
7.107E+00	3.936E+02	9.813E+02	4.443E+02	5.675E+01	9.050E+01	2.551E+01	1.187E+03	2.770E-01
8.607E+00	4.787E+02	1.117E+03	4.825E+02	5.516E+01	8.233E+01	2.054E+01	9.221E+02	3.521E-01
1.111E+01	6.166E+02	1.323E+03	5.339E+02	5.317E+01	7.574E+01	1.706E+01	6.810E+02	4.669E-01
1.411E+01	7.761E+02	1.550E+03	5.850E+02	5.109E+01	7.101E+01	1.506E+01	5.409E+02	5.739E-01
1.786E+01	9.677E+02	1.816E+03	6.415E+02	4.909E+01	6.702E+01	1.355E+01	4.536E+02	6.647E-01
2.236E+01	1.189E+03	2.118E+03	7.025E+02	4.657E+01	6.340E+01	1.272E+01	3.983E+02	7.345E-01
2.786E+01	1.445E+03	2.467E+03	7.725E+02	4.365E+01	5.963E+01	1.208E+01	3.599E+02	7.842E-01
3.436E+01	1.728E+03	2.854E+03	8.510E+02	4.070E+01	5.574E+01	1.137E+01	3.329E+02	8.135E-01
4.211E+01	2.044E+03	3.286E+03	9.391E+02	3.808E+01	5.198E+01	1.051E+01	3.131E+02	8.243E-01
5.086E+01	2.377E+03	3.741E+03	1.031E+03	3.579E+01	4.831E+01	9.468E+00	2.988E+02	8.204E-01
6.086E+01	2.735E+03	4.224E+03	1.126E+03	3.283E+01	4.474E+01	9.001E+00	2.877E+02	8.124E-01
7.236E+01	3.113E+03	4.739E+03	1.229E+03	2.940E+01	4.074E+01	8.575E+00	2.788E+02	7.952E-01
8.536E+01	3.495E+03	5.268E+03	1.341E+03	2.570E+01	3.640E+01	8.092E+00	2.715E+02	7.711E-01
9.986E+01	3.867E+03	5.796E+03	1.458E+03	2.164E+01	3.164E+01	7.562E+00	2.656E+02	7.425E-01
1.169E+02	4.235E+03	6.334E+03	1.587E+03	1.742E+01	2.662E+01	6.955E+00	2.605E+02	7.099E-01
1.344E+02	4.540E+03	6.800E+03	1.708E+03	1.346E+01	2.158E+01	6.138E+00	2.567E+02	6.813E-01
1.544E+02	4.809E+03	7.232E+03	1.831E+03	1.009E+01	1.751E+01	5.615E+00	2.534E+02	6.604E-01
1.746E+02	5.013E+03	7.586E+03	1.945E+03	7.365E+00	1.403E+01	5.041E+00	2.509E+02	6.431E-01
1.996E+02	5.198E+03	7.937E+03	2.071E+03	5.197E+00	1.119E+01	4.529E+00	2.488E+02	6.257E-01
2.246E+02	5.328E+03	8.217E+03	2.184E+03	3.510E+00	8.932E+00	4.099E+00	2.471E+02	6.122E-01
2.521E+02	5.424E+03	8.462E+03	2.297E+03	2.080E+00	6.999E+00	3.719E+00	2.456E+02	6.008E-01
2.821E+02	5.486E+03	8.672E+03	2.408E+03	8.381E-01	5.314E+00	3.384E+00	2.445E+02	5.917E-01
3.146E+02	5.514E+03	8.845E+03	2.518E+03	-2.116E-01	3.851E+00	3.071E+00	2.436E+02	5.849E-01
3.471E+02	5.507E+03	8.970E+03	2.618E+03	-1.199E+00	2.544E+00	2.829E+00	2.431E+02	5.815E-01
3.846E+02	5.462E+03	9.066E+03	2.724E+03	-1.628E-01	1.737E-01	3.876E+00	2.429E+02	5.802E-01
4.246E+02	5.455E+03	9.073E+03	2.879E+03	0.000E+00	0.000E+00	3.879E+00	2.428E+02	5.803E-01
4.671E+02	5.455E+03	9.073E+03	3.044E+03	0.000E+00	0.000E+00	0.000E+00	2.428E+02	5.803E-01

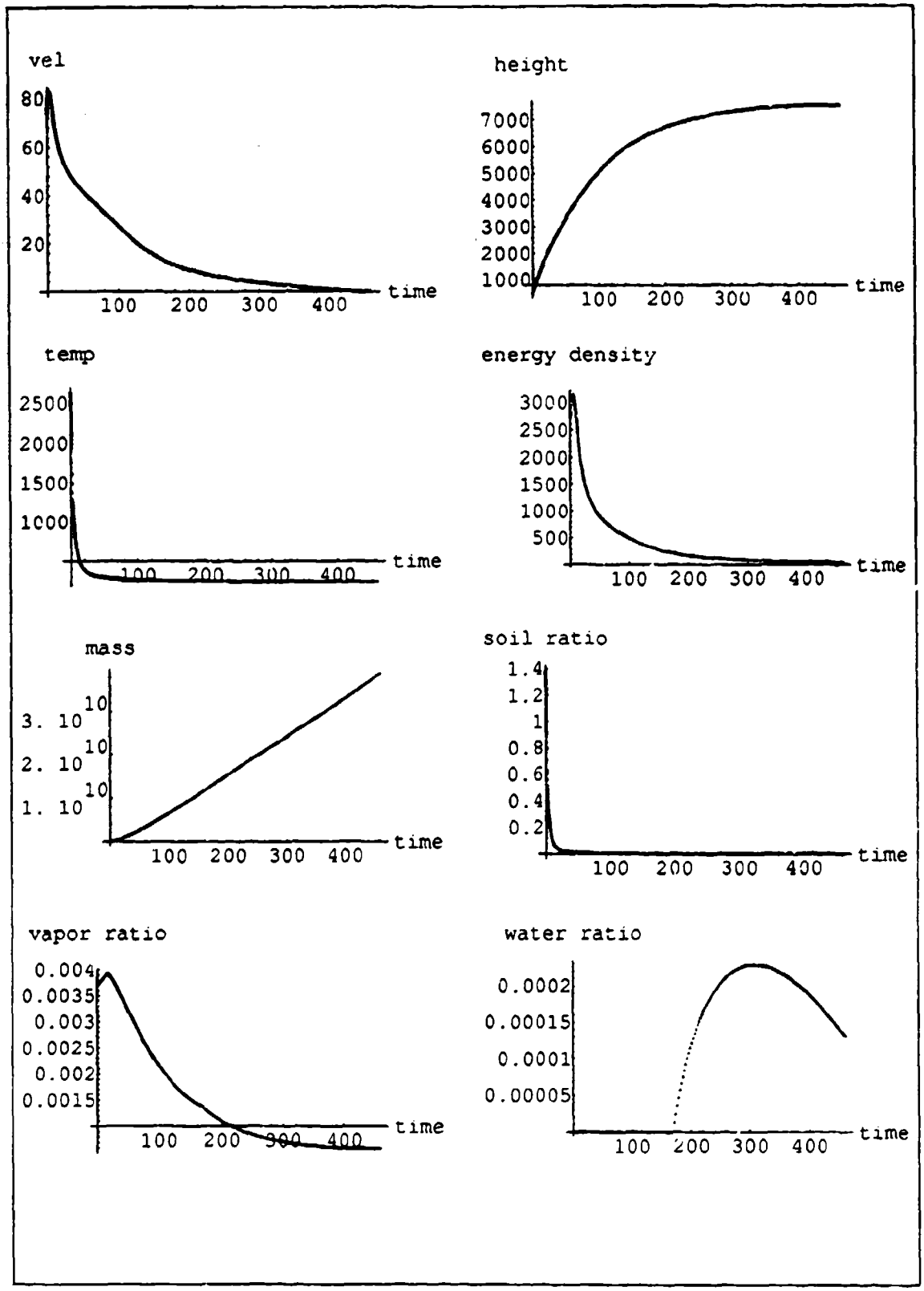

Figure 3: Basic Variables of DELFIC's CRM for the 1979 Test Case (MKS units)

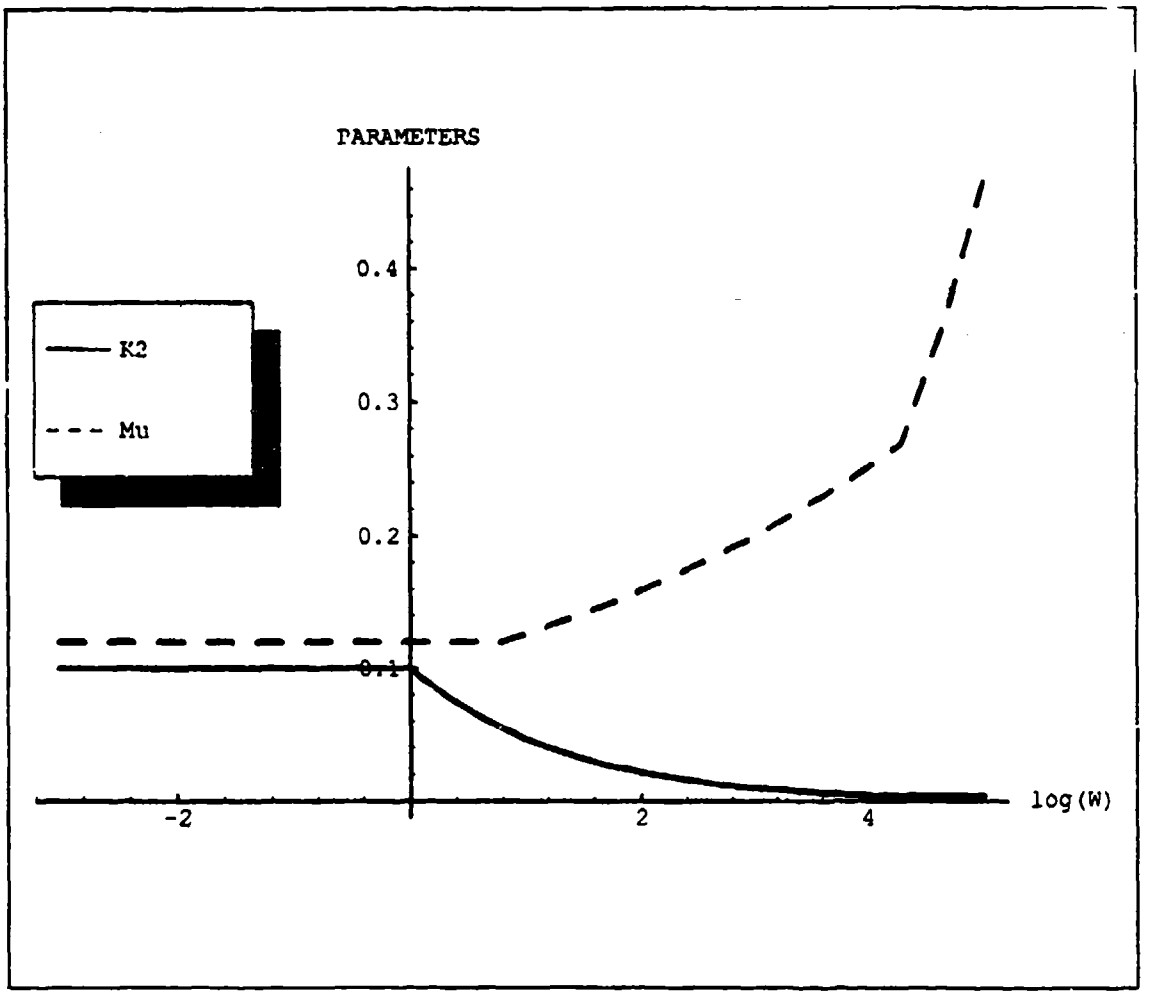

Figure 4: CRM Parameters for Entrainment (μ) and Eddy Viscous Drag (k_2) as a Function of the Log of the Yield (W in kt)

Modeling Fallout During Cloud Rise. The change in cloud mass during a time step dt must also account for the loss of soil mass, F, that may settle out during the rise.

$$\frac{dm}{dt} = \left.\frac{dm}{dt}\right|_{ent} - F \tag{20}$$

The settling rates of each particle size group must be calculated at each time step to compute their contribution to the value of F. A significant fraction of the bubble rise computation is taken up in computing this value. The contribution to the change of mass due to soil loss, when compared to the change due to entrained air, was found to be negligible by the author. All non-airbursts in the validation set were used to compare the effect of soil fallout on the basic variables. The effect of ignoring the soil loss was hardly noticeable on any burst and was well below a 1% change for all variables. The loss of condensed water was also modeled in the original CRM, but was considered negligible, and was no longer calculated in Norment's CRM-Revised.

Effect of Wind Shear. Huebsch has shown that the effect of wind shear on cloud rise is important. The CRM models wind shear by a replacement of variables in the entrainment equation. A physical explanation of the second term on the right below may be found in Huebsch's work (23:2-5). Basically the effect of shear on the cloud is to increase the surface to volume ratio, thereby increasing entrainment.

$$\mu \frac{S}{V} v \rightarrow \mu \left(\frac{S}{V} v + k_6 \frac{3}{2R_c} v_s \right) \tag{21}$$

where

k_6 = a constant

R_c = horizontal radius of the cloud (m)

v_s = wind velocity difference between the top and base of the cloud (m/s)

Cloud Shape and Volume. The volume of the cloud can be determined at any time by the ideal gas law for air, given the temperature, pressure, and mass of the cloud. Its dimensions are then determined by an assumption of its shape.

The original CRM assumed a sphere until the cloud top reached a user-defined tropopause altitude. The cloud's vertical radius was then frozen and any further growth was accommodated by horizontal expansion. Norment's CRM-Revised took a different approach. The vertical thickness of the cloud was assumed to be linearly dependent on the cloud's rise distance. The radius was then determined assuming a spheroidal shape. Though Norment claimed this would produce an oblate cloud, Huebsch's 1975 critique showed that the cloud could become prolate at late times.

Norment's response to Huebsch's critique was to fix the cloud shape as an oblate spheroid of eccentricity 0.75 based solely on observation and calculated from the cloud volume. Once the cloud stopped rising, however, the cloud would stop growing vertically and expand only radially, becoming more oblate. This is the current way the CRM computes the cloud's dimensions. Although this method seems to perform better than the previous methods, it still does not allow for the "collapse" of some clouds where the base continues to rise after the top has stopped rising. It also does not allow the top to overshoot and then oscillate about a final stabilized altitude. Both of these phenomena have been observed in US nuclear test events.

Termination of Cloud Rise and Expansion. Once the cloud has stopped rising, the CRM checks two conditions to determine horizontal stabilization (47:26-27). When either of the two conditions are met, the cloud expansion is terminated and the definition of the particle cloud is calculated for input to the DTM. The first condition is that the radial

growth rate has slowed down below a predetermined value which is a function of yield. The other is that the turbulent kinetic energy density in the cloud is reduced to ambient levels (also a function of yield) for the height of the cloud.

Work Done on DELFIC's Bubble Rise Subroutines

With the above explanation of the current version of the CRM, the work done by the author on the bubble rise modeling will now be presented. This section of the chapter is broken down into three subsections. The first subsection describes the corrections needed in the CRM subroutines to match the stated theory. The second subsection details the improvements implemented by the author in the model. The final subsection reviews the validation effort used to check the author's corrections and improvements.

A complete listing of the DELFIC code used in this research is on file in the Department of Engineering Physics, Air Force Institute of Technology, Wright-Patterson AFB, OH, 45433. The code includes the original 1979 version obtained by the author along with the corrections and improvements described in this report. All changes to the 1979 version are distinguished by comments within the code containing the author's initials 'vjj'.

Corrections Needed in the 1979 DELFIC CRM. In recovering the 1979 version of DELFIC from the documentation, McGahan had to add a MAIN program, since the documentation was lacking one. The CRM then compiled with no changes on a 386-SX-16 personal computer using Microsoft FORTRAN 5.1. To compile on a SPARC station 2 using SUN FORTRAN 1.4, two separate FORMAT statements had to be edited. These minor changes allowed the 1979 version of the CRM to be compiled without any warnings

or errors. Similar changes were needed to compile the entire DELFIC program including the DTM and OPM.

The 1979 documentation contains a test case's input and output which were used to verify that the code was running correctly (48:34-50). After the CRM was compiled successfully, the program's output was verified with that listed in Volume II of the 1979 documentation. Additional post-processors were built by the author with Mathematica to display the CRM variables as a function of time. DELFIC is fast on today's computers with the entire test case taking only 20 seconds on a 486-33 personal computer!

In studying the 1979 version, a few errors were found both in the document pertaining to the theory and in the source code. A discussion of these discrepancies and the corrections needed to remedy them are documented in a previous report by this author (25). One correction needed in the source code so it would match the 1979 documentation concerned the entrainment equation. This change made a noticeable difference in the output of the test case. While the remainder of the corrections didn't change the *test case output* significantly, they may affect other scenarios to a greater extent.

The discrepancy mentioned in section 2.3.5 (concerning a switch on the specific heat calculation of the cloud), on page 11 of this author's previous report (25), has now been resolved. The switch *is* needed in the calculation due to the derivation of the temperature equation. The soil temperature is at a different temperature than the gaseous cloud. It is assumed to stay at this lower temperature until the gaseous cloud cools to this temperature, at which time both soil and gases are cooled at the same rate. The interested reader should refer to the original CRM document (22).

Improvements. The single term form of the entrainment equation (See Eqn (12)) has been regarded as the correct form in the literature since Taylor (58), and is still accepted by the community today (32;54). Norment in his revision to the original CRM, attempted to derive the entrainment equation from the ideal gas law and empirical fits to observed cloud behavior. Huebsch critiqued Norment's version of the entrainment equation, considering it invalid and the cause of output discrepancies (24:12). His recommendation was to return to the single term version of the equation. Huebsch also asserted that the entrainment (μ) and eddy viscous drag (k_2) parameters should be constants, not parameters of yield as Norment had redefined them.

Upon investigating Norment's derivation, Huebsch's recommendations, and Norment's subsequent changes, it was decided that Huebsch's form of the entrainment equation was best. When Norment derived his version of the equation, he used some rigid empirical fits to the cloud's vertical thickness as a function of rise distance. He basically abandoned these empiricisms in his changes to the CRM's approach to cloud shape in 1977, but chose not to alter his entrainment equation. This makes his derivation questionable at best, and the single term form (as it still appears in the literature) should be used.

The literature also supports Huebsch in stating that the entrainment parameter, by definition, is a constant (12:7). There are similar physical arguments that support Huebsch's recommendation that the eddy viscous drag parameter too should be a constant (20:18-19). In his critique, Huebsch mentioned that Norment's combination of increasing μ and lowering k_2 with yield compensate somewhat for each other. This explains why agreement with observation is still achieved. It will be shown later that better agreement to atmo-

spheric nuclear test observations can be achieved using the single term entrainment equation and setting μ and k_2 to constants.

The reason Norment may have achieved acceptable results with his yield dependent fits for the parameters was due to their compensating effects on cloud rise. As the reader can see from Figure 4 on page 28, μ is raised while k_2 is lowered as yield increases past one kiloton. The result is to increase the effect of entrainment while lowering the effect of eddy viscous drag on the equations. When Norment reviewed Huebsch's recommendations, he tried a single term equation by setting μ and k_2 to 0.25 and 0.1 respectively. Although Huebsch stated these values as his best guess, he did say some testing was probably required to determine their best values. Norment did not report varying these values when testing the single term entrainment equation. The result of using the above values was an over prediction of entrainment and a poor match to observed cloud tops.

Upon further investigation, the discrepancy may be found in the cloud shape. Huebsch's original model used a spherical shape. Norment's 1977 revision was using a spheroidal shape. This implies a larger surface to volume ratio for Norment. Therefore, to maintain the same proportionality factor in front of the velocity term in the entrainment equation, one must reduce μ for a spheroid. In fact, the best value found here for μ was 0.12, which will be discussed in "Results and Comparisons" on page 72.

Validation. The effect of correcting and improving the cloud rise equations are determined by running actual atmospheric nuclear test cases. The results are then validated against recorded test data from these events. Input data files were created using the best available unclassified sources which describe the test events. Similarly, observation data

was gathered from published unclassified reports. Finally, the figure of merit used by Norment was used in this research to judge the performance of the changes.

Norment's Validation Set. In his 1970 revision of the CRM, Norment included an appendix which contained tabulations and plots from simulations of US atmospheric events (45:155-166). Although he used 56 shots, he only identifies the 54 unclassified ones. These 54 shots are the set used in this research for validation without excluding the lowest yield shot as Norment did in his 1977 validation of the CRM (See Table 5 on page 36 and Figure 5 on page 38) (46:18). Since Norment states that DELFIC is valid for shots from 1 ton to 100 MT (47;48), this 7.8 ton event is included in this author's validation studies. These 54 events include 39 airbursts, 13 near surface bursts, 1 surface burst, and 1 slightly buried burst. The yields included 14 sub-kiloton shots and 3 megaton range shots. Only 5 of the shots were from the Pacific Proving Grounds, including the four highest yield shots. The highest yield of the Nevada Test Site shots was 74 kilotons.

Cloud Top Observation Data. Since Norment did not cite any written reports as the source of inputs or observation values for his validation, it is impossible to know the reliability of his data. DASA 1251-EX-I and -II were used in this research for both the event data (yield, surface height, and height of burst) and the cloud-top observation data (16;17). This choice provides consistency between the different series (e.g. Castle and Plumbbob). It also lists the modern best estimates of the values and provides a basis for repeatability for future research done in this area. Most event data values agreed with those used by Norment in 1970.

Weather Input Data. An extensive search of the unclassified literature was undertaken to recover the written reports containing the recorded atmospheric conditions for

Table 5: Bubble Rise Validation Set Sorted by Yield

Operation	Shot Name	Yield (kt)	HOB (m)
Hardtack II	Humboldt	0.0078	7.62
Hardtack II	Catron	0.021	22.10
Hardtack II	Vesta	0.024	0.00
Hardtack II	DonaAna	0.037	137.16
Hardtack II	Hidalgo	0.077	114.91
Hardtack II	Quay	0.079	30.48
Hardtack II	Eddy	0.083	152.40
Hardtack II	RioArriba	0.09	22.10
Hardtack II	Wrangell	0.115	457.20
Plumbbob	Franklin	0.14	91.44
Plumbbob	Wheeler	0.197	152.40
Upshot-Knothole	Ray	0.2	30.48
Upshot-Knothole	Ruth	0.2	92.87
Sunbeam	JohnnieBoy	0.5	-0.58
Plumbbob	Laplace	1	228.60
Hardtack II	SantaFe	1.3	457.20
Hardtack II	Lea	1.4	457.20
Plumbbob	John	2	6096.00
Hardtack II	Mora	2	457.20
Hardtack II	DeBaca	2.2	457.20
Plumbbob	FranklinPrime	4.7	228.60
Hardtack II	Sanford	4.9	457.20
Hardtack II	Socorro	6	441.96
Plumbbob	Morgan	8	152.40
Plumbbob	Owens	9.7	152.40
Plumbbob	Kepler	10	152.40
Plumbbob	Wilson	10	152.40
Upshot-Knothole	Dixie	11	1835.51
Plumbbob	Doppler	11	457.20
Plumbbob	Fizeau	11	152.40
Plumbbob	Galileo	11	152.40
Plumbbob	Boltzman	12	152.40
Plumbbob	Charleston	12	457.20

Table 5: Bubble Rise Validation Set Sorted by Yield

Operation	Shot Name	Yield (kt)	HOB (m)
Plumbbob	Newton	12	457.20
Upshot-Knothole	Grable	15	159.72
Upshot-Knothole	Annie	16	91.44
Plumbbob	Diablo	17	152.40
Plumbbob	Shasta	17	152.40
Plumbbob	Stokes	19	457.20
Plumbbob	Whitney	19	152.40
Upshot-Knothole	Badger	23	91.44
Upshot-Knothole	Nancy	24	91.44
Upshot-Knothole	Encore	27	738.53
Upshot-Knothole	Harry	32	91.44
Plumbbob	Priscilla	37	213.36
Redwing	Lacrosse	40	5.18
Upshot-Knothole	Simon	43	91.44
Plumbbob	Smoky	44	213.36
Upshot-Knothole	Climax	61	406.60
Plumbbob	Hood	74	457.20
Castle	Koon	110	4.15
Redwing	Zuni	3500	2.74
Redwing	Tewa	5000	4.57
Castle	Bravo	15000	2.13

these shots (26;27;40). While most were available from DASIAC (8), the Plumbbob series had to be recovered from the original adiabatic chart entries. Microfilm recordings of these charts are held at Asheville, NC, and copies were obtained by the author (50). The weather data included the temperature, pressure, relative humidity (or dew point temperature), wind speed and direction for various altitudes from the surface to altitudes above the stabi-

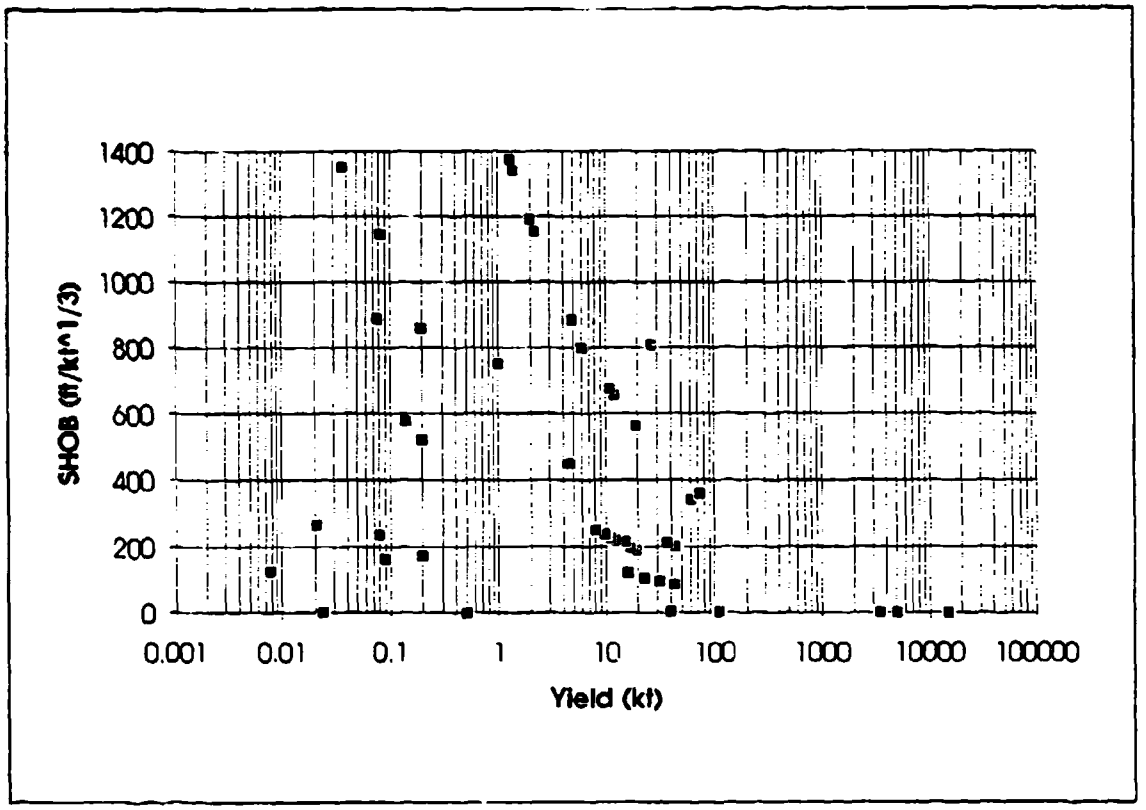

Figure 5: Validation Set (51 of 54 shots) Showing SHOB ($ft/kt^{1/3}$) vs. Yield (kt)

lized cloud top. All data was entered into the computer by the author for use in the CRM code. Every effort was made to ensure accuracy in the data entry.

Fractional Root Mean Square (FRMS) Error Definition. The figures of merit used by Norment to judge the performance of the 1977 version of the CRM were the FRMS deviation and the fractional mean deviation (FMD) (46:22)

$$FRMS = \sqrt{\frac{\sum_{N}\left(\frac{z_{obs} - z_{calc}}{z_{obs}}\right)^2}{N}} \tag{22}$$

$$FMD = \frac{\sum_{N}\left(\frac{z_{obs} - z_{calc}}{z_{obs}}\right)}{N} \qquad (23)$$

where

z_{obs}=observed cloud top height (m)

z_{calc}=calculated cloud top height (m)

N = number of shots in data set (54)

The same figures of merit were used in the validation of changes made in this research. Relative or fractional deviations were used due to the range of observed cloud heights used in these studies.

III. Particle Rise Dynamics

The purpose of this chapter is to explain the theory of particle rise in DELFIC's CRM. Both the current and proposed methods of particle rise are dependent on the results of the previous chapter (See "Bubble Rise Dynamics" on page 11). The present chapter begins in the first section by describing the levels of effort for particle rise simulation. The second section expands on the method of using vortex theory to model the flow of particles. The third section goes into the details of how this method is implemented in DELFIC's CRM. The final section reports the cases that were run and the method of comparison to hydrocode data and the current particle rise of the CRM. Actual results and comparisons will be found in Chapter IV.

Levels of Effort

There are three main ways of modeling particle rise dynamics. The first is the current method employed by DELFIC's CRM (one-dimensional). In addition, there are two primary ways of modeling the particle flow fields in two dimensions. The first is to use a 2-D hydrodynamics model. The second is to use an analytic solution to the fluid flow for a bubble rising in a still fluid. The flow field method is a computationally cheaper way of obtaining increased fidelity of particle rise simulation in DELFIC without resorting to computationally expensive hydrocodes.

Current DELFIC Modeling. This is a simplified description of a very complex algorithm used to determine the particle distribution in the stabilized cloud. The 1-D particle rise subroutine in the CRM takes the history of the stored bubble rise variables and traces the upward motion of an initially uniformly distributed cloud. Then, allowing for fallout

(or particle settling) during the rise, the particles are followed in their path up through the atmosphere to stabilization. Once the end time of the stored variable table is reached (See Table 4 on page 26), the particles are fixed in their vertical locations and the stabilized cloud is thus defined. This algorithm then stores the description of the stabilized cloud so that it can be used in the DTM of DELFIC (47:27-30).

Source Initial Location. The particle cloud is represented as a cylinder with a top, bottom, and radius that match the top, bottom, and radius of the spheroidal bubble defined in the previous chapter (See Figure 6 on page 42). The mass of particles in the cloud is assumed to be uniform in its spatial distribution at the beginning of the particle rise calculations.

Since the CRM does not calculate a radial distribution of mass, the cloud is only subdivided into a set of vertical layers. The number of layers, *KDI*, is input by the user or chosen by the code to be $KDI = 15 + \ln(W \text{ in kilotons})$. These uniformly loaded layers are represented as cylindrical disks (or parcels). This vertical stack of disks in the initial cloud is repeated for each particle size bin in the particle size distribution. The particle size bins are represented by a geometric mean group diameter, bounded by upper and lower boundary particle diameters.

Particle Size Distribution. DELFIC contains three different particle size distribution options: log normal, power law, and tabular input. The default distribution chosen by the code is log normal. This log normal distribution has a mean diameter of 130 microns and a geometric standard deviation of 4. This distribution was determined from downwind

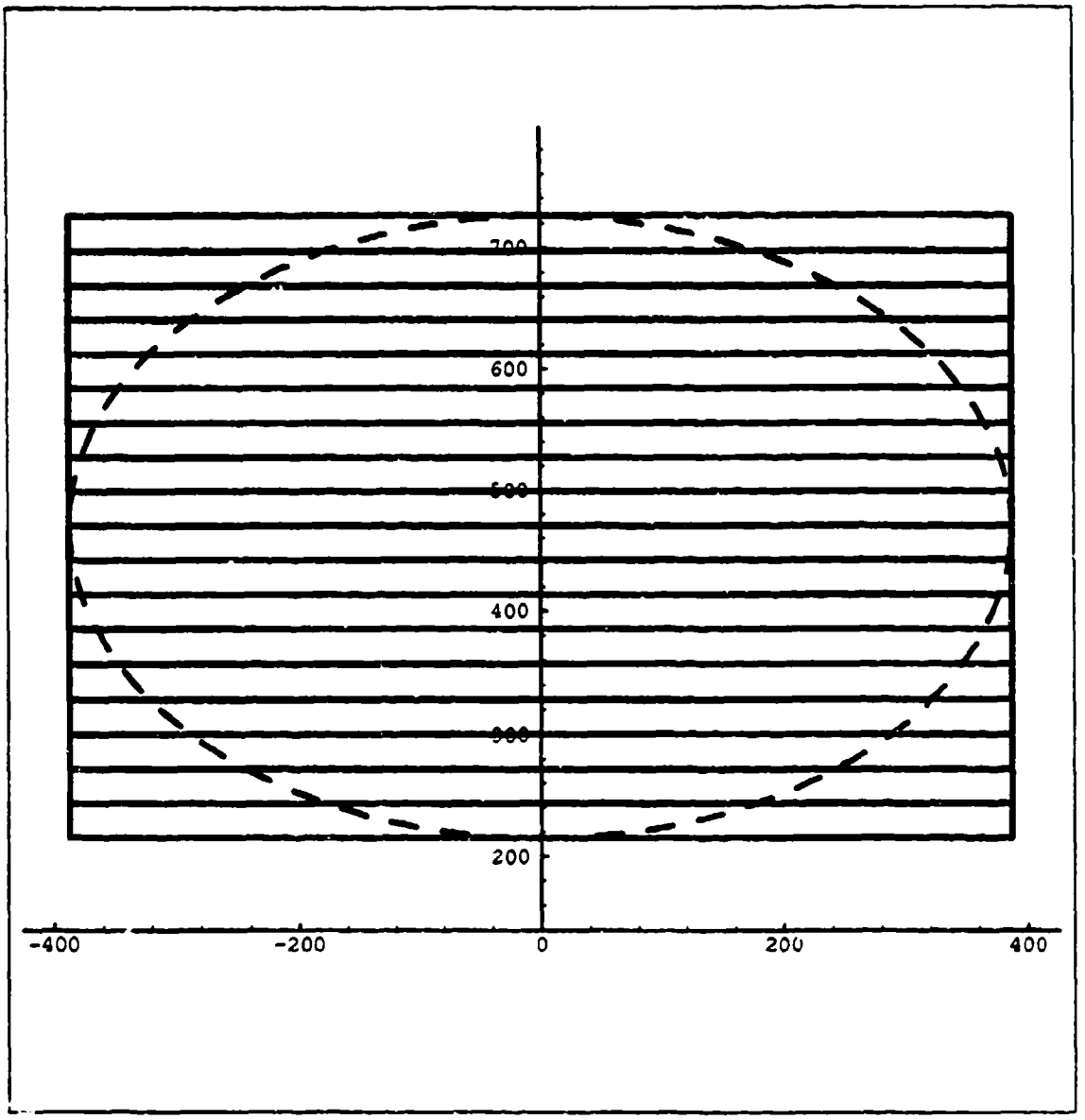

Figure 6: Cross Section of Current CRM Initial Particle Cylinder With Disk Structure Based on Bubble Vertical and Radial Dimensions (dashed) in Meters

samples of fallout and is well accepted by the fallout community. The particle sizes for a 50 group distribution are shown in Table 6 on page 43.

The hydrocode TASS on the other hand has two different particle size distributions: one for ejecta mass and one for scoured mass. Both distributions are determined using

Table 6: Default Particle Size Distribution for DELFIC (50 Groups)

Group	Mean Diameter (m)	Lower Boundary (m)	Upper Boundary (m)
1	0.32686E-02	0.22399E-02	0.47695E-02
2	0.18155E-02	0.14714E-02	0.22399E-02
3	0.12845E-02	0.11214E-02	0.14714E-02
4	0.10108E-02	0.91113E-03	0.11214E-02
5	0.83632E-03	0.76766E-03	0.91113E-03
6	0.71296E-03	0.66217E-03	0.76766E-03
7	0.62008E-03	0.58067E-03	0.66217E-03
8	0.54709E-03	0.51546E-03	0.58067E-03
9	0.48794E-03	0.46189E-03	0.51546E-03
10	0.43885E-03	0.41696E-03	0.46189E-03
11	0.39736E-03	0.37867E-03	0.41696E-03
12	0.36175E-03	0.34559E-03	0.37867E-03
13	0.33082E-03	0.31669E-03	0.34559E-03
14	0.30367E-03	0.29119E-03	0.31669E-03
15	0.27962E-03	0.26852E-03	0.29119E-03
16	0.25816E-03	0.24821E-03	0.26852E-03
17	0.23888E-03	0.22991E-03	0.24821E-03
18	0.22146E-03	0.21332E-03	0.22991E-03
19	0.20563E-03	0.19822E-03	0.21332E-03
20	0.19119E-03	0.18440E-03	0.19822E-03
21	0.17795E-03	0.17172E-03	0.18440E-03
22	0.16577E-03	0.16003E-03	0.17172E-03
23	0.15453E-03	0.14922E-03	0.16003E-03
24	0.14412E-03	0.13919E-03	0.14922E-03
25	0.13445E-03	0.12986E-03	0.13919E-03
26	0.12544E-03	0.12116E-03	0.12986E-03
27	0.11702E-03	0.11302E-03	0.12116E-03
28	0.10914E-03	0.10539E-03	0.11302E-03
29	0.10174E-03	0.98212E-04	0.10539E-03
30	0.94774E-04	0.91456E-04	0.98212E-04
31	0.88211E-04	0.85082E-04	0.91456E-04
32	0.82015E-04	0.79058E-04	0.85082E-04
33	0.76153E-04	0.73355E-04	0.79058E-04

Table 6: Default Particle Size Distribution for DELFIC (50 Groups)

Group	Mean Diameter (m)	Lower Boundary (m)	Upper Boundary (m)
34	0.70599E-04	0.67946E-04	0.73355E-04
35	0.65326E-04	0.62807E-04	0.67946E-04
36	0.60313E-04	0.57917E-04	0.62807E-04
37	0.55537E-04	0.53254E-04	0.57917E-04
38	0.50979E-04	0.48800E-04	0.53254E-04
39	0.46620E-04	0.44537E-04	0.48800E-04
40	0.42443E-04	0.40447E-04	0.44537E-04
41	0.38430E-04	0.36513E-04	0.40447E-04
42	0.34564E-04	0.32718E-04	0.36513E-04
43	0.30826E-04	0.29044E-04	0.32718E-04
44	0.27198E-04	0.25469E-04	0.29044E-04
45	0.23655E-04	0.21969E-04	0.25469E-04
46	0.20165E-04	0.18510E-04	0.21969E-04
47	0.16685E-04	0.15039E-04	0.18510E-04
48	0.13129E-04	0.11461E-04	0.15039E-04
49	0.92895E-05	0.75292E-05	0.11461E-04
50	0.51597E-05	0.35360E-05	0.75292E-05

power law relationships and range in size from 1 micron to 2 centimeters for scoured mass and 50 microns to 1 meter for ejecta mass (9:3). Since the hydrocodes use dynamic loading for assigning mass from these two phenomena, it cannot be determined a priori what the particle size distribution of the total cloud mass will be at stabilization. For this reason, and the fact that the particle size distribution of DELFIC is based on fallout studies, the default distribution of DELFIC is used in the current research.

One-Dimensional Particle Rise. An individual parcel (a given particle size at a given altitude) is traced through the bubble rise variable table (See Table 4 on page 26) to determine its rise history. For particle rise simulations, the top and base of each parcel are

followed separately with the upper particle size boundary corresponding to the base of the parcel and the lower particle size boundary used for the parcel top. The upward velocity of the top or base is determined by its location relative to the bubble's top and base locations for the particular time in its history.

For a given time, the upward velocity for a parcel wafer (top or base) is found from the top and base rise rates. If the wafer is within the main cloud, the velocity is found by linearly interpolating with altitude between the top and base velocity values. A wafer exactly at the cloud center altitude will have an upward velocity equal to the average of the top and base velocities. If the wafer is below the cloud base, the velocity is calculated by linearly interpolating between the base rise rate and a zero rise rate for the surface altitude.

Gravity Settling. The only way a wafer that starts within the main cloud can get below the cloud base is to have a downward component to its velocity vector. This component comes from gravity settling. Larger particles will have a higher terminal velocity due to gravity. This implies that the base wafers represented by the upper boundary size will fall faster than the top wafers which use the lower boundary particle size. This, combined with the fact that the cloud does not collapse but rather expands, means that individual parcels are stretched vertically.

If a wafer never leaves the main cloud, its final radius will be that of the main cloud at vertical stabilization. If wafers fall below the base of the main cloud, their radius is set to the radius of the cloud at the time it departs the base of the main cloud. Once a parcel has reached the end of the bubble rise history, it stops its vertical rise. If a parcel base and top have different radii, the parcel may be subdivided in the vertical dimension. Each subdivided parcel is given a radius depending on its location in the tapered parent parcel. This

method of subdividing parcels which have at least partially fallen out of the main cloud is how a fallout stem is defined in the DELFIC stabilized cloud.

Shot Time Wind Shifting. The final subroutine in the CRM adjusts the stabilized parcels in the horizontal direction due to the ambient winds. This is a way of modeling the asymmetry of stabilized clouds above ground zero that were observed in the atmospheric nuclear tests. Each parcel's center is adjusted according to the wind velocity and the amount of time it spends in each wind altitude layer.

Original CRTIM Included a 2-D Option. As a note, it should be pointed out that the 1967 version of the Cloud Rise/Transport Interface Module (CRTIM) had the option of accepting input for a two-dimensional description of the particle cloud (22:3-1,3-2). This capability was in anticipation of someday linking its transport module to a hydrocode solution of the rising cloud. Unfortunately this capability was removed from the 1-D particle rise and wind shifting subroutines which describe the stabilized particle cloud.

Modeling with Hydrocodes. A second method of computing the particle's rise dynamics is with hydrocodes. Hydrocodes follow the variables in a multicell framework. This allows the variables to change in multiple dimensions. As the result of solving a set of partial differential equations, a two-dimensional representation of all the variable solutions are determined. Therefore the velocity of the flow is known with both vertical and radial components.

With hydrocodes, the stabilized dust cloud is determined by the use of trace particles. Each trace particle represents a certain amount of mass in the cloud. Trace particles are added when modeling the addition of mass from ejecta or sweepup. The sizes and weights of these trace particles are determined by the particle size distributions used in these codes

and the amount of soil being injected into the cloud. Once in the multicell framework, the particles are moved by the forces determined by the local state of the cloud.

Modeling with Vortex Theory. An alternative to solving all of the variables in two dimensions is to use the theory of bubbles rising in a still fluid. The conservation equations as described in the previous chapter can be solved and the bubble's rise history stored. By knowing just the rise velocity and dimensions of the bubble, the two-dimensional flow in and around the main cloud can be analytically determined. The vortex flow field models the circulation within the rising cloud. Some assumptions concerning the fluid flow are needed. The current 1-D CRM approach contains no circulation!

VORDUM. One such code which used this approach is the Vortex Dust Model (VORDUM). VORDUM uses empirical fits to the velocity and dimensions of the bubble as a function of time instead of solving a set of conservation equations (7;64;65). Its fits, therefore, do not take into account any variation due to atmospheric conditions in computing the bubble rise solution. The empiricisms are based solely on yield and height of burst.

Radioactive Dust. DELFIC's CRM is concerned solely with the radiation hazard of the fission fragments as they appear in the engulfed soil and weapon debris mixture. VORDUM is a systems-level code for producing the *total* dust environment (radioactive and nonradioactive) of a nuclear explosion for fratricide and radar communication studies. It makes no attempt to determine what dust is radioactive, nor does it concern itself with dust particles once they are grounded. This is in contrast to DELFIC which ultimately calculates the location and intensity of only the grounded radioactivity.

Circulation. A limitation to the vortex flow theory, is that the flow is directly related to the rise velocity. This means that when the bubble stops rising vertically, the

model will revert back to a one-dimensional gravity settling model (equivalent to the current CRM). If only from flow inertia, one would expect some residual circulation after the rise has stopped. To model the residual circulation after the rise has stopped, a full 2-D hydrodynamics solution could be used, but not without the added expense of running such a code.

Theory Used in Vortex Particle Rise Module

The motivation for using an analytic flow field solution is that it matches the observed patterns of rising nuclear clouds. The toroidal shape of the flow pattern (See Figure 1 on page 3) is reproduced with such a solution, unlike the current DELFIC modeling. The cloud properties needed for the solution are available from the bubble rise solution. Finally, the velocity distribution predicted by this type of solution has been shown to match laboratory experiments (30; 60).

To understand vortex flow fields, some theory from classical fluid dynamics needs to be reviewed. The topics covered in this section begin with a discussion of vortices in general and Hill's spherical vortex in particular. From this, the definition of a streamline is presented with application to the rising bubble. Velocity vectors can then be derived from the knowledge of the streamlines, and used for particle motion. The application of an image vortex is presented which will help account for the boundary with the ground. Some of the more recent theory covering spheroidal vortices is then discussed.

Vortices. When a buoyant bubble rises in a denser atmosphere a vortex circulation is induced. Analytic solutions to this circulation are found within classical fluid dynamics texts (3:526; 19; 29:245; 37:578-579; 57). There are three main categories for these solu-

tions: ring vortices, spherical vortices, and spheroidal vortices. Ring vortices differ from the other two types in that the vorticity is concentrated in a smaller core region of the flow (56:7).

When modeling nuclear clouds with analytic solutions, certain assumptions are required. The assumptions which allow one to use an analytic solution to the flow field are as follows. It is assumed that the flow in and around the rising bubble is steady. Also, it is assumed that the fluid is inviscid and incompressible. The irrotational flow outside the bubble is assumed to be the potential flow in a still fluid about a moving sphere. The normal component of the velocity must vanish at the sphere boundary while the tangential velocity must remain continuous (56:12).

Hill's Spherical Vortex . Hill's spherical vortex is described by Batchelor as "one extreme member of a family of vortex rings" (3:526). The extremity is that its vorticity occupies the entire sphere, rather than only a limited region.

The solution for Hill's spherical vortex is obtained by solving for the flow past a stationary sphere. The solution for a sphere moving in a still fluid is then obtained by superimposing on the entire system an equal but opposite potential flow. Hill showed that a solution to the equations below predicts the flow in and about a fluid moving past a stationary sphere (56:13).

$$\frac{1}{r^2(\sin\theta)^2}\left[\frac{\partial}{\partial r}\left(\frac{1}{\sin\theta}\frac{\partial\psi}{\partial r}\right)+\frac{\partial}{\partial\theta}\left(\frac{1}{r^2\sin\theta}\frac{\partial\psi}{\partial\theta}\right)\right]=0 \qquad \text{for } r\le a \tag{24}$$

$$\frac{1}{r^2(\sin\theta)^2}\left[\frac{\partial}{\partial r}\left(\frac{1}{\sin\theta}\frac{\partial\psi}{\partial r}\right)+\frac{\partial}{\partial\theta}\left(\frac{1}{r^2\sin\theta}\frac{\partial\psi}{\partial\theta}\right)\right] = A(\psi) \quad \text{for } r > a \tag{25}$$

where

r = radius coordinate for spherical coordinate system (m)

θ = angle from axis of motion in spherical coordinate system

ψ = streamfunction of the flow to be solved for

a = radius of the sphere (m)

$A(\psi)$= arbitrary function of ψ

Streamlines and Streamfunctions. A streamline is a curve everywhere parallel to the direction of flow. Streamlines represent lines of constant streamfunction, ψ (53:23-24). The above equations are solved by requiring the streamfunction to vanish, and the tangential velocity to be continuous, at the sphere surface, i.e.,

$$\psi = 0 \quad \text{at} \quad r = a \tag{26}$$

$$\frac{1}{r\sin\theta}\frac{\partial\psi}{\partial r} \quad \text{is continuous at} \quad r = a \tag{27}$$

The final boundary condition is that the flow approaches the potential flow about a solid sphere as it approaches the free field stream (56:13).

$$\psi \rightarrow -\frac{1}{2}Ur^2(\sin\theta)^2 \quad \text{as } r \rightarrow \infty \tag{28}$$

where

U = velocity of the moving body of fluid (m/s)

The above equations and boundary conditions are solved to obtain the solution for a fluid flowing past a stationary sphere. The free field stream function ($\frac{1}{2}Ur^2(\sin\theta)^2$) is superimposed on the previous answer to get the solution for a moving sphere in a still fluid. The streamfunctions for the flow inside and outside Hill's spherical vortex moving in a still fluid are then (56:175)

$$\psi = Ur^2(\sin\theta)^2\left(\frac{5}{4} - \frac{3}{4}\frac{r^2}{a^2}\right) \qquad \text{inside sphere} \tag{29}$$

$$\psi = \frac{1}{2}Ua^3\frac{(\sin\theta)^2}{r} \qquad \text{outside sphere} \tag{30}$$

The streamlines for this solution are shown in Figure 7 on page 52.

Velocity Vectors. The velocity components for both inside and outside the spherical vortex can be found by differentiating the appropriate streamfunction. The radial and tangential velocities are defined by (56:35-36)

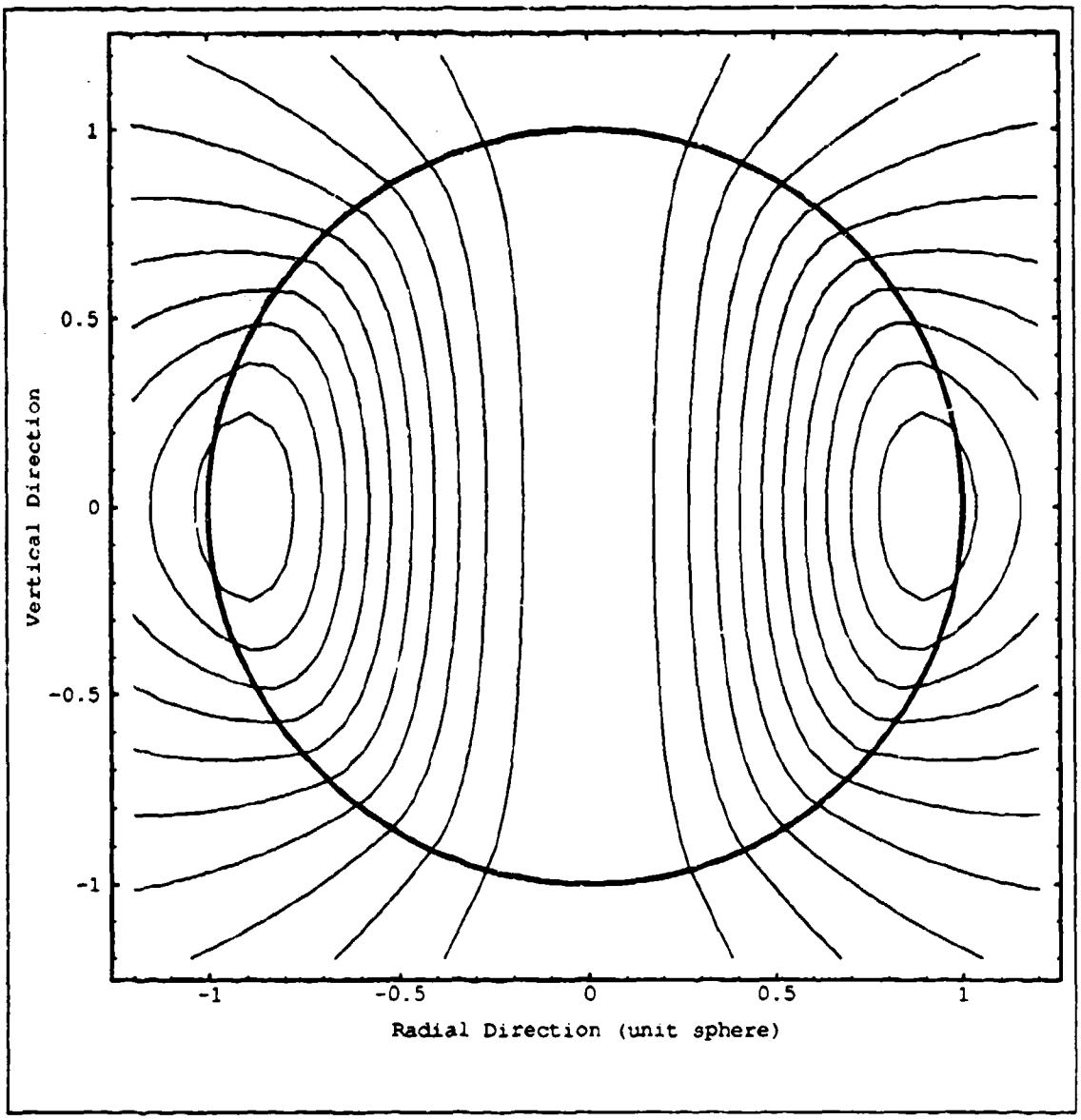

Figure 7: Streamlines for Hill's Spherical Vortex (cross sectional view of unit sphere)

$$U_r = \frac{1}{r^2 \sin\theta} \frac{d\psi}{d\theta} \tag{31}$$

$$U_\theta = -\frac{1}{r \sin\theta} \frac{d\psi}{dr} \tag{32}$$

This yields a radial velocity of

$$U_r = U\cos\theta\left(1 - \frac{a^3}{r^3}\right) \qquad \text{outside sphere} \tag{33}$$

$$U_r = -\frac{3}{2}U\cos\theta\left(1 - \frac{r^2}{a^2}\right) \qquad \text{inside sphere} \tag{34}$$

and a tangential velocity of

$$U_\theta = -U\sin\theta\left(1 + \frac{1}{2}\frac{a^3}{r^3}\right) \qquad \text{outside sphere} \tag{35}$$

$$U_\theta = \frac{3}{2}U\sin\theta\left(1 - \frac{2r^2}{a^2}\right) \qquad \text{inside sphere} \tag{36}$$

These equations are then transformed into cylindrical coordinates for implementation in the code to give the vertical and radial components of the particle's velocity. A vector field of the velocity shows the *magnitude* of the flow in different locations, whereas the stream-line figure gave only a qualitative view of the direction of flow (See Figure 8 on page 54).

From this figure, one can see the difference compared to the 1-D model of the current CRM. Not only is there the addition of a radial component, but there is variation of the vertical component based on location in the sphere. The vertical component varies from 2.5U at the center to -0.5U at the edge of the sphere, along the vortex midplane.

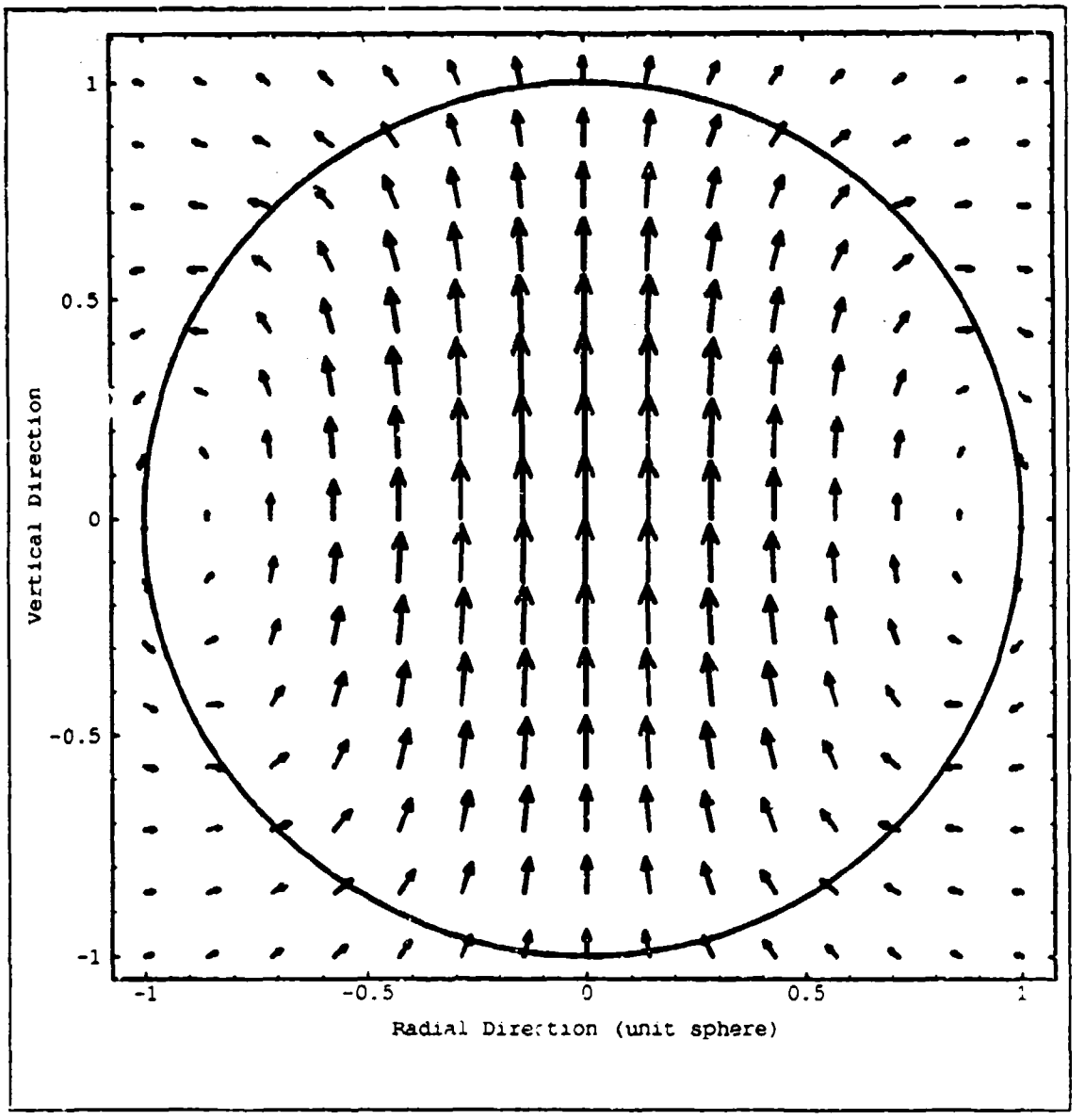

Figure 8: Vector Field for Hill's Spherical Vortex (unit sphere with unit velocity)

Image Vortex. A mirror image of the spherical vortex is created at an equal distance on the other side of the ground plane. This new vortex has the same dimensions and speed as the real vortex but moves in the opposite direction. This has the effect of canceling out the vertical components and doubling the radial component at the ground surface. This not

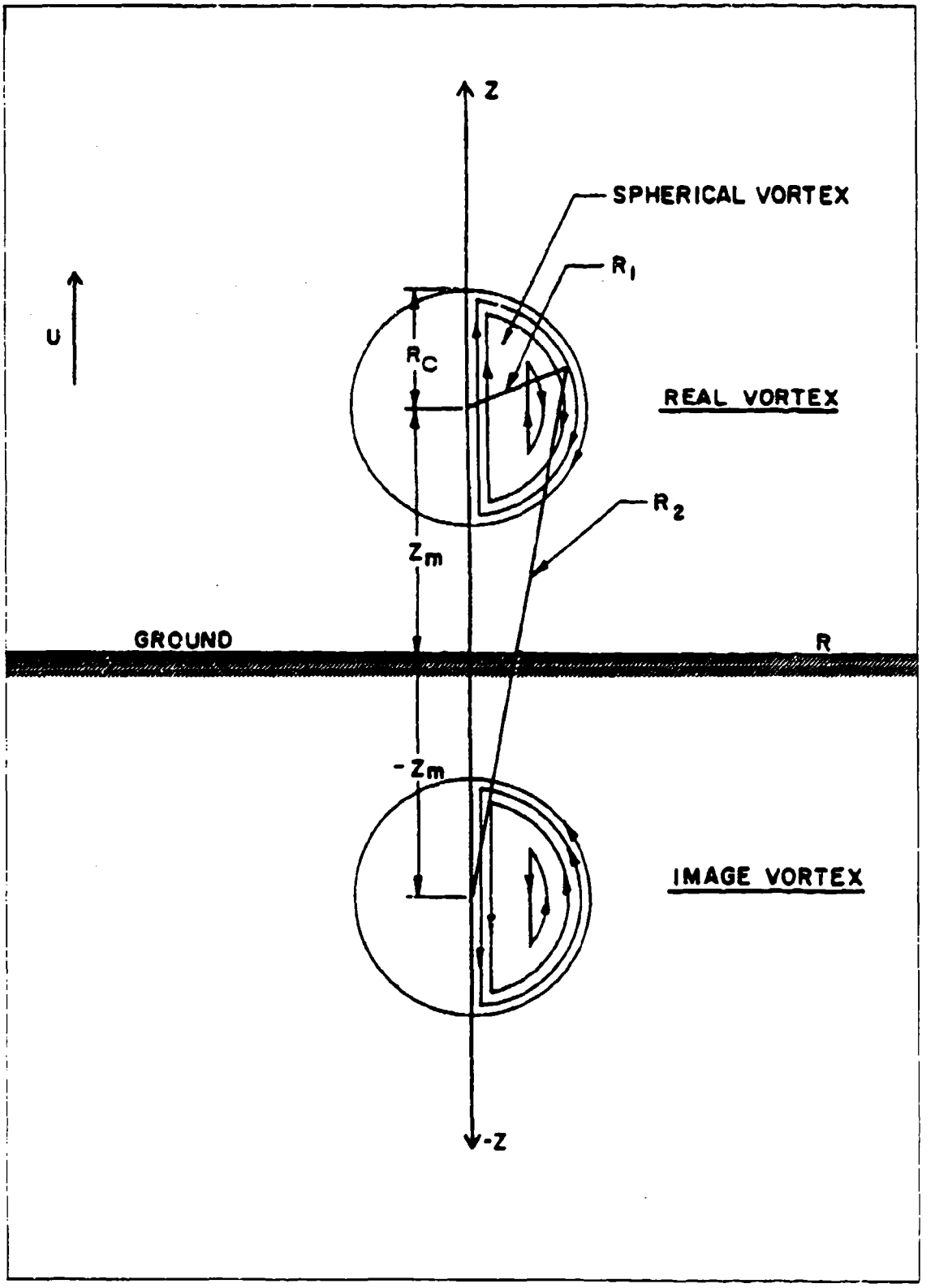

Figure 9: Direction and Location of Image Vortex Sphere (35:42)

only satisfies the condition that flow cannot enter the ground plane, but also helps simulate the intense surface winds which are known to occur for near surface nuclear bursts (56:60).

After the image vortex is included, there are now three possible locations for a particle: inside both the real and imaginary vortices, inside the real vortex and outside the imaginary vortex, and outside both the real and imaginary vortices. After conversion to cylindrical coordinates and inclusion of the image's effect, the vertical and radial components of velocity are found to be the following.

Inside both the real and imaginary vortices:

$$U_Z = U\left[\frac{1}{2}\left(5 - \frac{6R^2 + 3Z_1^2}{a^2}\right) - \frac{1}{2}\left(5 - \frac{6R^2 + 3Z_2^2}{a^2}\right)\right] \tag{37}$$

$$U_R = U\left(\frac{3}{2}\frac{RZ_1}{a^2} - \frac{3}{2}\frac{RZ_2}{a^2}\right) \tag{38}$$

where

U_Z = the vertical velocity (m/s)

U_R = the radial velocity (m/s)

R = the radial distance from the axis of symmetry (m)

Z_1 = the vertical distance from the midplane of the real vortex (m)

Z_2 = the vertical distance from the midplane of the imaginary vortex (m)

Inside the real vortex and outside the imaginary vortex:

$$U_Z = U\left[\frac{1}{2}\left(5 - \frac{6R^2 + 3Z_1^2}{a^2}\right) - a^3\frac{Z_2^2 - \frac{1}{2}R^2}{(R^2 + Z_2^2)^{5/2}}\right] \tag{39}$$

$$U_R = U\left[\frac{3}{2}\frac{RZ_1}{a^2} - \frac{\frac{3}{2}RZ_2a^3}{(R^2 + Z_2^2)^{5/2}}\right] \tag{40}$$

Outside both the real and imaginary vortices:

$$U_Z = U\left[a^3\frac{Z_1^2 - \frac{1}{2}R^2}{(R^2 + Z_1^2)^{5/2}} - a^3\frac{Z_2^2 - \frac{1}{2}R^2}{(R^2 + Z_2^2)^{5/2}}\right] \tag{41}$$

$$U_R = U\left[\frac{\frac{3}{2}RZ_1\ a^3}{(R^2 + Z_1^2)^{5/2}} - \frac{\frac{3}{2}RZ_2a^3}{(R^2 + Z_2^2)^{5/2}}\right] \tag{42}$$

The effect of the image vortex on the velocity field for a sphere intersecting the ground is shown in Figure 10 on page 58. Note the vectors at ground level have no vertical component.

Spheroidal Vortices. A solution similar to Hill's spherical vortex was found for spheroids by O'Brien (49). This solution was investigated by this and other authors, but not

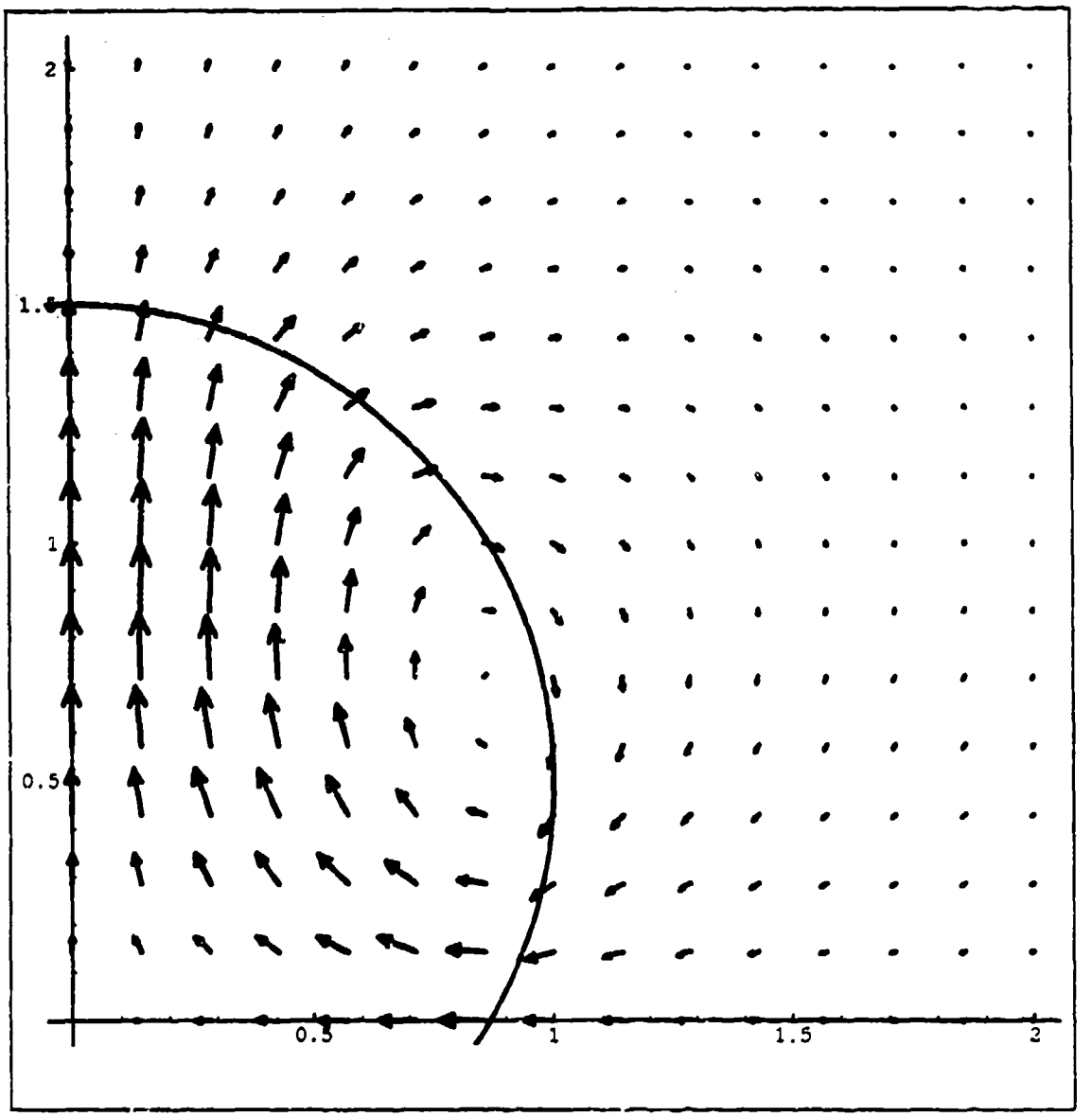

Figure 10: Velocity Field for Sphere Intersecting the Ground (Image Vortex Included)

implemented in the current research. It was implemented in the VORDUM dust code by Shannon and he reports that "results from the spheroidal vortex VORDUM model do not differ greatly from the spherical vortex VORDUM model results...and applications of the

spheroidal vortex flow field to define dust environments for use in system studies may not be warranted" (56:174).

Perturbation Theory. A final note concerning the results of this author's literature search is in order. Pozrikidis mathematically showed that an initially spherical vortex which becomes transformed (due to axisymmetric perturbations) to an oblate shape, entrains the outside irrotational fluid. This fluid enters the rotational fluid from the rear stagnation point and travels along the vortex boundary. He states that this action reduces the oblate vortex to a nearly steady vortex ring (51).

His mathematical description is qualitatively similar to the shape history of real nuclear clouds. Such clouds start as near perfect spherical fireballs and are deformed during their intense motion upwards into oblate spheroids. Some researchers have even modeled nuclear clouds as vortex rings (11).

Vortex Implementation in DELFIC's Current CRM

On the basis of the previous theory, this section describes how the author has implemented vortex flow into the CRM of DELFIC to produce a two-dimensional description of the stabilized cloud. The major subsections discuss the modeling choices made by the author to complement the theory of the previous section. The first subsection shows how the bubble rise history is used in the description of the vortex region. The second subsection reviews the modeling of the initial soil distribution for the radioactive dust. This is followed by a brief review of particle settling and the force balance needed to determine the particle acceleration equations. The last major phenomenon modeled is the correction

for the expansion of the bubble. The final subsection describes the solution method used to calculate the particle histories.

Input from Bubble Rise History. As in the current CRM, particle rise is dependent on the results of the bubble rise equations. The history of the cloud's velocity and dimensions are needed to describe fully the flow field using the theory described above. In addition, the temperature of the cloud and its density are needed to determine the viscosity and the drag force on the particles. A major question that still remains is how one relates the visible oblate bubble to the domain of the vortex sphere.

Visible Cloud Spheroid vs. Vortex Sphere. In matching the oblate spheroid to a domain more conducive to flow field simulation, some modeling choices had to be made. In the present research the top of the bubble was matched to the top of the vortex sphere region. The radius of the sphere was then matched to the radius of the bubble. This produced a vortex region which encompassed most of the visible cloud and included a region below the cloud (See Figure 11 on page 61).

The region below the cloud but still within the vortex sphere helps simulate the updraft in the stem. Also, since the stagnation point for the center of circulation of a rising sphere is above the midplane of the expanding sphere, the particles will concentrate within the visible oblate sphere which is also centered above the midplane (60:201).

Initial Particle Locations. The initial location of the soil in the cloud must now be determined and a set of trace particles described. Each of these trace particles must be assigned a fraction of the soil mass based on their location and an assumption of the soil loading in the cloud before the cloud begins its rise. The effects of sweepup and time dependent loading will also be discussed.

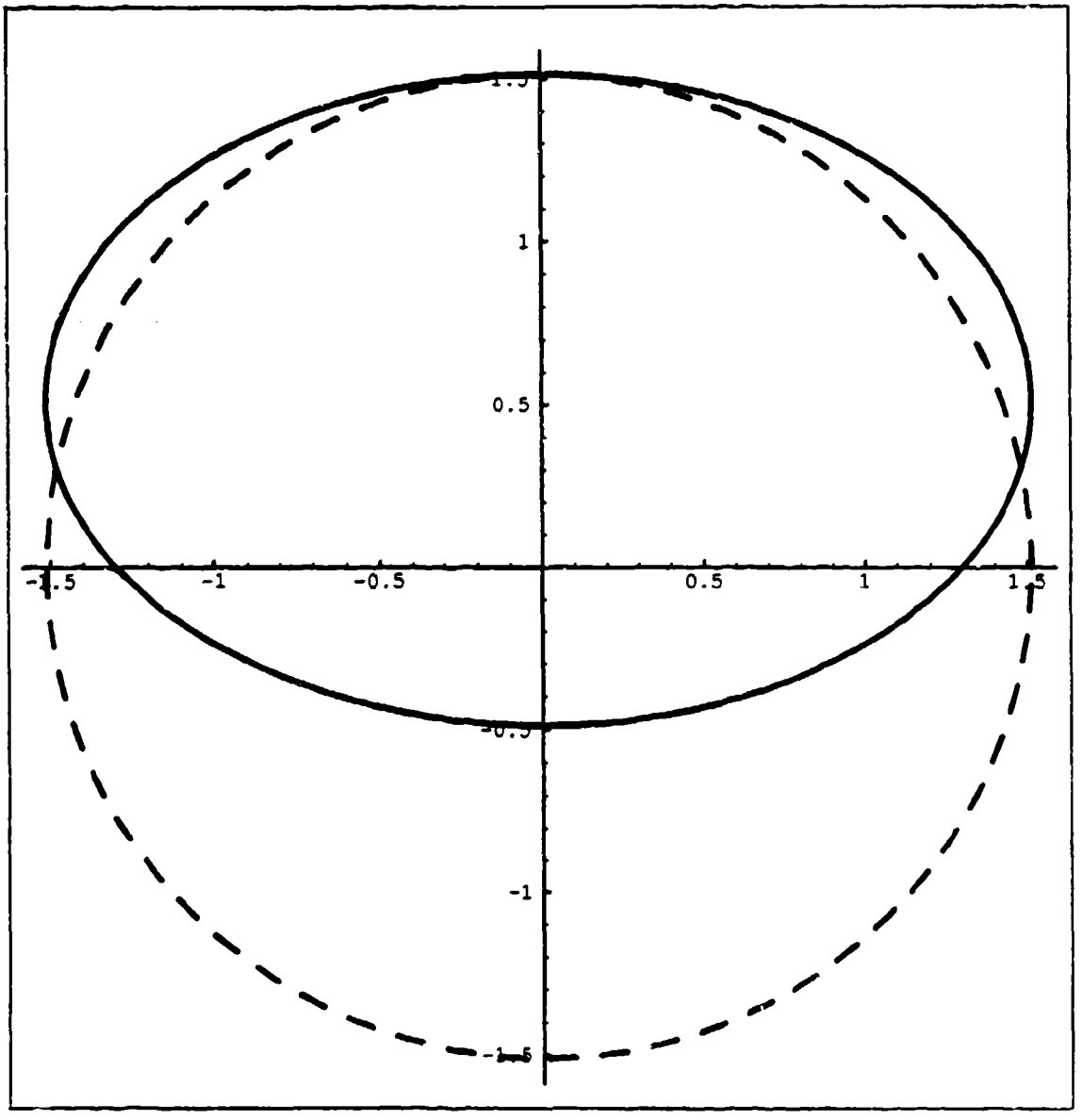

Figure 11: Visible Oblate Bubble (solid) in Relation to Vortex Sphere (dashed)

Main Source Cylinder. The initial location of the soil particles is assumed to be a cylinder with the initial cloud top and radius (See Figure 12 on page 62). This is similar to the current assumption in DELFIC's CRM with one difference. The difference in the new model is that the cylinder is assumed to be touching the ground instead of hovering in

space. This accounts for the pedestal of very early time dust clouds and is similar to the way VORDUM originally modeled its ejecta source (7:204).

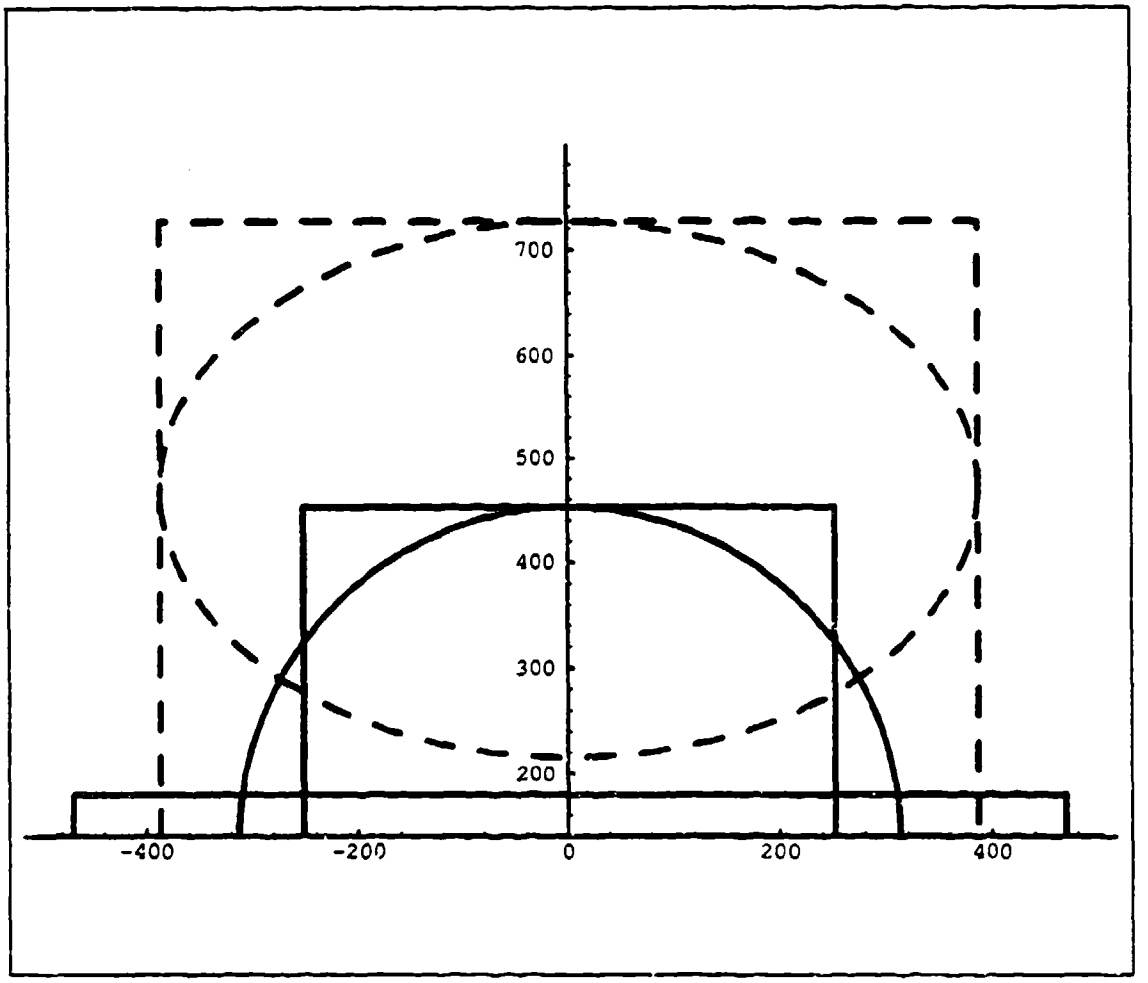

Figure 12: Vortex Particle Source Cylinder and Initial Bubble (both dashed) and VORDUM's 2-Cylinder Sources in Relation to Initial Fireball (distances in meters)

Sweepup Source Cylinder. The original VORDUM also included a second source cylinder, a shorter but wider sweepup cylinder. This second cylinder modeled the dust which is not directly engulfed by the fireball but is eventually swept into the fireball or its

stem due to the flow-induced surface winds. Although VORDUM's dust loading was immediate, as is DELFIC's, the initial time of particle tracking was later than in DELFIC (nominally 30 seconds). The question remains which of this dust is part of the *radioactive* dust that eventually contributes to the fallout dose on the ground.

McGahan showed that the debris in the ejecta (VORDUM's first cylinder) has a vastly different final location in the stabilized cloud when compared to the stabilized sweepup dust. One may conjecture that the nonradioactive sweepup dust may attach itself to the radioactive ejecta debris if they are in the same location of the cloud. This area of overlap between the two sources appears to be small from initial investigations (36:77). One source cylinder is used in this research.

The main source cylinder dimensions chosen in this model virtually engulf the VORDUM two cylinder source. The vortex sphere domain in DELFIC also starts earlier in the rise, and therefore at a lower altitude. The effect is that the majority of the particles start above the vortex midplane and with a greater initial radial distribution. It was found that the particles which start lower in the domain, or closer to the axis, take a longer time to enter the toroidal core, if at all. The particles which start higher in the domain, or away from the axis, enter the toroidal core faster.

Time Dependent Loading. As in the original CRM, the new model for particle rise does not include a time dependent loading of the cloud. Instead, the entire soil mass is assumed to be in the cloud at the initial time. The soil that does enter at later times (not modeled here) may not make it into the vortex sphere and if so may not end up being collocated with the radioactive debris from the weapon.

Also all particles are assumed to be solid from the start with essentially their final radius, and are tracked accordingly. This is a minor approximation since all clouds simulated in this study cooled to below soil solidification after the first few seconds of their rise simulations ($<t_i + 5$ sec).

Number of Trace Particles. In determining the number of trace particles, one must choose a number small enough for reasonable run times but large enough for reasonable approximation of the radioactive dust densities. In the current CRM, the cloud is divided into a one-dimensional stack of cylindrical parcel To make the new option for particle rise easy to implement, this same number of vertical grid points was chosen. In addition, the new routine has *KDI* horizontal grid points for starting trace particles. This gives KDI^2 number of trace particles for each size class run. For a typical run with 50 size classes, this gives approximately 20,000 (=20x20x50) trace particles to describe the soil loading of the cloud at any time. This number met both of the aforementioned criteria and had the ease of user input already set up in the current CRM.

Particle Weighting. Once the number of trace particles is chosen, their starting locations within a 2-D vertical cross section of the initial source cylinder are determined. Each particle size group contains an identical uniform grid of trace particles from the axis to the outer cylinder radius. A fraction of the cylinder's volume is determined by the 3-D annulus the trace particle represents. The particle's weight is then determined by the number of particle sizes and the fraction of the cylinder's volume its starting annulus represents. This amount of mass weighting stays with the particle and is output with the history of the particle's rise for loading information.

Particle Settling. The particle acceleration equations can be found by equating the force on the particle to the sum of the forces of gravity and drag (35:48).

$$F_p = F_g + F_D \tag{43}$$

$$\frac{4}{3}\pi r_p^3 \rho_m \dot{V}_Z = -\frac{4}{3}\pi r_p^3 \rho_m g - \frac{\pi r_p^3 \rho_a C_D}{d}(V_Z - U_Z)\left[(U_Z - V_Z)^2 + (U_R - V_R)^2\right]^{\frac{1}{2}} \tag{44}$$

where

F_p = force on the particle (kg m/s^2)

F_g = gravity force (kg m/s^2)

F_D = drag force (kg m/s^2)

V_Z = particle vertical velocity (m/s)

V_R = particle radial velocity (m/s)

r_p = particle radius (m)

d = particle diameter (m)

ρ_m = particle (mass) density (kg/m^3)

ρ_a = air (or cloud) density (kg/m^3)

C_D = coefficient of drag

which becomes

$$\dot{V}_Z = -g - \frac{3}{4}\frac{\rho_a}{\rho_m}\frac{C_D}{d}(V_Z - U_Z)\left[(U_Z - V_Z)^2 + (U_R - V_R)^2\right]^{\frac{1}{2}} \quad (45)$$

$$\dot{V}_R = -\frac{3}{4}\frac{\rho_a}{\rho_m}\frac{C_D}{d}(V_R - U_R)\left[(U_Z - V_Z)^2 + (U_R - V_R)^2\right]^{\frac{1}{2}} \quad (46)$$

An alternative to calculating the above accelerations is to assume that the particle is in equilibrium with the flow field. The particles are then given the flow velocity plus a correction for gravity. This correction is called the slip correction. The slip correction assumes the particle immediately achieves its terminal velocity of fall. The method of calculating this terminal velocity is the same as in the current CRM (47:24-25). The particle's location is determined to be in the cloud or out of the cloud, and its corresponding environment temperature and density are found. With this information and the particle's diameter, its viscosity and drag coefficient can be calculated.

Lagrangian Transport vs. Slip Correction. The hydrocode TASS uses a Lagrangian transport routine to follow particles greater than 1000 microns (1 mm). This is in contrast to assigning the particle the flow velocity minus the terminal velocity in the vertical direction. This assumes that particles less than a millimeter are in equilibrium with the flow, while those above may not be. This criteria was maintained in the current research.

The cutoff value used in TASS (1 mm) was investigated in the vortex flow field code developed. It was discovered that not only do one millimeter particles behave as if they

are in equilibrium with the flow, but so do particles as large as 2.5 mm. Particles larger than this may not be in equilibrium with the flow. but their fraction of the particle size distribution for DELFIC is negligible (<2%). Therefore using the assumption of being in equilibrium with the flow and substituting a slip velocity for Lagrangian transport will not significantly affect the result of DELFIC's particle rise. The savings in computer time when using a slip correction is substantial, and therefore the switch for Lagrangian transport in the new particle rise model of DELFIC may be removed if desired.

TASS vs. DELFIC. The DELFIC settling subroutine is based on the work of Davies and Beard (47:25). The particle settling equations used in TASS are based on a modified Stokes drag term (2:19). In TASS, the drag coefficient for a perfect sphere is multiplied by 1.5 for a rough sphere approximation. With this method of calculating the drag, TASS will predict a slightly larger terminal velocity (lower drag force) than DELFIC for the larger particles (0.5 mm) if the same particle density is used. TASS, however, assumes a lighter density for the dust particles (2.0 vs. 2.6 kg/m^3) which compensates for the difference in the drag parameter. The stabilized heights for the same particle using the two codes differ by less than 100 meters, therefore, DELFIC's settling subroutine is still used.

Radial Expansion. The last major modeling effort included in the new particle rise subroutines is a correction for the radial expansion of the cloud. All of the velocity equations presented in this chapter thus far are for a vortex sphere of constant size rising in the air. Since DELFIC's bubble is actually expanding continuously during its rise, a correction is needed for the particle's velocity equations.

The expansion correction in this research is taken to be proportional to the location of the particle and the current bubble expansion rates. From the bubble rise history, the base rate, top rate, and radial rate are determined for the time of interest. These values are used to determine the vertical and radial expansion rates for the particles within the visible oblate cloud. A particle's radial velocity will increase by the fraction of its radial distance to the radius of the cloud, multiplied by the radial expansion rate. Likewise, particles in the cloud will expand vertically commensurate with their distance from the cloud center to the top or base.

Integration of the Particle Equations. Once all the velocity components are resolved from the underlying forces and corrections, the particle's trajectory is calculated by integration. The method of integration chosen is a fifth-order Runge-Kutta with an adaptive stepsize to ensure accuracy and optimum run times (52:701-715). The numerical method chosen was well documented and its performance checked with analytically solvable equations. A main calling routine for the vortex particle rise module was created (VPRM) as well as a subroutine to calculate the derivatives of the particle's trajectory for integration (DERIVS).

Comparison Cases and Types of Comparisons

The vortex particle rise model as described above was then used to simulate a number of different cases. The cases used include the Single Burst Nuclear Cloud Database (SBNCD) and the 1979 DELFIC test case. These cases were used to investigate the effect of using vortex flow in modeling stabilized nuclear [illegible] (See Table 7 on page 69). A number of different ways of displaying the [illegible]

Table 7: Vortex Particle Rise Comparison Cases

Case	Yield (kt)	Scaled Height of Burst ($ft/kt^{1/3}$)
91A01	300	0
91A02	300	50
91A03	300	120
91B01	100	0
91B02	100	50
91B03	100	120
91F01	800	0
91F02	800	50
91H01	20	0
1979 Test Case	50	0

Particle Plots. One form of output is plots of trace particles as a function of time for different size classes. Although these were not used for comparison with hydrocode data or the current CRM, they do help show the effect vortex rise has on the trajectories of trace particles. The effects of radial expansion, particle settling, and the toroidal flow are easily seen by these plots.

Density Contours. The primary means of comparing the vortex particle rise results with the hydrocode data are with density contour plots. These plots have all been run for the SBNCD cases and were available on the DNA CRAY at Los Alamos. The plots are presented in the next chapter and give both a radial and vertical description of the mass loading of the cloud at various times from one minute to stabilization. Plots for other times and other variables are also on the CRAY (9).

Grid Size and Contour Levels. All the density contours shown in the next chapter were generated by using 500 meter grid cells in both radial and vertical dimensions and

summing the mass of the tracer particles which lie within the cell. From this data, contour lines were calculated which show the mass density in 10^{-x} g/cc where x is an integer from 10 down to the highest density present. It is currently thought that the visible cloud has a density of around 10^{-8} g/cc (6). The plots shown in the next chapter (TASS and DELFIC) are for soil loading only. TASS plots for water content are also available but are not considered in this research.

Mass vs. Altitude Loading. The primary purpose in comparing vortex particle rise to the CRM's current particle rise was to see if the particles stabilize at different altitudes. In particular, would the larger particles attain higher altitudes similar to preliminary comparisons with TASS. For this reason, mass versus altitude was chosen as the means for comparing the current CRM to the vortex particle rise results Another reason mass versus altitude was chosen was that the CRM, as it's currently setup, has no radial distribution.

Fallout Contours and Radial Distribution. The final comparison made was a preliminary review of the implications vortex particle rise has on one set of fallout contours. Since the primary purpose for upgrading DELFIC is to improve the DoD's fallout prediction capability, the fallout contour is of utmost concern. To fully see how a radial distribution affects fallout contours requires an investigation of the DTM and OPM of DELFIC. Since this was not within the scope of the current research, conclusions drawn can only be preliminary in nature.

Link to DELFIC's DTM. To produce fallout contours using DELFIC's DTM and OPM required giving up the radial definition of the stabilized particle cloud. The distribution of stabilized particles was loaded into DELFIC's current disk-like structure and writ-

ten to tape. The sizes of the disks (both vertical and radial) were chosen to be similar to disks created by the CRM, with the only difference being the amount of mass in each disk. The DTM/OPM's method of assigning mass (activity) in the radial dimension was used for the generation of fallout maps. The OPM uses a bivariate gaussian distribution which is distorted elliptically (downwind and crosswind) based on diffusion during the transport. The difference in vertical loading, therefore, is the only difference investigated in the fall-out contour comparison study.

IV. Results and Comparisons

This chapter presents the results and comparisons of the two main areas of research conducted by the author. The chapter is organized into two sections, bubble rise and particle rise. The first section gives the results of comparing the bubble rise subroutines to observation. The second main section gives a comparison of vortex theory particle rise to the current CRM particle rise and to hydrocode results.

Bubble Rise

This section presents the results obtained from the different versions of the CRM described in "Work Done on DELFIC's Bubble Rise Subroutines" on page 31. The following subsections show the performance of the 1979, corrected, and improved versions of the CRM. The 1979 version is the documented code as provided to the author. The corrected version is the code with the programming errors removed. The improved version is the code with the single term entrainment equation and constant parameters. The three different versions are compared to actual observations from the US atmospheric nuclear test events. This is followed by a discussion of observation error and a discussion of the figure of merit chosen. Finally, a couple of examples of the time-dependent performance of the improved CRM are given.

The performance of stabilized bubble prediction lies in matching observed nuclear cloud values, in particular stabilized cloud tops. Norment points out that the cloud top, by its very nature, is crucial to the art of predicting fallout, the ultimate goal of DELFIC The cloud top value determines what wind layer values are to be used in transporting the radioactivity. It is also noted that cloud top recordings are by far the most reliable data from the

atmospheric nuclear tests. Cloud bases and radii, on the other hand, are ill-defined due to the presence of a stem and the wind shearing of the clouds. Norment emphasizes the fact that the least important property is the observed cloud base, since stabilized particle positions in the cloud may not correspond with this visible base value (46:21). Of course temporal performance of the rising cloud needs to be considered and is also reported here.

The decision was made to repeat the validation of the 1979 and newer versions of the CRM in the same manner as Norment's 1977 validation effort. Therefore, the figures of merit used were the fractional root mean square error (FRMS), and the fractional mean deviation (FMD). Both were described in the section titled "Fractional Root Mean Square (FRMS) Error Definition" on page 38. It should be noted at this point that the FMD for the entire set of validation shots may be deceiving since overpredictions can balance out underpredictions. The deviation for an individual shot is of value since it tells if the model overpredicts or underpredicts the height, depending on its sign (negative and positive respectively).

The FRMS is chosen as the primary figure of merit since it sums absolute error in either direction. The combination of the FRMS applied to the cloud *top* values was chosen to adjust the constants in the improved model (to be discussed later). The results of predicting cloud bases are shown since observation values were available for most of the shots (49 of 54). Radii observations were not widely available, and so are not presented at all. Table 8 on page 74 and Table 9 on page 76 present the results of the bubble rise part of the research. The values shown are for the 1979 version of the CRM as well as the corrected and improved versions of the code. They are all relative to the burst height (HOB plus surface altitude).

Table 8: Cloud Top Comparison of Models to Observation (relative to burst point)

Shot	Yield (kt)	Observed Cloud Top (m)	Calculated Cloud Top (m)			Fractional Deviation		
			1979	Corrected	Improved	1979	Corrected	Improved
Humboldt	0.0078	1050	759	827	1038	0.28	0.21	0.01
Catron	0.021	1344	1061	1170	1415	0.21	0.13	-0.05
Vesta	0.024	1760	2282	2294	2247	-0.30	-0.30	-0.28
DonaAna	0.037	1940	2831	2802	2796	-0.46	-0.44	-0.44
Hidalgo	0.077	2267	2172	2258	2515	0.04	0.00	-0.11
Quay	0.079	1722	1548	1543	1768	0.10	0.10	-0.03
Eddy	0.083	1925	2368	2137	2635	-0.23	-0.11	-0.37
RioArriba	0.09	2870	1895	1975	2559	0.34	0.31	0.11
Wrangell	0.115	1653	1627	1640	1861	0.02	0.01	-0.13
Franklin	0.14	3772	4175	4253	4179	-0.11	-0.13	-0.11
Wheeler	0.197	3740	3374	3396	3684	0.10	0.09	0.01
Ray	0.2	2644	2121	2141	2524	0.20	0.19	0.05
Ruth	0.2	2833	2838	2946	3051	0.00	-0.04	-0.08
JohnnieBoy	0.5	3612	2575	2565	2818	0.29	0.29	0.22
Laplace	1	4592	4709	4736	4819	-0.03	-0.03	-0.05
SantaFe	1.3	3753	3550	3569	4254	0.05	0.05	-0.13
Lea	1.4	3449	3931	3925	4536	-0.14	-0.14	-0.32
Mora	2	3906	4339	4374	4521	-0.11	-0.12	-0.16
John	2	6008	4197	4197	4540	0.30	0.30	0.24
DeBaca	2.2	3601	3878	3811	4989	-0.08	-0.06	-0.39
FranklinPrime	4.7	8249	5467	5480	5841	0.34	0.34	0.29
Sanford	4.9	6530	4946	4986	5942	0.24	0.24	0.09
Socorro	6	6207	5776	5792	6287	0.07	0.07	-0.01
Morgan	8	10755	6374	6379	6773	0.41	0.41	0.37
Owens	9.7	9231	8033	7999	7407	0.13	0.13	0.20
Wilson	10	9226	6409	6389	7987	0.31	0.31	0.13
Kepler	10	7069	7612	7611	7648	-0.08	-0.08	-0.08
Fizeau	11	10811	7780	7833	7915	0.28	0.28	0.27

Table 8: Cloud Top Comparison of Models to Observation (relative to burst point)

Shot	Yield (kt)	Observed Cloud Top (m)	Calculated Cloud Top (m)			Fractional Deviation		
			1979	Corrected	Improved	1979	Corrected	Improved
Galileo	11	9830	7554	7573	8029	0.23	0.23	0.18
Doppler	11	9836	7731	7685	7307	0.21	0.22	0.26
Dixie	11	10654	8099	8092	8681	0.24	0.24	0.19
Boltzman	12	8615	10524	10517	9887	-0.22	-0.22	-0.15
Newton	12	8021	7958	8008	8057	0.01	0.00	0.00
Charleston	12	8012	6779	6823	6801	0.15	0.15	0.15
Grable	15	9570	6164	6147	6425	0.36	0.36	0.33
Annie	16	11178	9365	9480	10039	0.16	0.15	0.10
Shasta	17	8264	9347	9215	8717	-0.13	-0.12	-0.05
Diablo	17	8239	8884	8837	9171	-0.08	-0.07	-0.11
Whitney	19	7624	8459	8474	9042	-0.11	-0.11	-0.19
Stokes	19	9545	8494	8497	8732	0.11	0.11	0.09
Badger	23	9513	7554	7568	8897	0.21	0.20	0.06
Nancy	24	11244	8807	8823	9217	0.22	0.22	0.18
Encore	27	11125	8908	8911	9246	0.20	0.20	0.17
Harry	32	11642	11844	11997	12640	-0.02	-0.03	-0.09
Priscilla	37	11955	10782	10774	11150	0.10	0.10	0.07
Lacrosse	40	11582	7410	9164	8983	0.36	0.21	0.22
Simon	43	12028	12140	12183	12181	-0.01	-0.01	-0.01
Smoky	44	10004	11290	11298	11181	-0.13	-0.13	-0.12
Climax	61	11382	12084	12092	12053	-0.06	-0.06	-0.06
Hood	74	12884	12719	12724	13245	0.01	0.01	-0.03
Koon	110	16150	15549	15713	14995	0.04	0.03	0.07
Zuni	3500	24076	25195	27341	27282	-0.05	-0.14	-0.13
Tewa	5000	30171	26613	29399	29520	0.12	0.03	0.02
Bravo	15000	34745	35450	37085	36118	-0.02	-0.07	-0.04
					FMD	0.08	0.06	0.01
					FRMS	0.20	0.19	0.18

Table 9: Cloud Base Comparison of Models to Observation (relative to burst point)

Shot	Yield (kt)	Observed Cloud Base (m)	Calculated Cloud Base (m)			Fractional Deviation		
			1979	Corrected	Improved	1979	Corrected	Improved
Humboldt	0.0078	593	450	471	688	0.24	0.21	-0.16
Catron	0.021	277	646	724	957	-1.33	-1.61	-2.45
Vesta	0.024		1577	1601	1642			
DonaAna	0.037	568	1657	1682	1942	-1.92	-1.96	-2.42
Hidalgo	0.077	1048	1297	1381	1740	-0.24	-0.32	-0.66
Quay	0.079	960	921	923	1219	0.04	0.04	-0.27
Eddy	0.083	858	1477	1419	1634	-0.72	-0.65	-0.90
RioArriba	0.09	2108	1187	1238	1699	0.44	0.41	0.19
Wrangell	0.115	739	984	994	1289	-0.33	-0.35	-0.75
Franklin	0.14	2949	2674	2804	2984	0.09	0.05	-0.01
Wheeler	0.197	2825	2104	2114	2539	0.26	0.25	0.10
Ray	0.2	1089	1326	1343	1676	-0.22	-0.23	-0.54
Ruth	0.2	1949	1551	1705	2147	0.20	0.13	-0.10
JohnnieBoy	0.5	2240	1629	1638	1921	0.27	0.27	0.14
Laplace	1	2763	3054	3077	3417	-0.11	-0.11	-0.24
SantaFe	1.3	2229	2230	2226	2899	0.00	0.00	-0.30
Lea	1.4	1925	2468	2468	3054	-0.28	-0.28	-0.59
Mora	2	1315	2845	2871	3150	-1.16	-1.18	-1.40
John	2		2702	2708	3100			
DeBaca	2.2	1315	2372	2358	3367	-0.80	-0.79	-1.56
FranklinPrime	4.7	4896	3601	3605	3979	0.26	0.26	0.19
Sanford	4.9	2415	3112	3129	3827	-0.29	-0.30	-0.58
Socorro	6	4378	3825	3839	4292	0.13	0.12	0.02
Morgan	8	6488	4183	4187	4594	0.36	0.35	0.29
Owens	9.7	4659	5464	5442	5107	-0.17	-0.17	-0.10
Wilson	10	6178	4209	4193	5169	0.32	0.32	0.16
Kepler	10	4600	5100	5077	5172	-0.10	-0.10	-0.12
Fizeau	11	6849	5241	5268	5451	0.23	0.23	0.20

Table 9: Cloud Base Comparison of Models to Observation (relative to burst point)

Shot	Yield (kt)	Observed Cloud Base (m)	Calculated Cloud Base (m)			Fractional Deviation		
			1979	Corrected	Improved	1979	Corrected	Improved
Galileo	11	3734	5017	5021	5471	-0.34	-0.34	-0.47
Doppler	11	5264	5045	5027	4940	0.04	0.05	0.06
Dixie	11	6996	5260	5251	5713	0.25	0.25	0.18
Boltzman	12	5567	7258	7246	6759	-0.30	-0.30	-0.21
Newton	12	4058	5181	5218	5411	-0.28	-0.29	-0.33
Charleston	12	4354	4643	4684	4806	-0.07	-0.08	-0.10
Grable	15	5913	3866	3861	4233	0.35	0.35	0.28
Annie	16	7216	5917	5953	6614	0.18	0.18	0.08
Shasta	17	3387	6118	6036	5872	-0.81	-0.78	-0.73
Diablo	17	4581	5960	5920	6306	-0.30	-0.29	-0.38
Whitney	19	3967	5570	5568	6133	-0.40	-0.40	-0.55
Stokes	19	6497	5449	5439	5758	0.16	0.16	0.11
Badger	23	5550	4758	4772	5762	0.14	0.14	-0.04
Nancy	24	6520	5782	5801	6214	0.11	0.11	0.05
Encore	27	6858	5474	5476	5981	0.20	0.20	0.13
Harry	32	7070	7213	7377	8105	-0.02	-0.04	-0.15
Priscilla	37	6164	6914	6909	7392	-0.12	-0.12	-0.20
Lacrosse	40	6096	5180	5856	6011	0.15	0.04	0.01
Simon	43	8065	7907	7948	8090	0.02	0.01	0.00
Smoky	44		7566	7566	7677			
Climax	61	9035	7883	7891	8141	0.13	0.13	0.10
Hood	74	8921	8065	8065	8737	0.10	0.10	0.02
Koon	110		9875	10035	9649			
Zuni	3500	14932	13623	15016	15374	0.09	-0.01	-0.03
Tewa	5000		14017	16369	16435			
Bravo	15000	16853	20938	22055	20240	-0.24	-0.31	-0.20
					FMD	-0.12	-0.14	-0.29
					FRMS	0.47	0.49	0.66

Observation. The observed values of the cloud tops were taken from Refs 16 and 17, and for the majority were given to the nearest kilofoot (305 m). The values for cloud tops and bases are plotted as a function of yield in Figure 13 on page 79. No mention was made to the estimated error in the observation in these references. A search was made of the old weapon test (WT) reports to try and get a rough idea of the appropriate error, but to no avail.

One study did comment on reasons why early data was considered questionable. It stated that some data were considered unreliable due to the lack of a drift correction when the cloud vectored toward the camera. Some data were inaccurate due to manual operation of the theodolite equipment or conflicting results with the camera data (14:14).

To get a feeling for the impact of observation error on the FRMS value, a simple sensitivity study was done. For the purpose of this side study, it was assumed that all shots in the validation set contained the same amount of absolute error and the FRMS was calculated. The FRMS associated with this exact amount of error is shown along with the value of the FMD for the entire set in Table 10 on page 80. As can be seen from the table, if one assumes the observed values can be off by one kilofoot (305 m), the FRMS is already approaching 0.1.

Norment presented results of his validation study using the FRMS and FMD values (46:27). These numbers are shown in Table 11 on page 80. Included in the table are the values for a set of 53 shots (54 minus Humboldt) and 60 shots (54 plus 6 classified shots). Also listed are the results obtained when the author ran the tabulated values in Norment's 1970 simulation study of the 54 shots. Norment did not calculate his own value for FRMS with the 1970 version of the CRM.

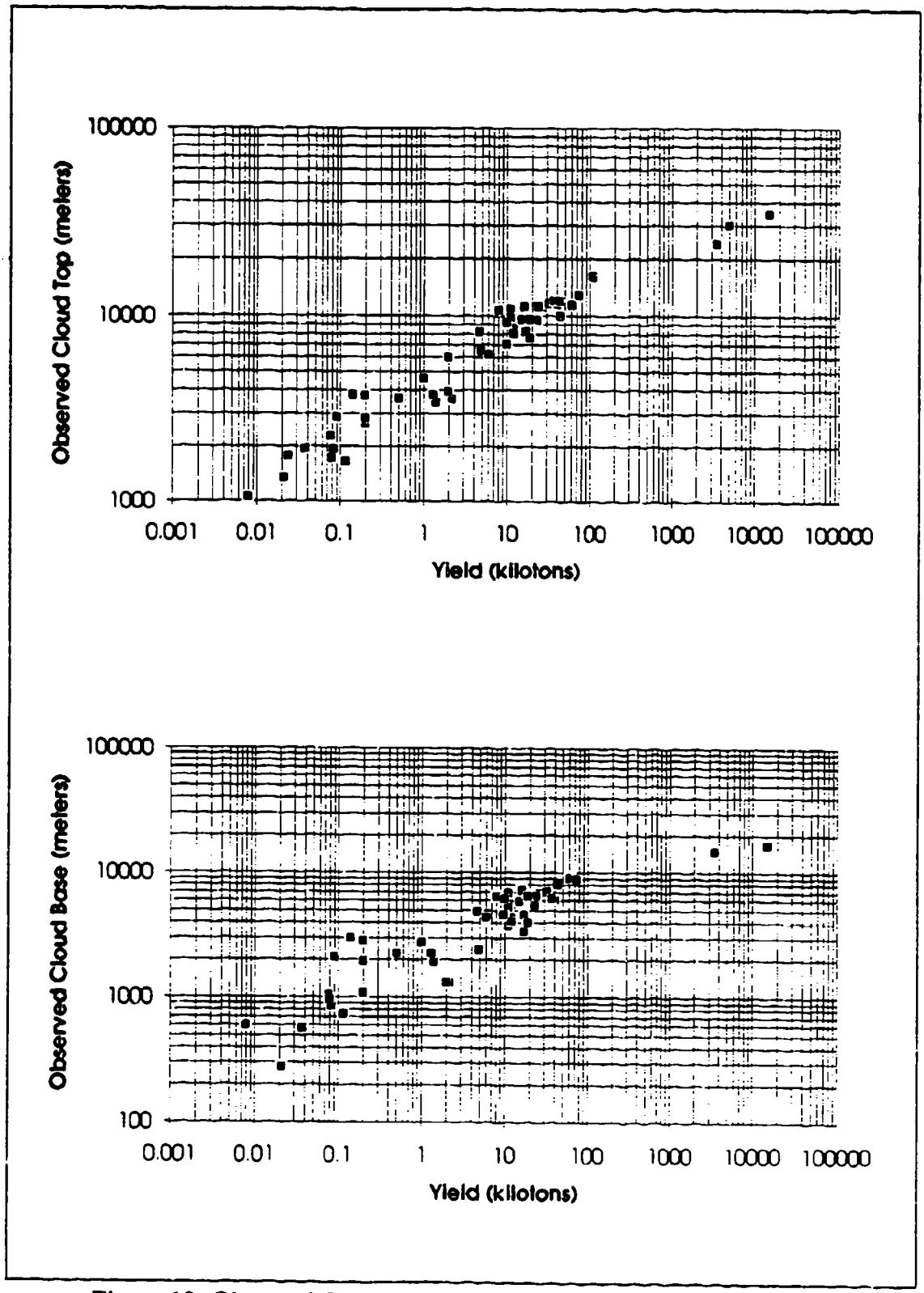

Figure 13: Observed Cloud Tops and Bases Relative to Burst Heights

Table 10: Sensitivity of FRMS and FMD to a Constant Error in the Cloud Top Value

Assumed Error (ft)	FRMS	FMD
1000	0.089	0.066
2000	0.177	0.132
3000	0.266	0.197
4000	0.354	0.263
5000	0.443	0.329

Table 11: Cloud Top FRMS and FMD for the 1970 & 1977 Versions of the CRM

	1970 (54 shots)	1977 (53 shots)	1977 (60 shots)
FMD	0.16	-0.009	0.002
FRMS	0.24	0.15	0.14

1979 Version. First, the 1979 version of the CRM was used to calculate the cloud tops and bases of the validation set. The results of these runs are plotted in Figure 14 on page 81 as well as being listed in Table 8 on page 74 and Table 9 on page 76 (which show the values for the FRMS figure of merit).

The first question that comes to mind is why the 1979 version of the model performs worse than the previously tabulated values for the 1977 version. Since Norment did not tabulate the data used to compute the reported FRMS values in 1977, there is no way of knowing why the 1979 CRM performs worse. The 1979 CRM was checked line by line by the author and the test case cloud top listed in the documentation was duplicated to all four significant digits. Therefore, the 1979 FRMS value is used as a baseline for comparison, and the 1977 values are held suspect.

Corrected Version. After making the corrections mentioned in "Corrections Needed in the 1979 DELFIC CRM" on page 31, the set of 54 shots was again run. The results of

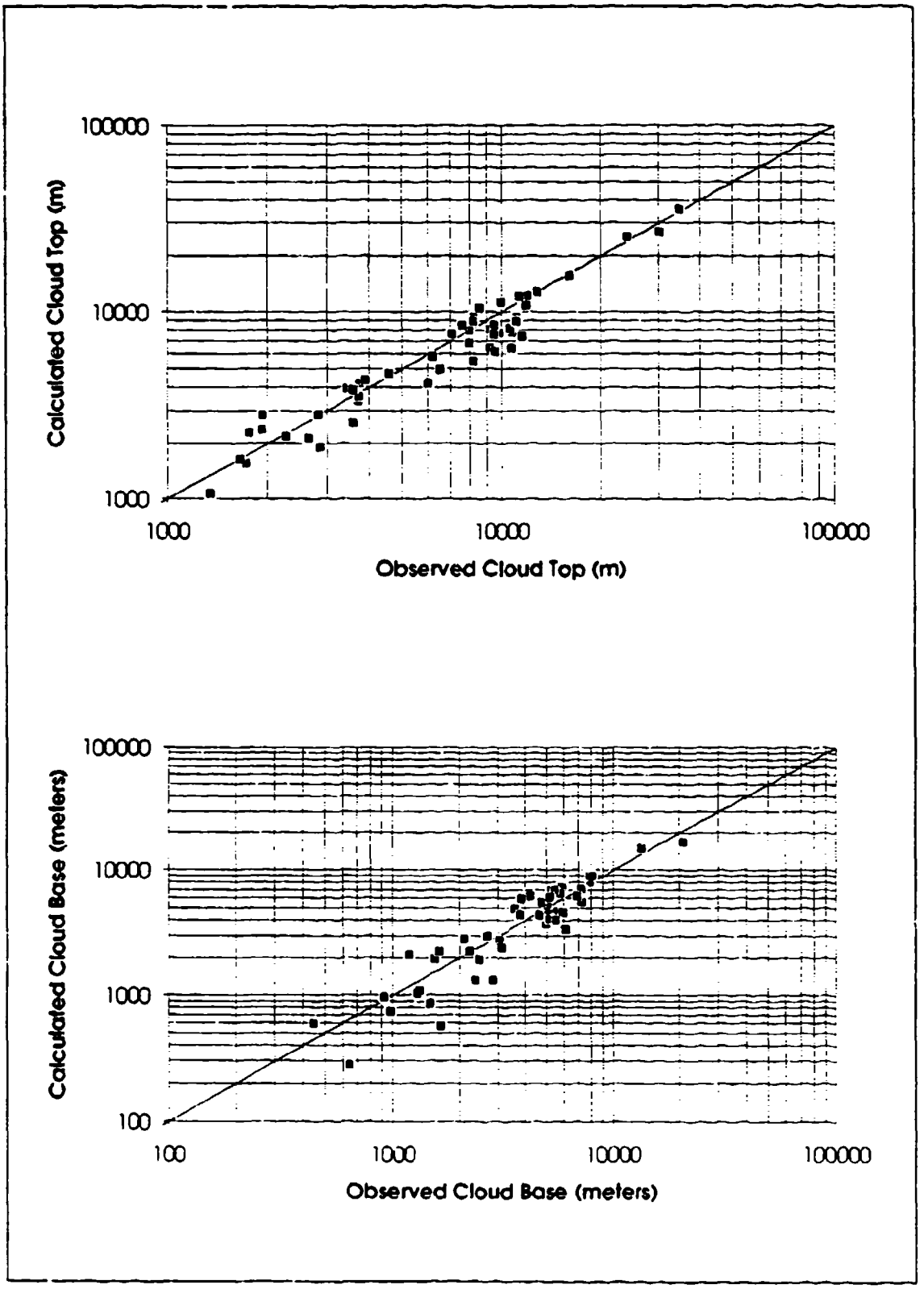

Figure 14: 1979 CRM Cloud Tops and Bases (relative to burst heights)

this newer version of the CRM are plotted in Figure 15 on page 83. As can be seen from Table 8 on page 74, the FRMS value decreases slightly from 0.20 to 0.19 after making the suggested corrections.

Improved Version. The improved version of the CRM represents a change back to a single term entrainment equation and constant values for the entrainment (μ) and eddy viscous drag (k_2) parameters. The optimum values for the parameters were found by running a matrix of values for the pair. The suggested ranges by Huebsch (21:72) were tried initially. His range for the entrainment parameter (0.15 to 0.25) was too high, most likely due to the model's change in cloud shape modeling (See "Cloud Shape and Volume" on page 30). A range of smaller values (0.08 to 0.15) closer to the values used in the 1979 version was tried. As for the eddy viscous drag parameter, values from Huebsch's highest recommended value (0.125) down to 0.0 were tried.

The FRMS results of varying the entrainment and eddy viscous drag parameters are shown in Figure 16 on page 84. As can be seen from the saddle shape of the figure, there is a compensating effect when lowering the value of one parameter while raising the other. It was found that the minimum value for the ranges considered was FRMS=0.18. This value is achieved with more than one combination of parameters. The pair chosen was μ=0.12 and k_2=0.1. These values correspond to the 1979 CRM values for yields up to a kiloton (See Figure 4 on page 28).

The results of using these values along with a single term entrainment equation are shown in Figure 17 on page 85. As can be seen from Table 8 on page 74, the FRMS value decreases again from 0.19 to 0.18 after making these improvements. This stands in con-

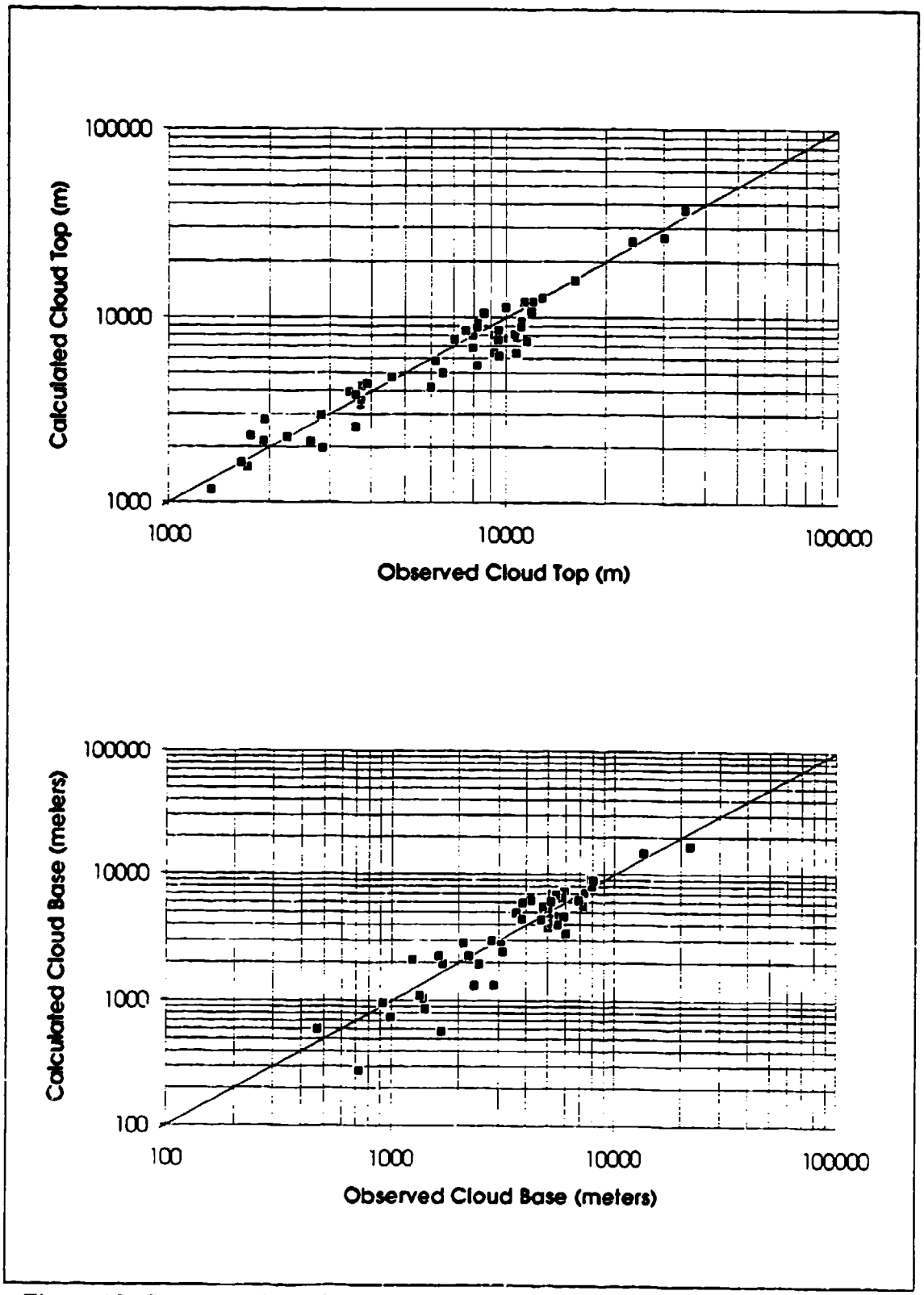

Figure 15: Corrected 1979 CRM Cloud Tops and Bases (relative to burst heights)

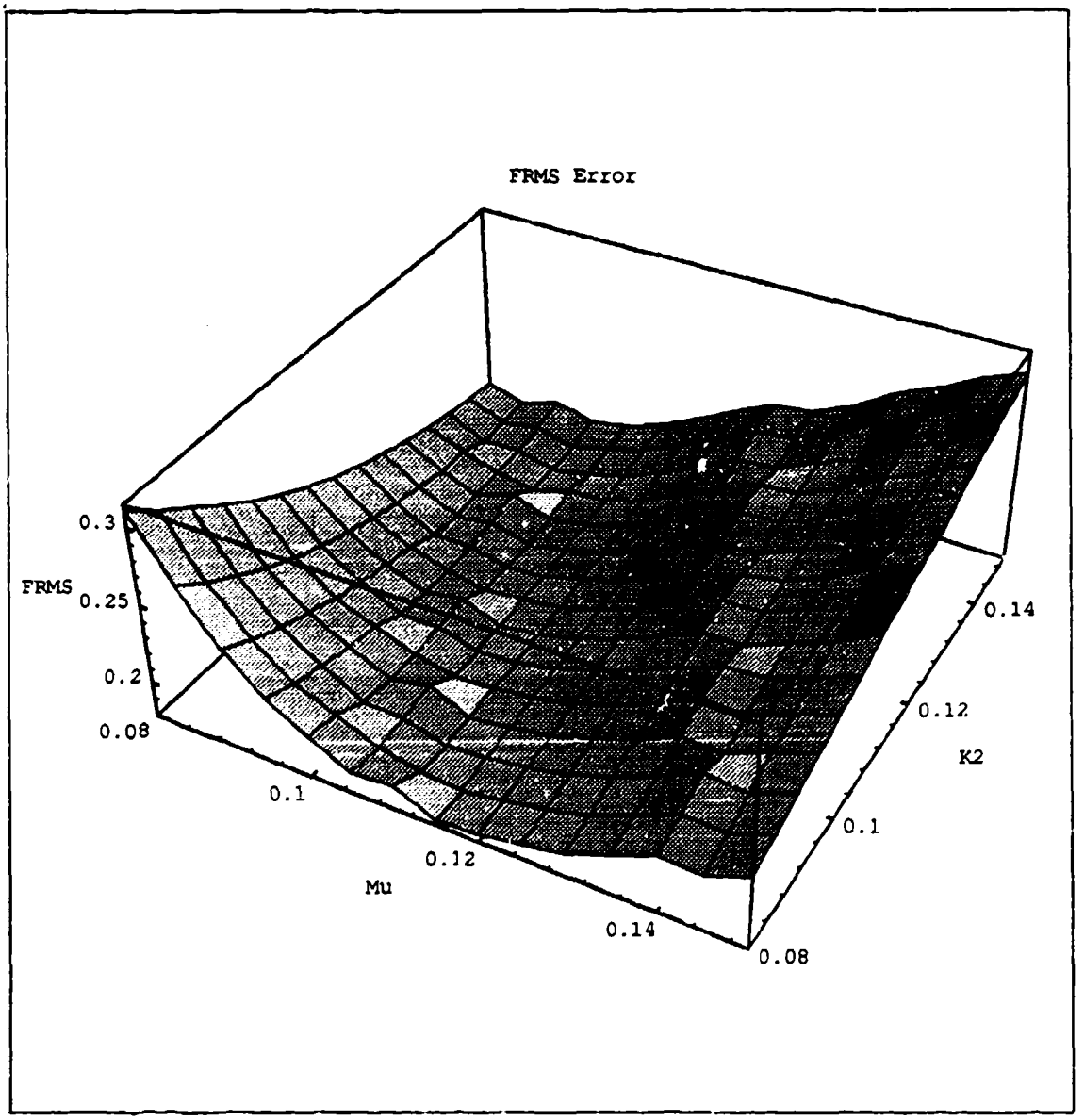

Figure 16: FRMS Values for Entrainment (μ) and Eddy Viscous Drag (k_2) Parameter Combinations

trast to comments made in Norment's 1977 report: "Extensive calculations...have shown that it is not possible to adequately ...atch calculated with observed results if single, yield independent values are used for these [μ and k_2] parameters" (46:40). One could argue

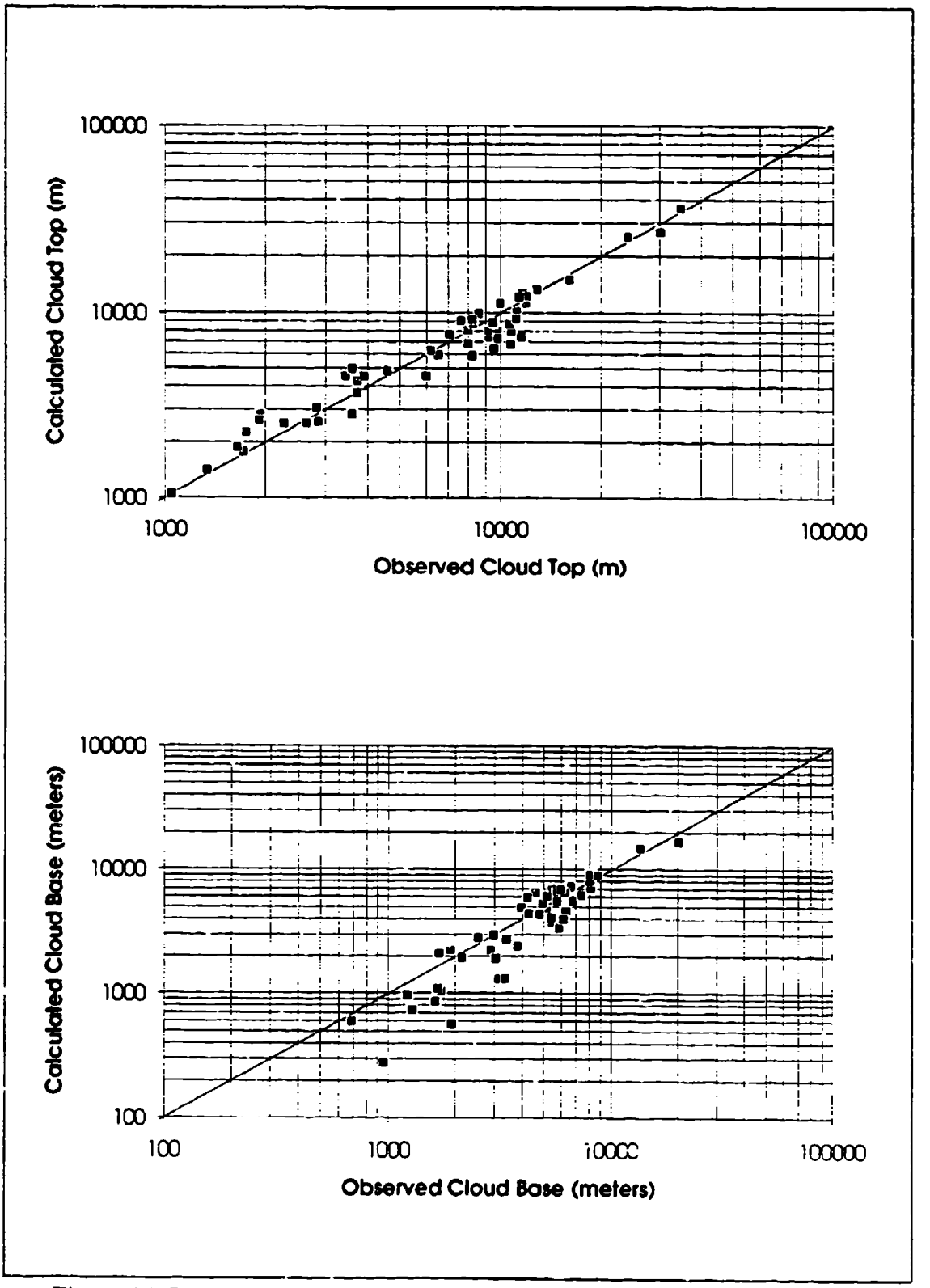

Figure 17: Improved CRM Cloud Tops and Bases (relative to burst heights)

that the FRMS with constant parameters (See Figure 16 on page 84) is still not "adequate", but it is certainly an improvement.

The FMD also reduces substantially for the whole group. However this may imply that there are just as many underpredictions as overpredictions. But this near zero FMD combined with the fact that the FRMS is reduced, implies a somewhat better fit to observed cloud tops with the chosen yield independent parameters. The figure of merit for the cloud *bases* on the other hand gets about 30-40% worse. Considering the scatter in the observed data (See Figure 13 on page 79), and the fact that cloud bases are ill-defined, not too much can be implied from this result.

Time Dependent Results. The temporal performance of the bubble rise is the final area to be discussed. Although the figures of merit chosen were not related to the rate of rise, the way a cloud gets to its final height does play a part in determining the strength of the flow in the particle rise modeling. Figure 18 on page 87 and Figure 19 on page 88 show the calculated time history plots of shots Castle Bravo and Upshot-Knothole Simon. These cases were chosen since Norment used them in his 1977 study and temporal plots were available from DASA 1251-EX (16;17). These references contain temporal plots for 16 of the 54 shots in the set.

While the results for both Simon and Bravo are excellent as far as matching cloud tops, both achieve the desired value earlier than observation. The Bravo simulation (See Figure 18 on page 87) shows the cloud top stabilizing at 3 minutes, while the observation (See Figure 20 on page 89) puts vertical stabilization at 4.5 minutes. The observation also shows oscillation in the cloud top height following the apogee, which is typical for high yield shots. The observed cloud base continues to rise even at 10 minutes while, by the

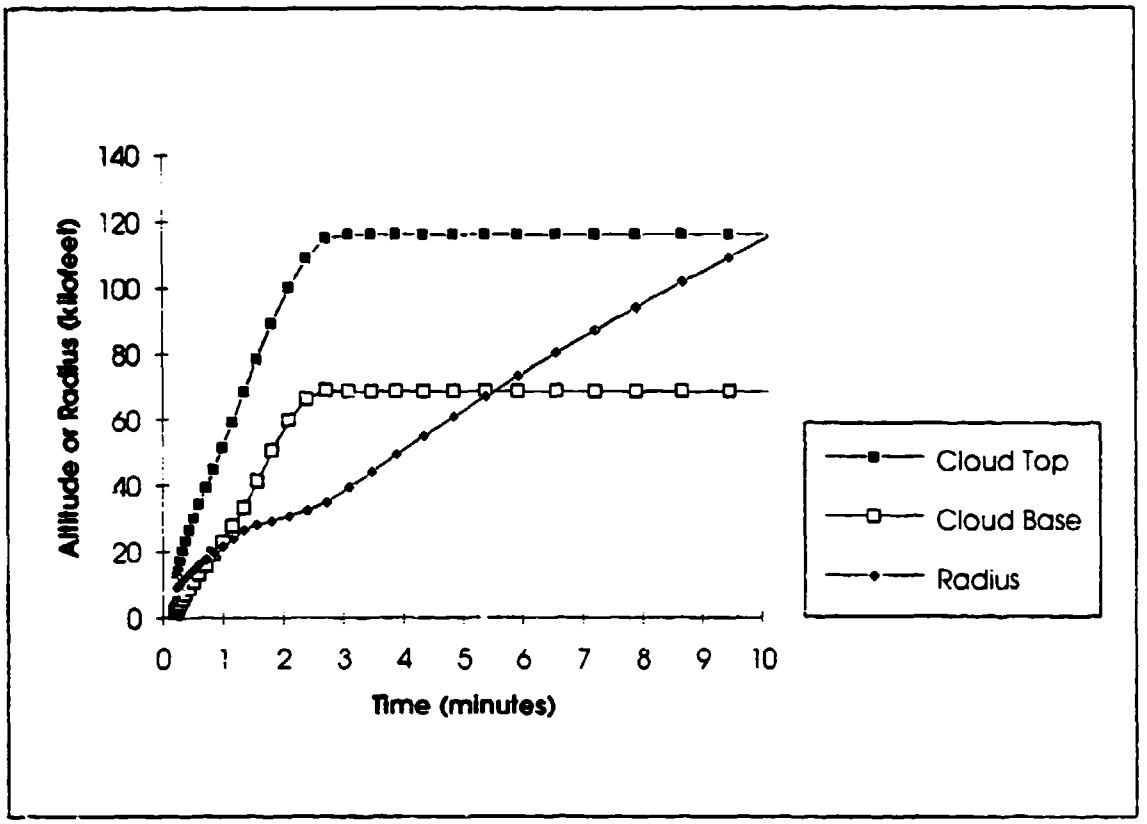

Figure 18: Calculated Cloud Dimensions: Operation Castle Shot Bravo

nature of the CRM modeling, the simulated cloud base is made to stop rising at the same time as the top.

The simulation of Simon (See Figure 19 on page 88) shows the cloud top achieving vertical stabilization at 7 minutes while observation (See Figure 21 on page 90) puts vertical stabilization at 10 minutes. With Simon, however, the observed base vertically stabilizes at 7 minutes, identical to the simulation. It should be noted that the simulated vertical stabilization times for both of these shots was about the same as those simulated in Norment's 1977 study. While these two simulations both stabilize the cloud top earlier than

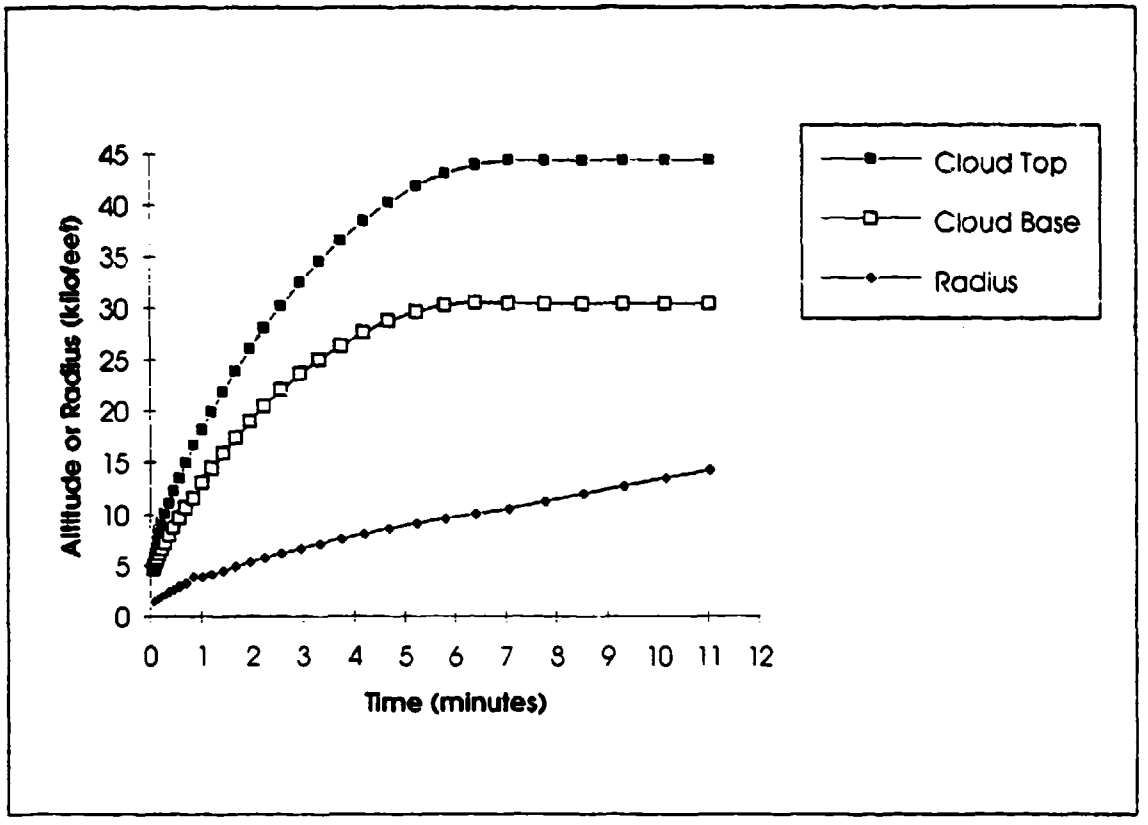

Figure 19: Calculated Cloud Dimensions: Operation Upshot-Knothole Shot Simon

observation, other simulations (e.g. Upshot Knothole events Annie and Ruth) stabilize the cloud top later than observation.

Particle Rise

This second major section of the chapter presents the results of running the particle rise subroutines which use the vortex flow field equations. There are two main comparisons to be shown: 1) vortex particle rise to hydrocode dust modeling, and 2) vortex particle rise to DELFIC's 1-D particle rise. Before these comparisons are made, however, sample snapshots of the trace particles' histories are given for physical insight.

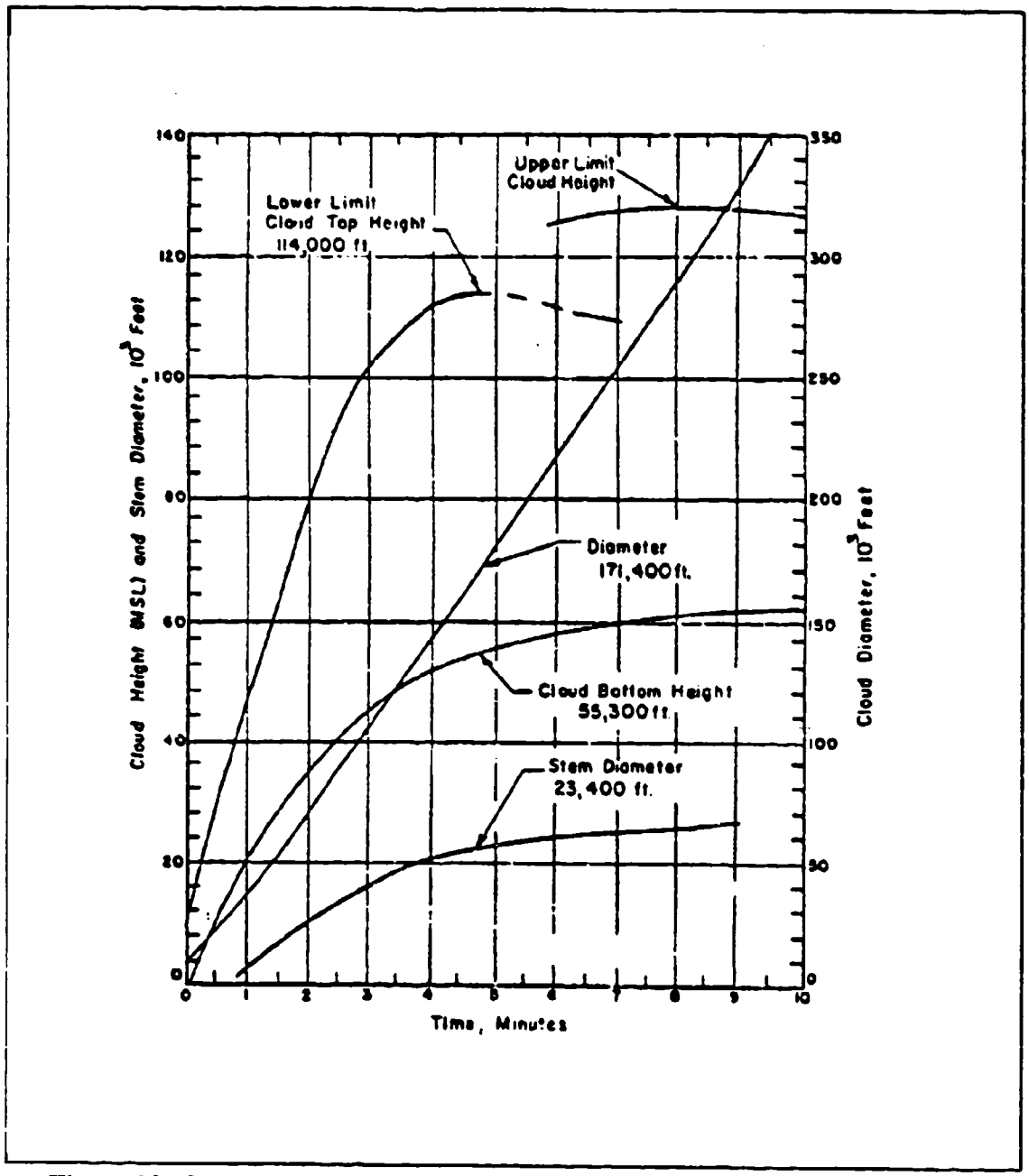

Figure 20: Observed Cloud Dimensions: Operation Castle Shot Bravo (17:68)

Particle Plots. Animation of the trace particles is a useful tool for evaluating the code's functioning and overall performance. Animation in Mathematica was used as an integral part of the particle rise research. It allowed the author to view the effects of the

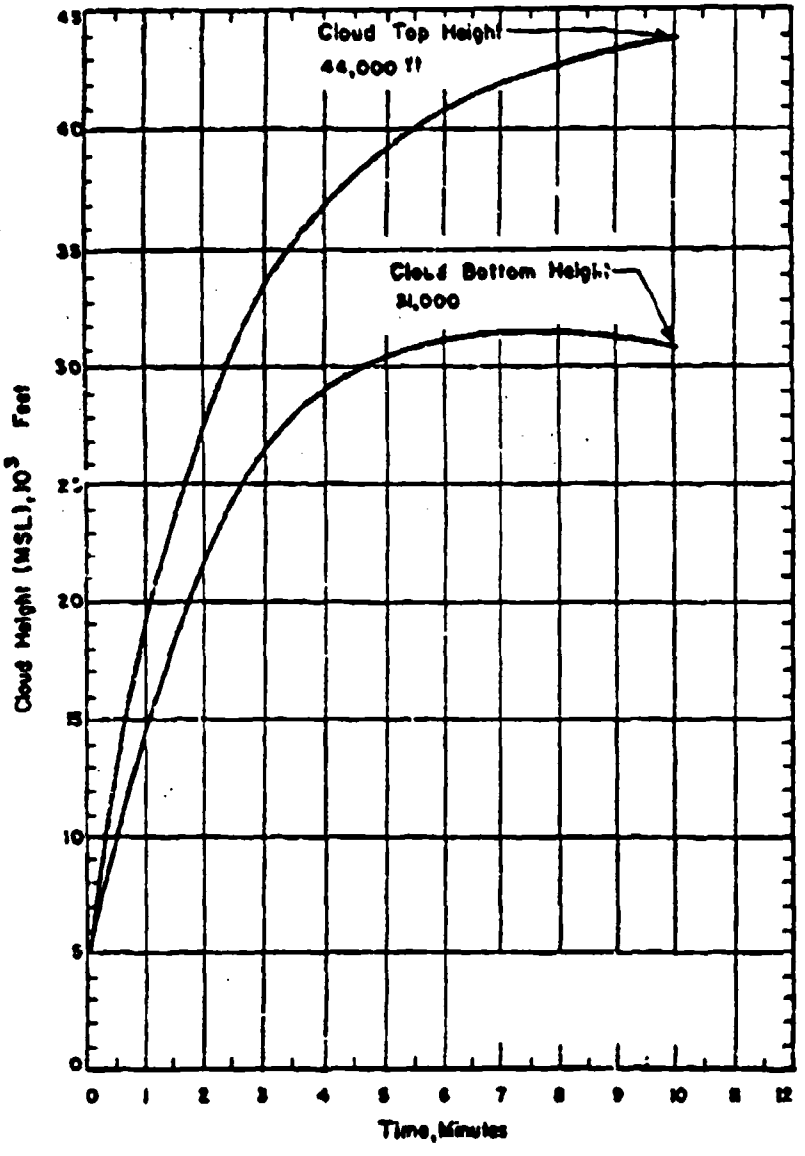

Figure 21: Observed Cloud Dimensions: Operation Upshot-Knothole Simon (16:141)

submodel choices such as gravity settling, radial expansion, and initial source location.

Although animation is not able to be placed in this report, a sample of a sequence of snapshots can be given.

In Figure 22 on page 92 the positions of trace particles are shown from initial time (4.35 sec) to stabilization time (608.1 sec) along with the whole-minute snapshots. The sequence represents the 1979 test case using the improved CRM. For this figure there are 5 particle size groups (22, 60, 130, 277, and 768 microns), each with a 20 by 20 grid of starting locations, for a total of 2000 trace particles. One must keep in mind that the trace particles do not all have equal weights (of mass or radioactivity). This is due to the fact that each trace particle represents an annulus at the radius where it originates. Therefore, particles starting at the outer radii have a larger weight than those starting at the inner radii.

The first few snapshots show how the vortex flow quickly moves the dust out into a torus away from the axis. In addition, one can see the number of trace particles in the center of the torus is sparser than at the surface of the torus. In the second row of snapshots, the reader can see that the cloud has reached vertical stabilization. After this, radial expansion is seen, as the particle sizes also start to separate. The larger particles fall first and some exit the cloud before stabilization. Once they fall below the cloud base they no longer are affected by the expansion correction. The last snapshot shows the different groups, with the two smallest groups overlapping each other. This occurs because neither of these smaller groups has an appreciable terminal velocity.

Dust Density Contour Plots. The first set of comparisons to be made is to the hydrocode dust plots. Each of the 9 different cases described in Table 7 on page 69 are plotted. Plots are provided for both DELFIC with vortex flow and TASS hydrocode results. Each

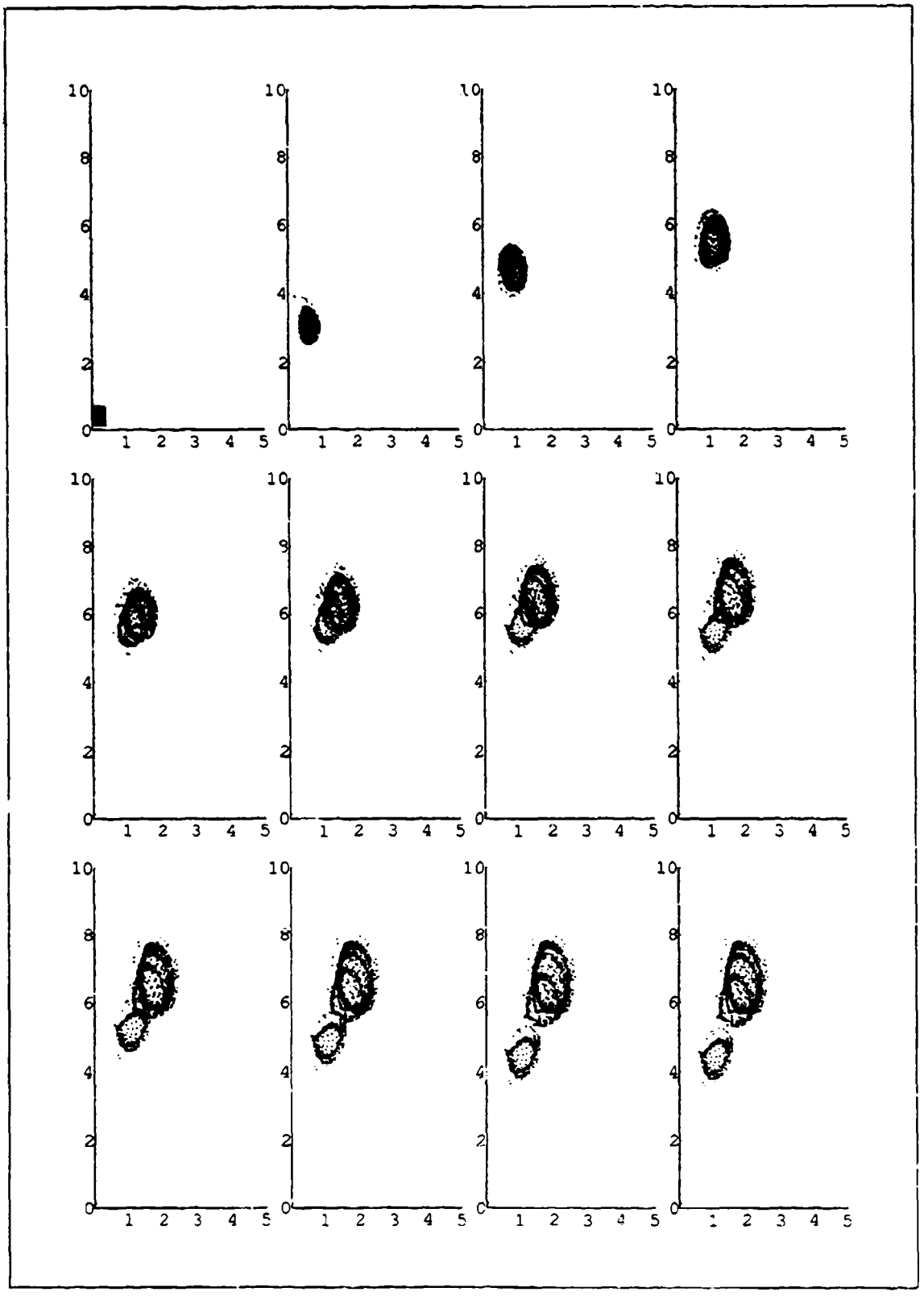

Figure 22: Cross Section of Particle Cloud with 5 Trace Particle Sizes as it Rises (snapshots every minute: initial time to stabilization time; distances in kilometers)

required multiple plots per simulation for times from one to ten minutes. The plots are shown in Figure 23 on page 94 through Figure 40 on page 111 for comparison. Shown are the total dust contours at levels of 10^{-10} g/cc and higher by factors of 10. These simulations were run with the full number of particle size groups shown in Table 6 on page 43.

DELFIC with Vortex. The radioactive particles being simulated quickly rise up and out into a torus. There is only a small amount of this dust which shows up in the stem or pedestal at early times. After vertical stabilization, radial expansion becomes the dominant force along with gravity settling. The dust contours above the main cloud base expand out, emphasizing the void on the axis of the cloud. Particle settling of the larger groups does form a visible stem at late times.

These plots show that the dust that originates in the cloud at 4-5 sec, is *not* uniformly distributed radially at later times. When the cloud stops rising, the vortex flow stops and the particles move under the influence of gravity and expansion only. This phase of the particle modeling is limited in that it does not account for any diffusive motion of the particles back to the areas of lower concentration. It also turns off the toroidal flow without allowing for a residual continuation of this flow after vertical stabilization.

TASS Output. The hydrocode output does account for both diffusion and a gradual decay of the flow field velocity after vertical stabilization. This residual motion may account for a retardation of vertical settling in the TASS results. Also noticeably different is the presence of an appreciable stem throughout the history of the dust cloud. The TASS dust clouds also reach a higher altitude than DELFIC, especially the highest near-surface bursts with SHOB=120 ft/kt$^{1/3}$ (See "Appendix A: Cloud Tops" on page 127).

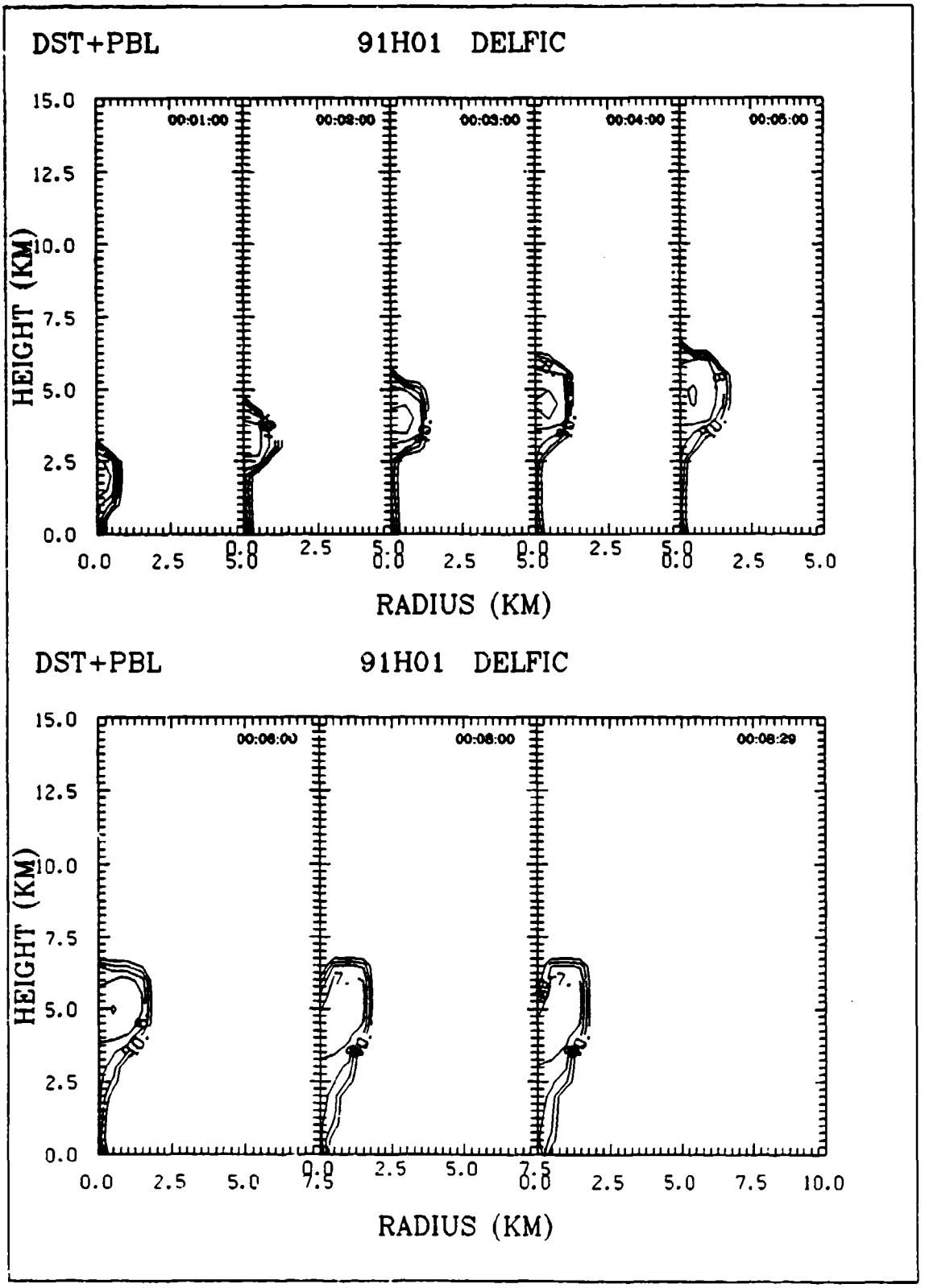

Figure 23: 91H01 (20 kt 0 SHOB) DELFIC Density Contours (10^{-x} g/cc)

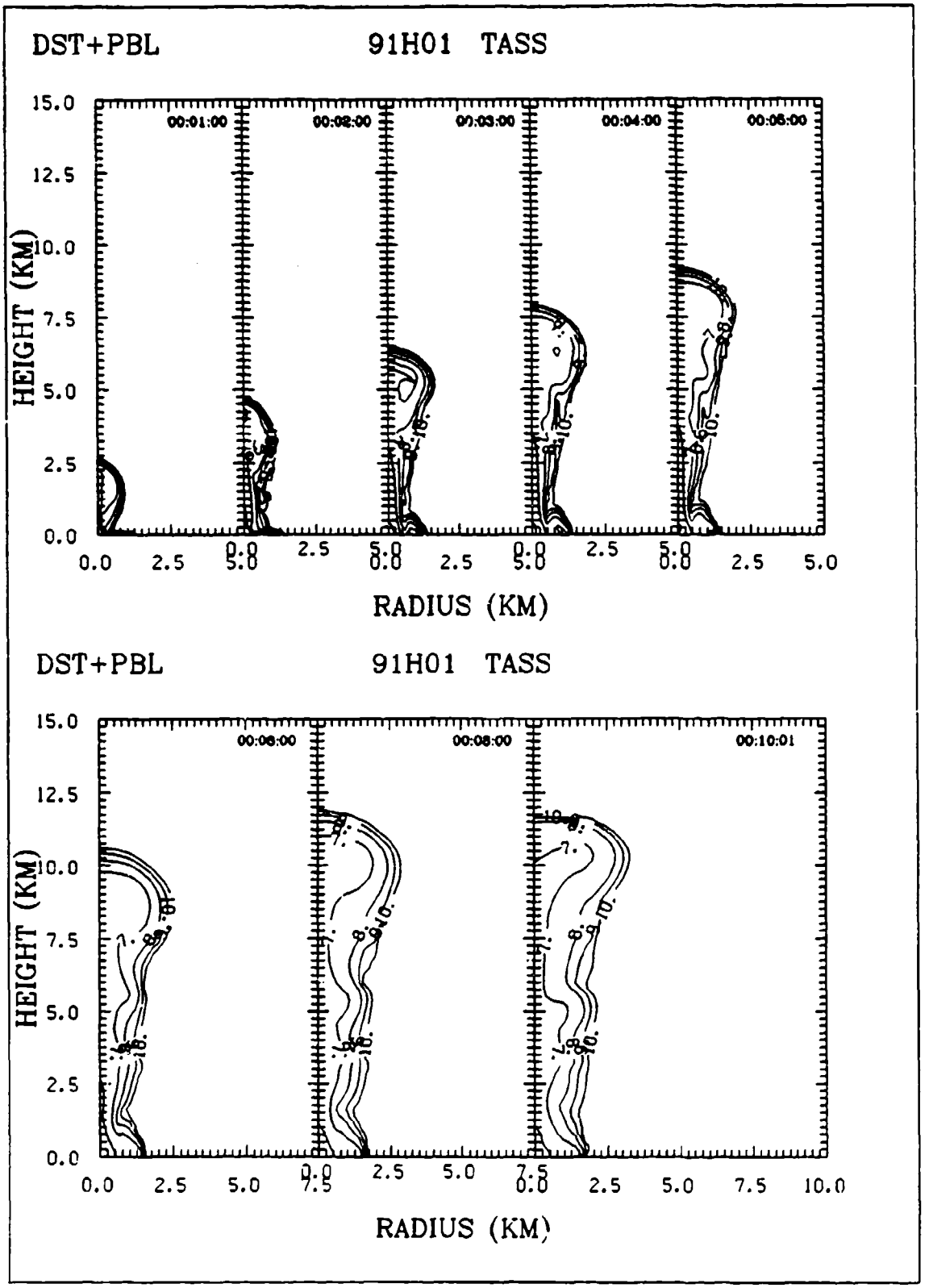

Figure 24: 91H01 (20 kt 0 SHOB) TASS Density Contours (10^{-x} g/cc)

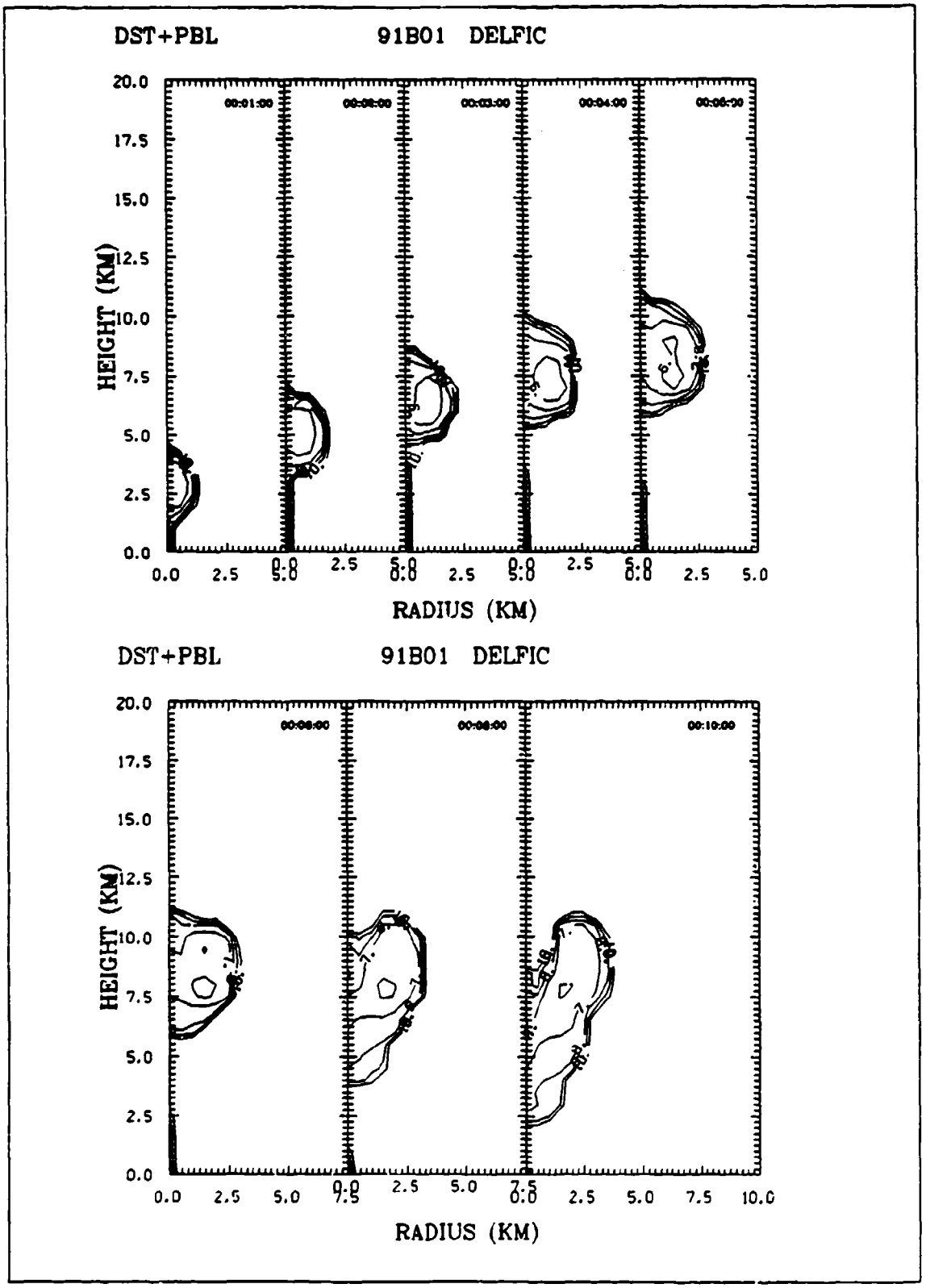

Figure 25: 91B01 (100 kt 0 SHOB) DELFIC Density Contours (10^{-x} g/cc)

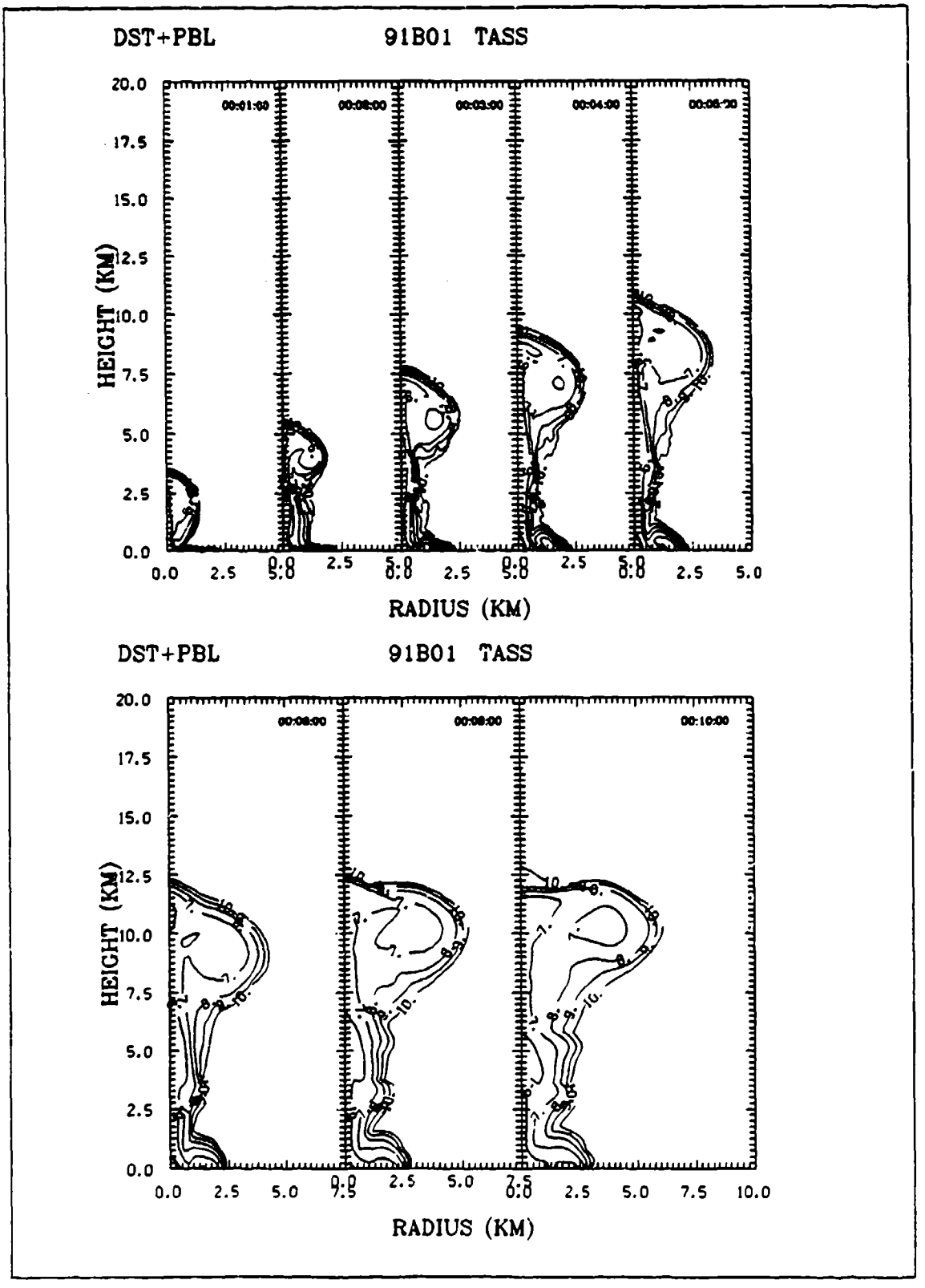

Figure 26: 91B01 (100 kt 0 SHOB) TASS Density Contours (10^{-x} g/cc)

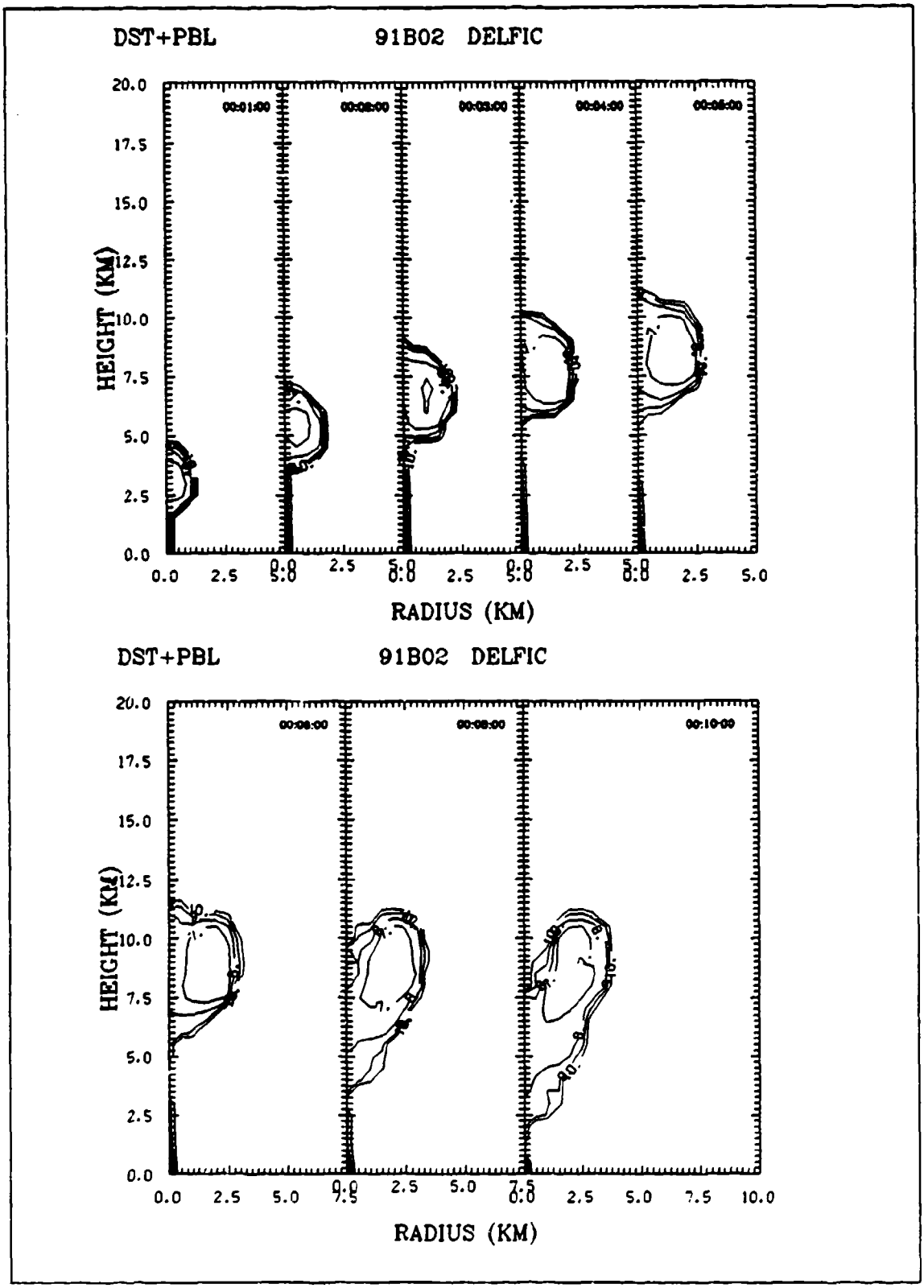

Figure 27: 91B02 (100 kt 50 SHOB) DELFIC Density Contours (10^{-x} g/cc)

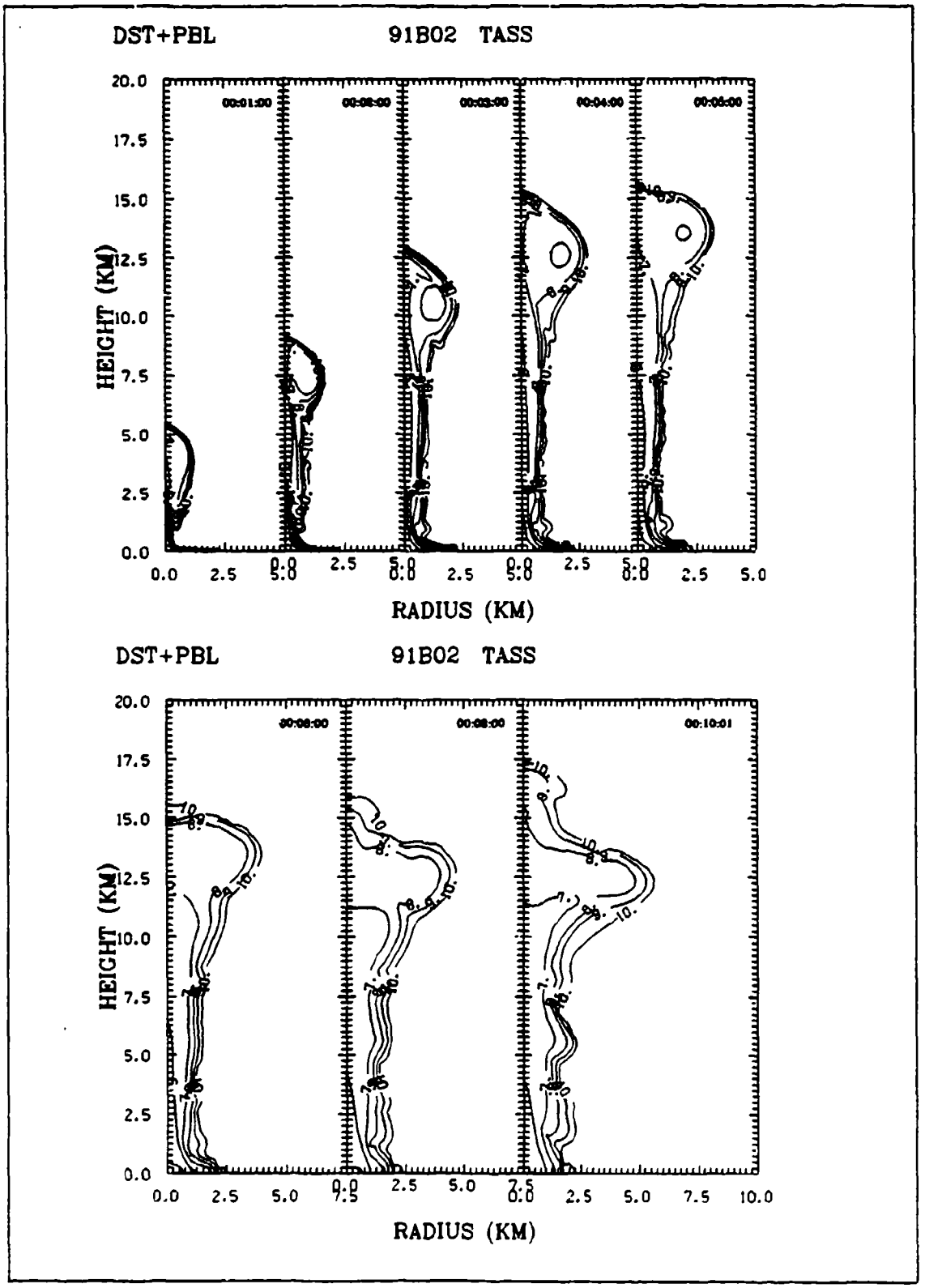

Figure 28: 91B02 (100 kt 50 SHOB) TASS Density Contours (10^{-x} g/cc)

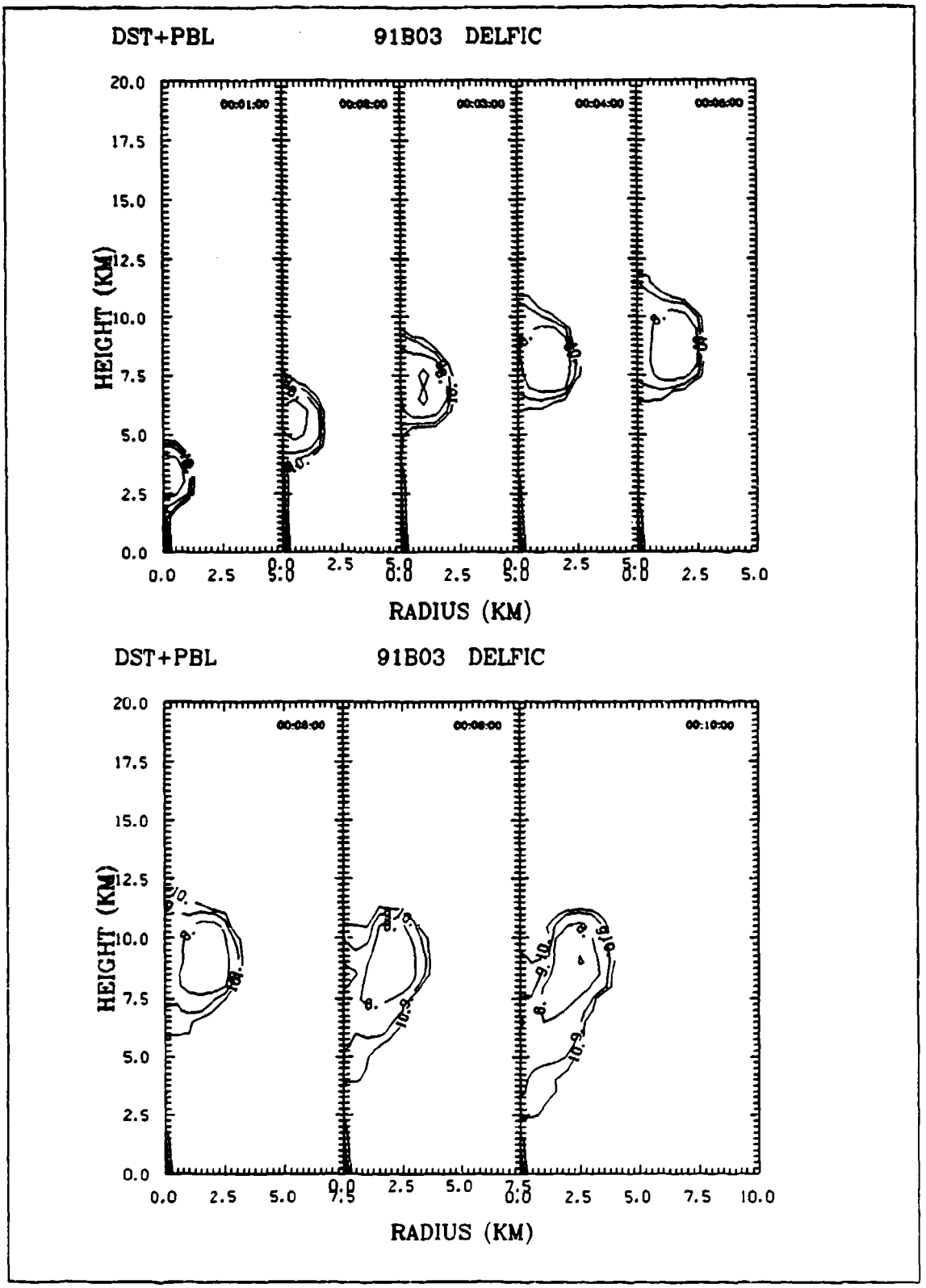

Figure 29: 91B03 (100 kt 120 SHOB) DELFIC Density Contours (10^{-x} g/cc)

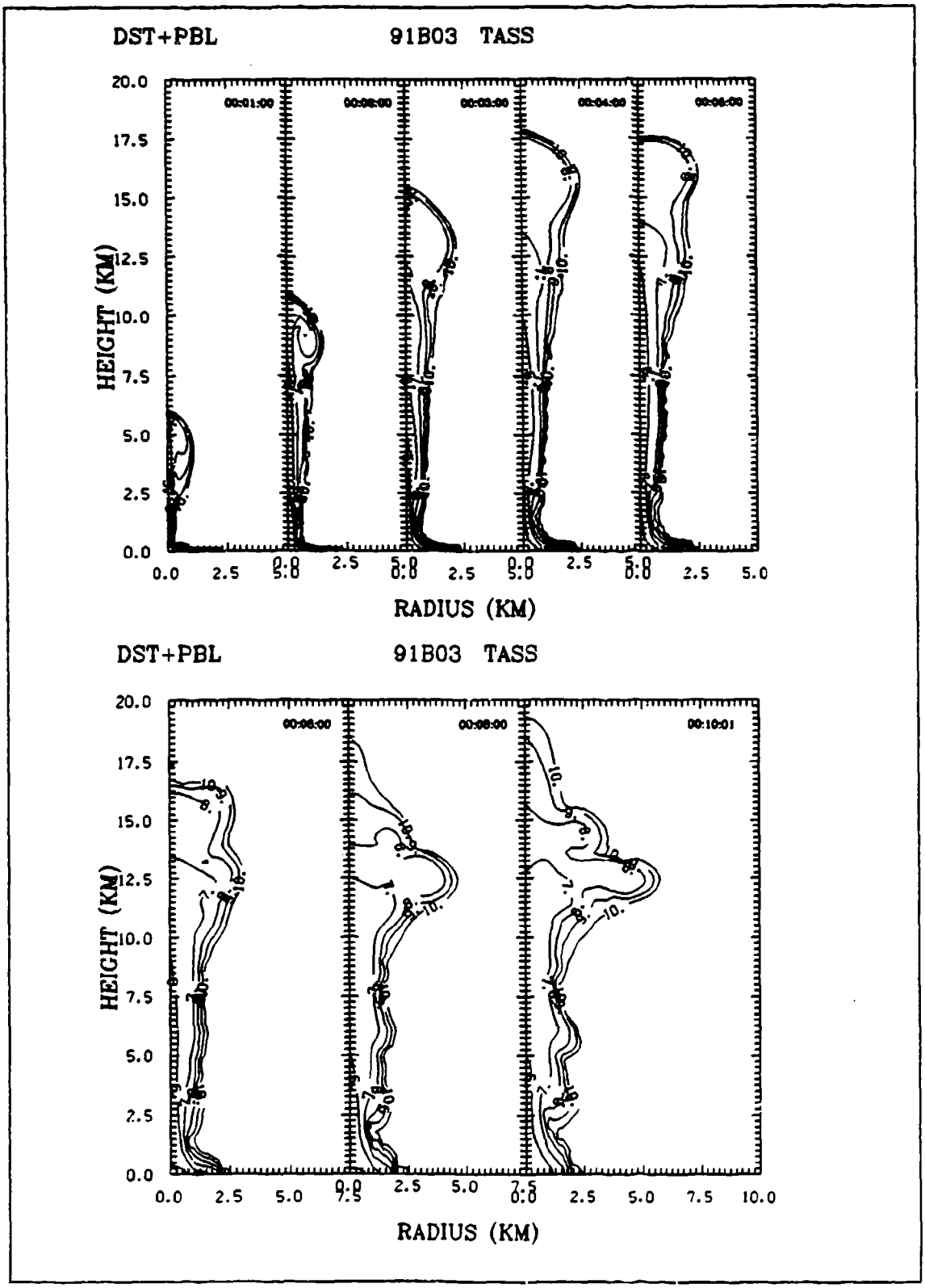

Figure 30: 91B03 (100 kt 120 SHOB) TASS Density Contours (10^{-x} g/cc)

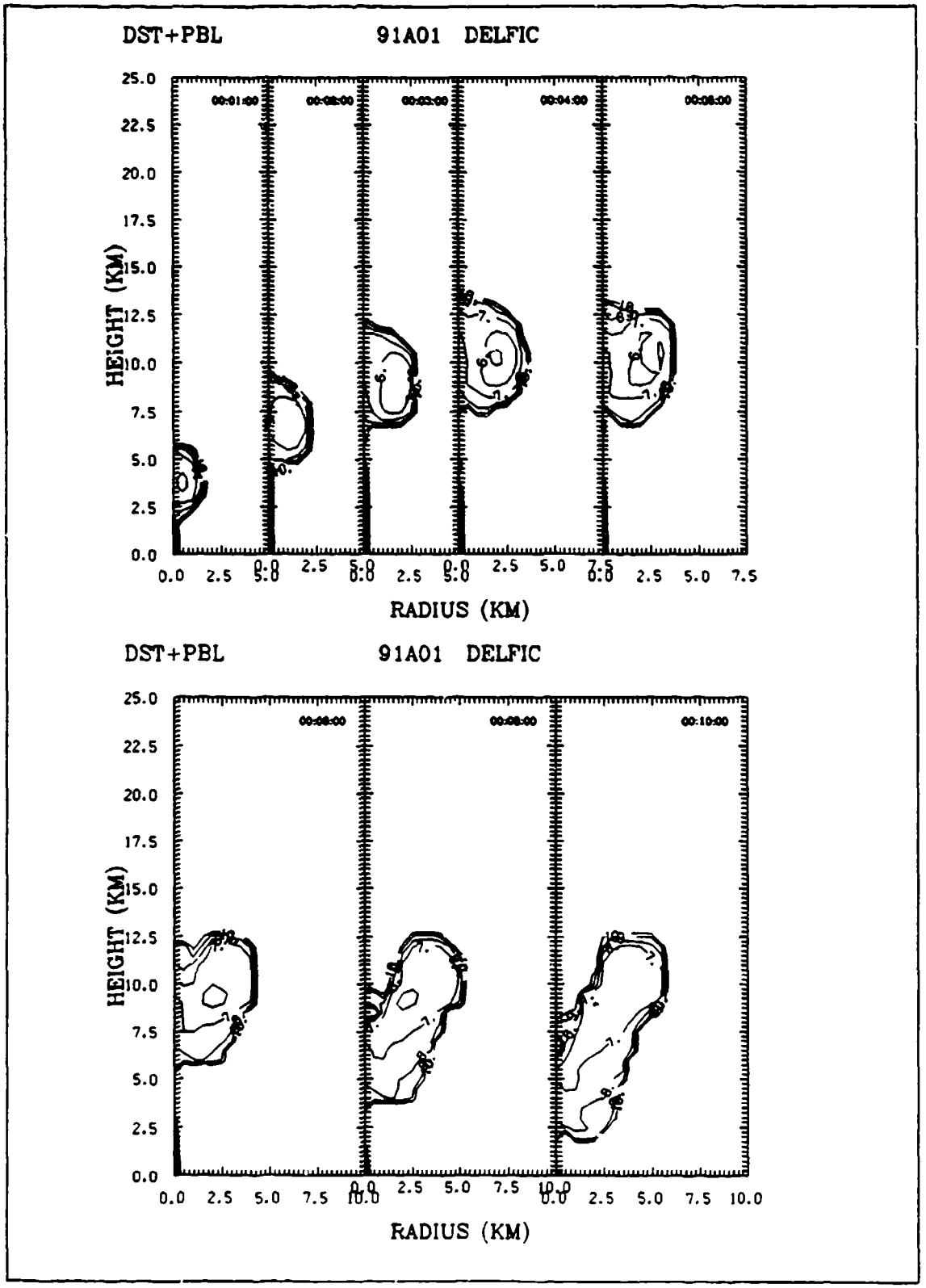

Figure 31: 91A01 (300 kt 0 SHOB) DELFIC Density Contours (10^{-x} g/cc)

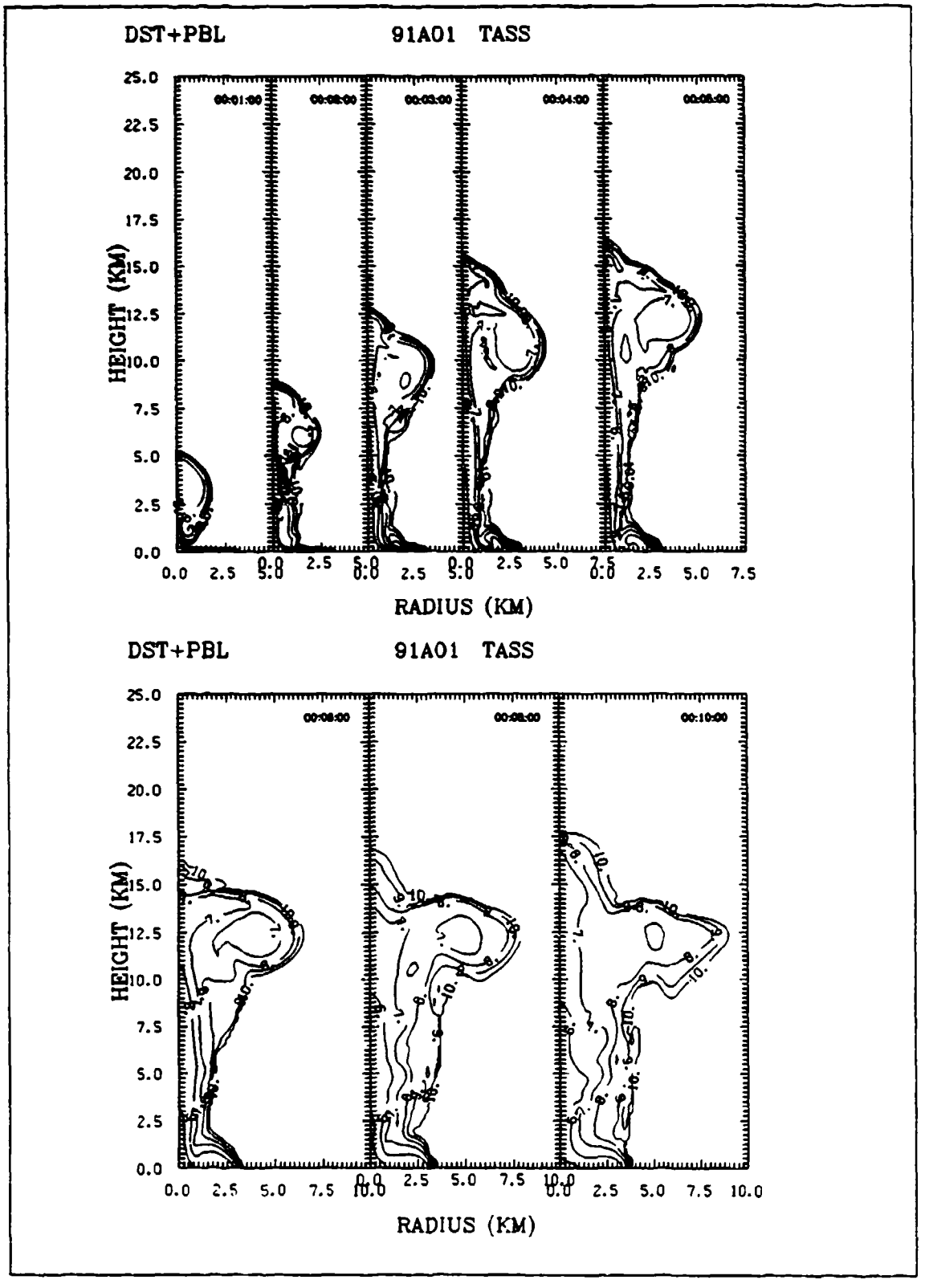

Figure 32: 91A01 (300 kt 0 SHOB) TASS Density Contours (10^{-x} g/cc)

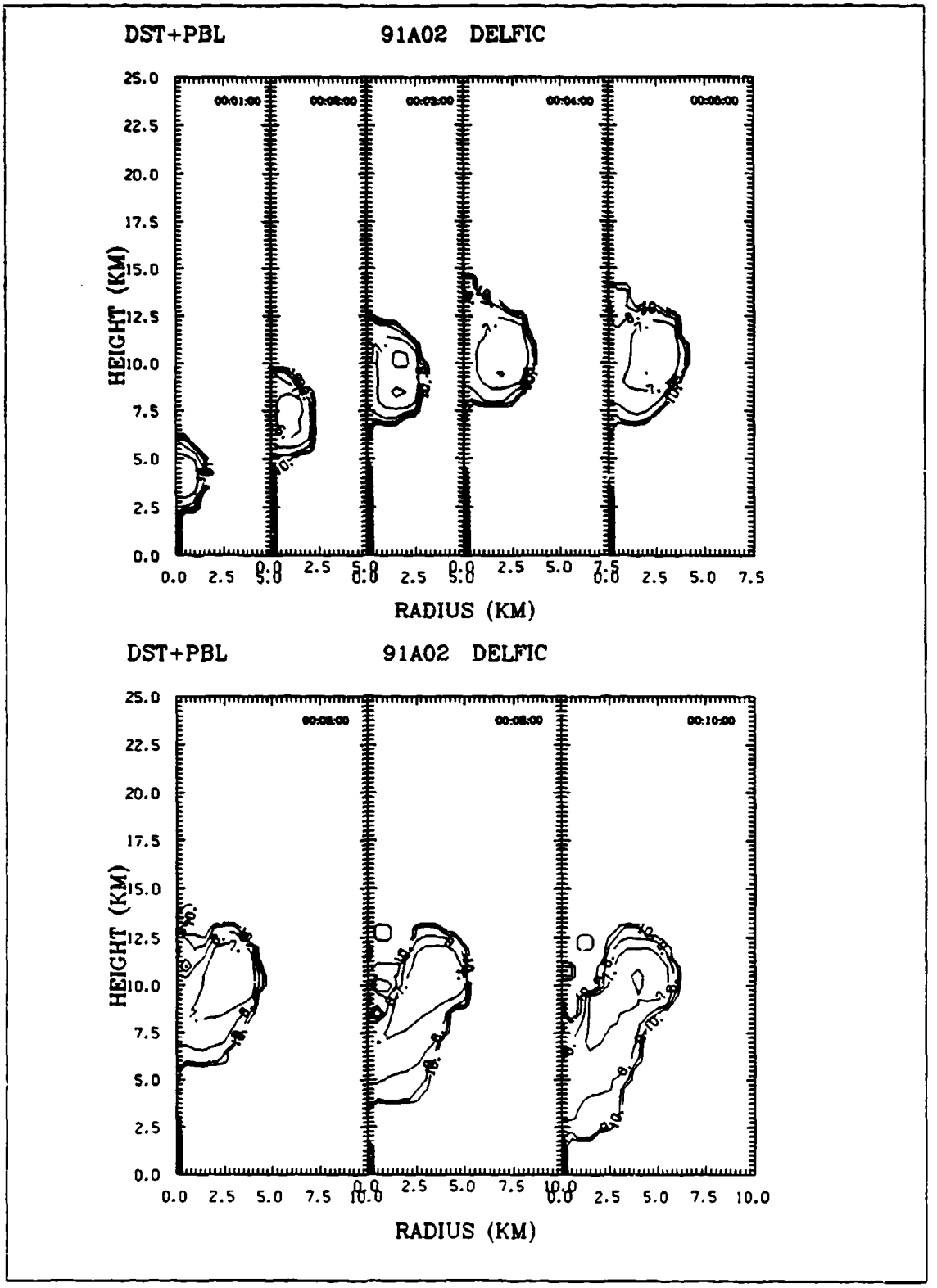

Figure 33: 91A02 (300 kt 50 SHOB) DELFIC Density Contours (10^{-x} g/cc)

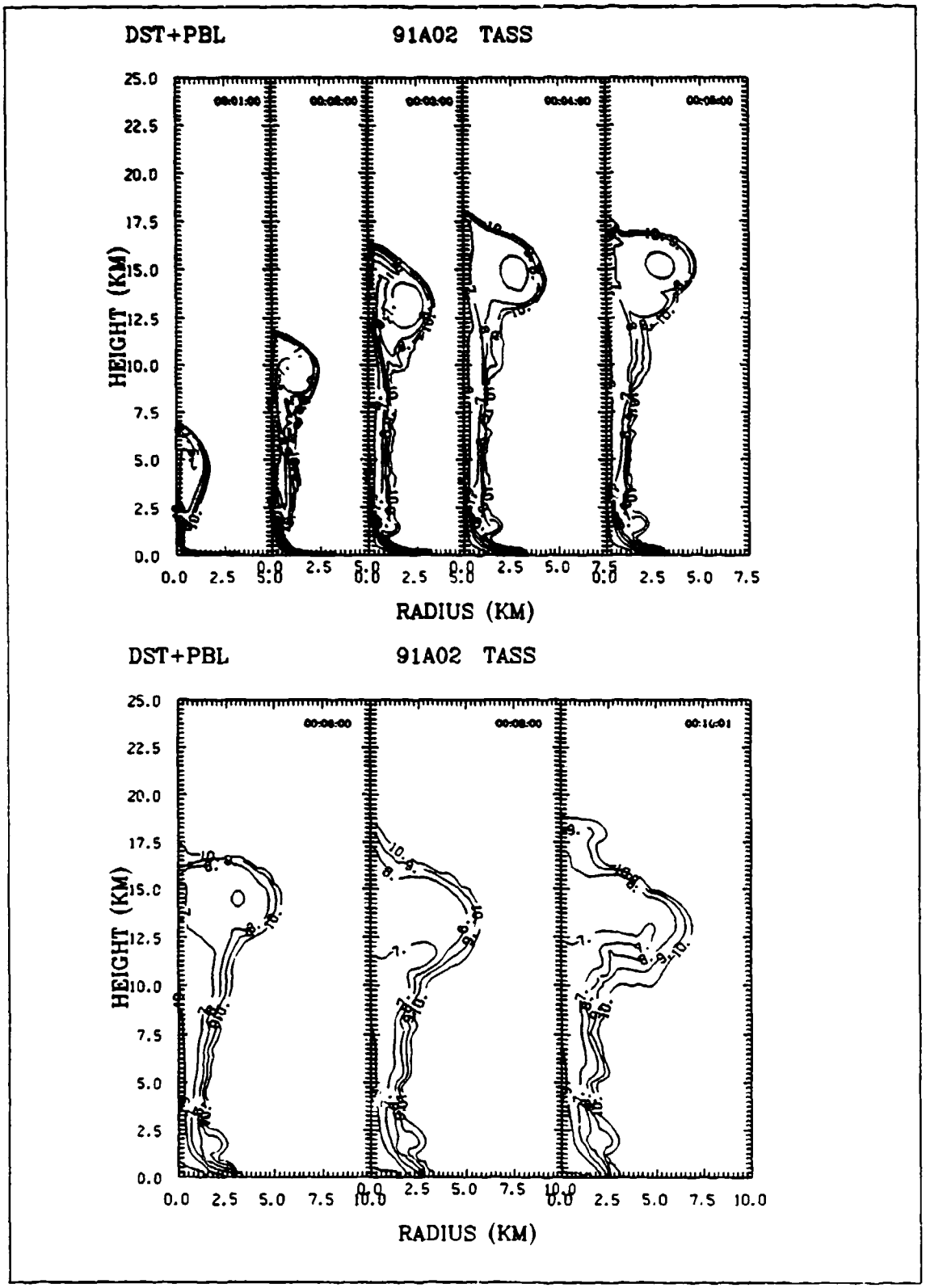

Figure 34: 91A02 (300 kt 50 SHOB) TASS Density Contours (10^{-x} g/cc)

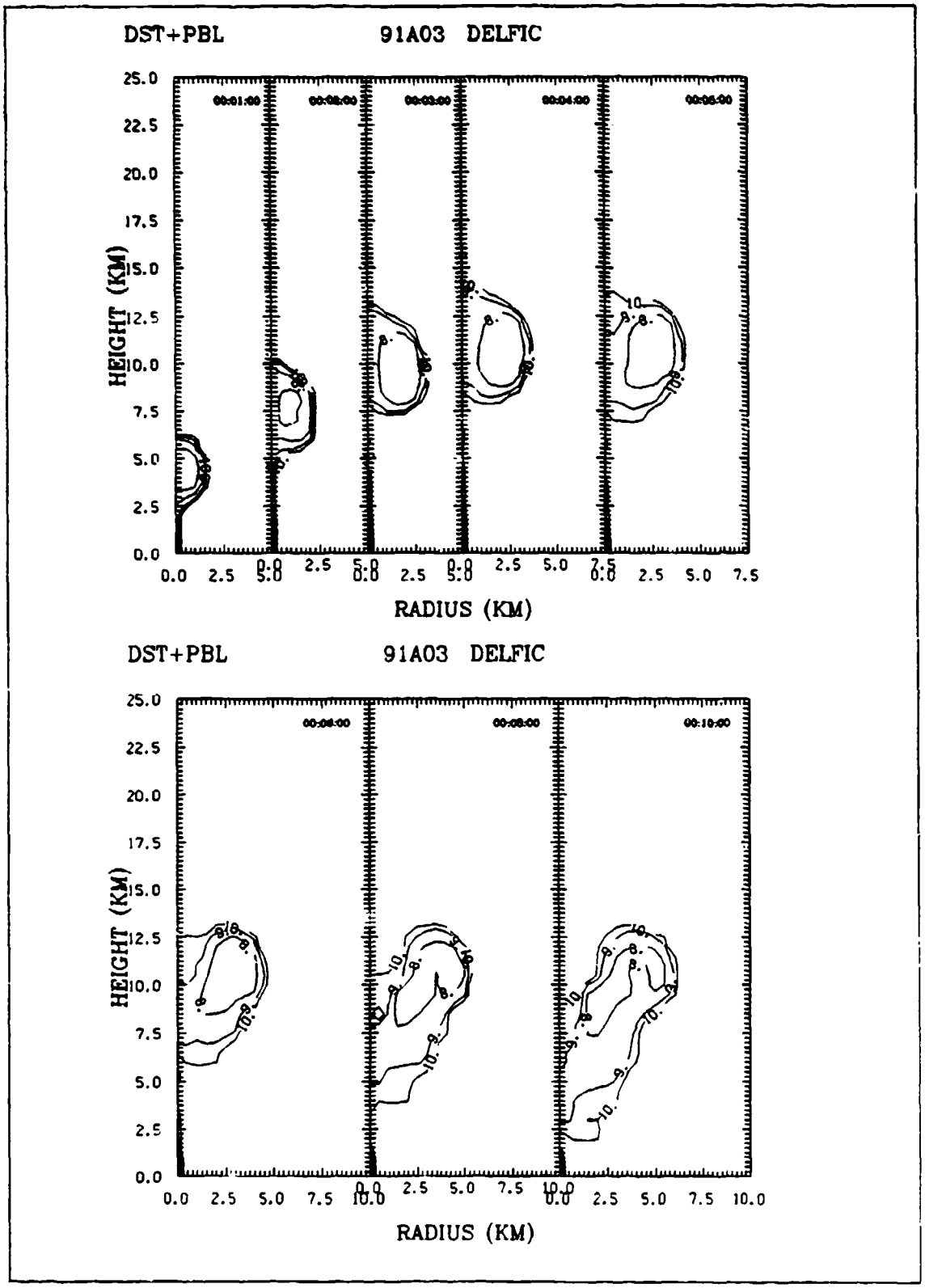

Figure 35: 91A03 (300 kt 120 SHOB) DELFIC Density Contours (10^{-x} g/cc)

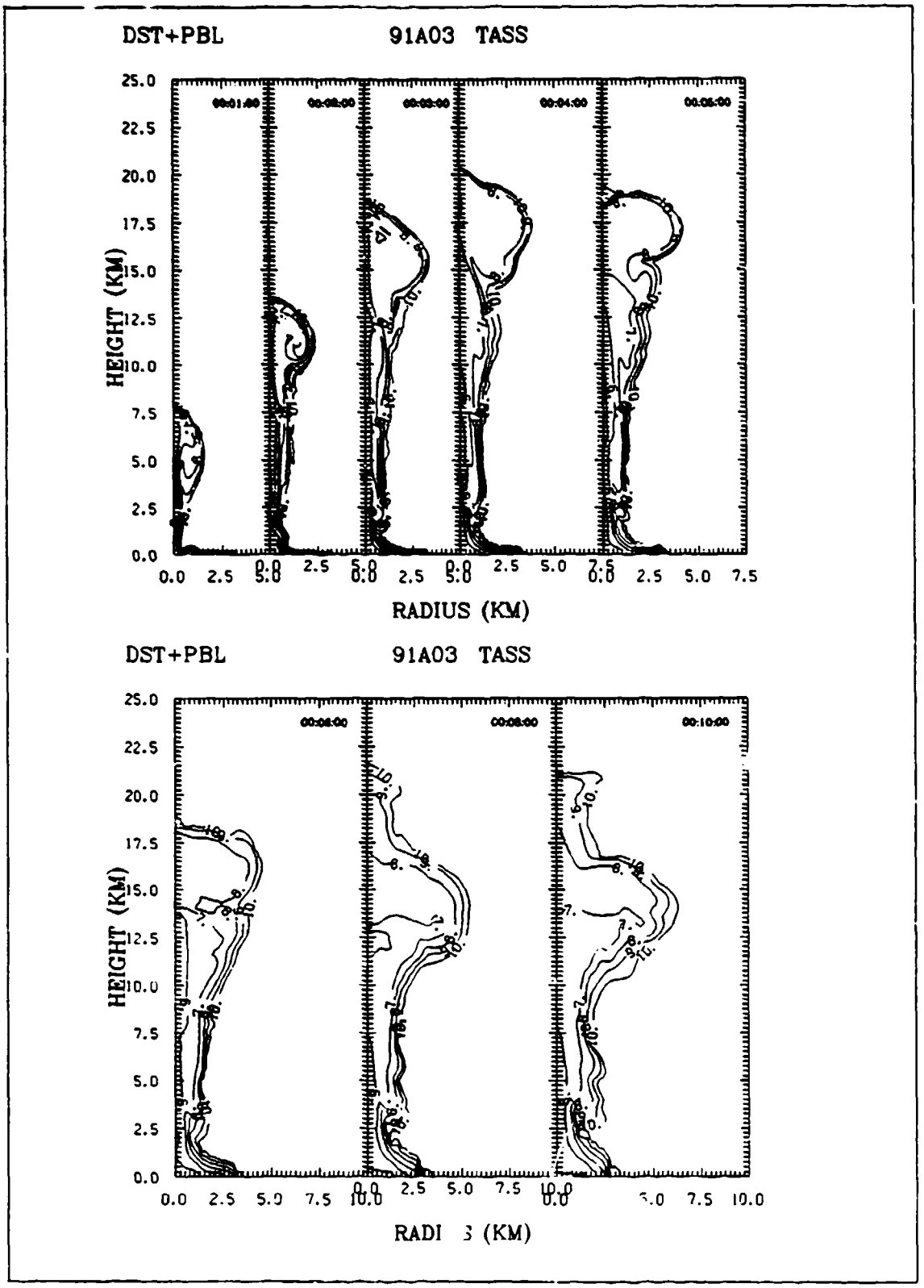

Figure 36: 91A03 (300 kt 120 SHOB) TASS Density Contours (10^{-x} g/cc)

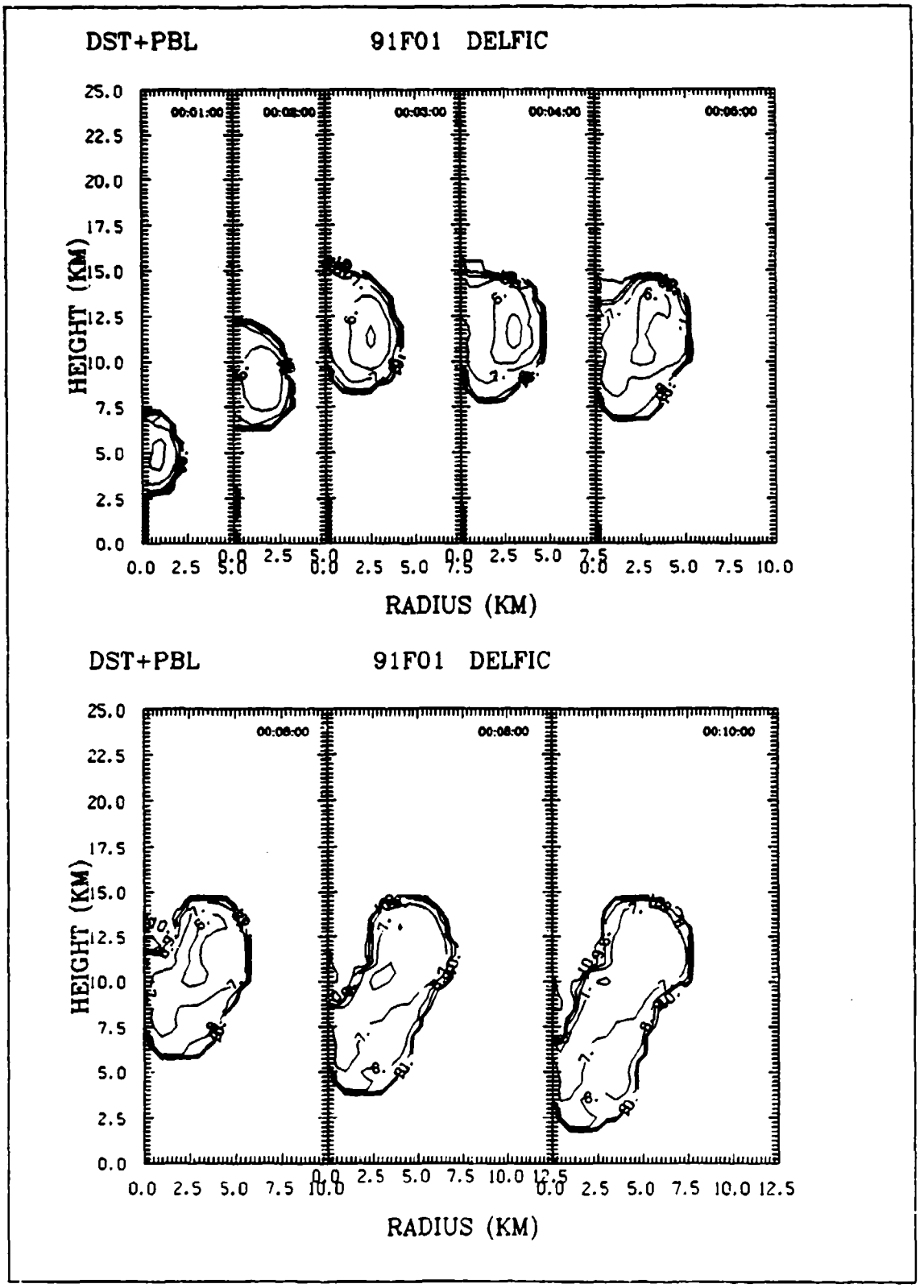

Figure 37: 91F01 (800 kt 0 SHOB) DELFIC Density Contours (10^{-x} g/cc)

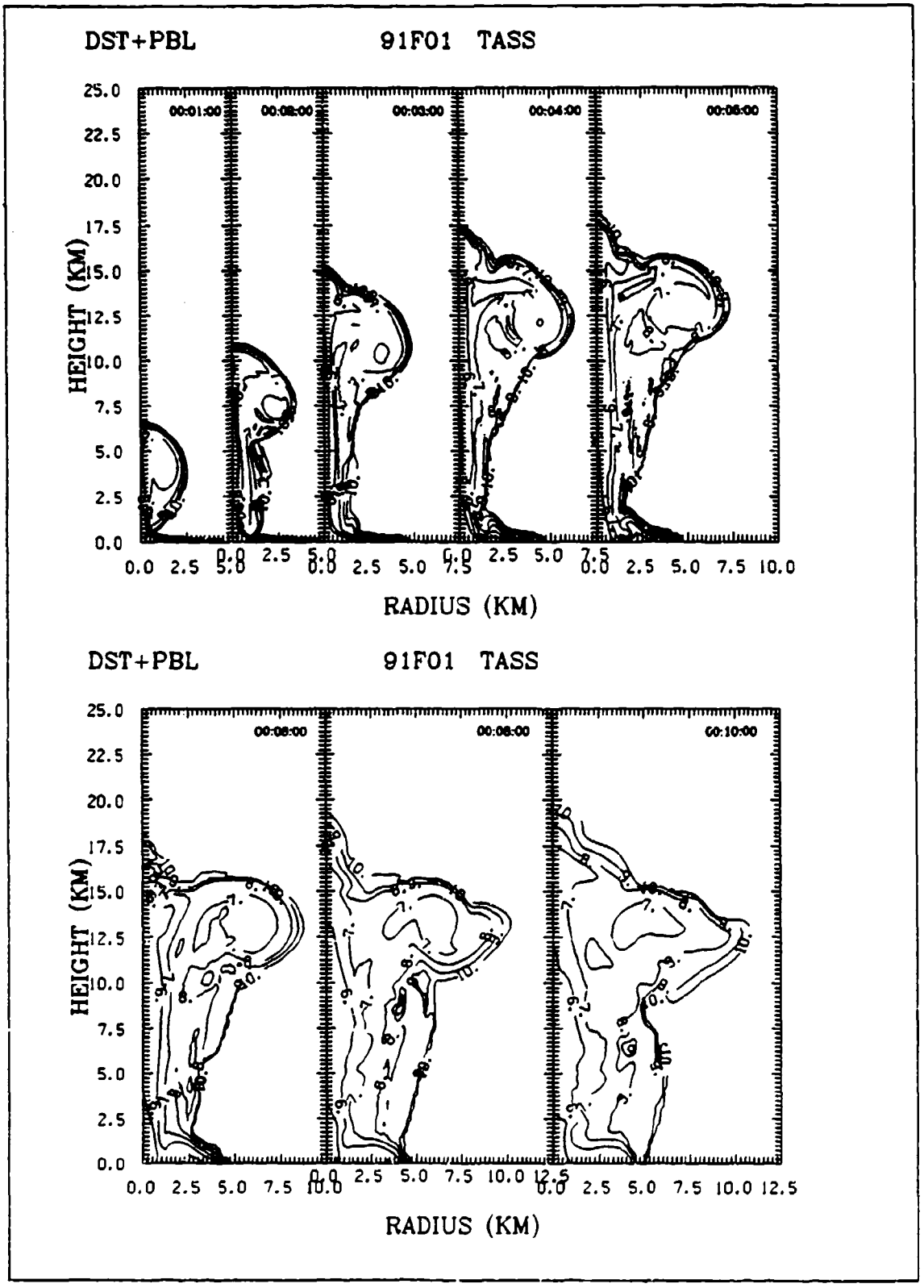

Figure 38: 91F01 (800 kt 0 SHOB) TASS Density Contours (10^{-x} g/cc)

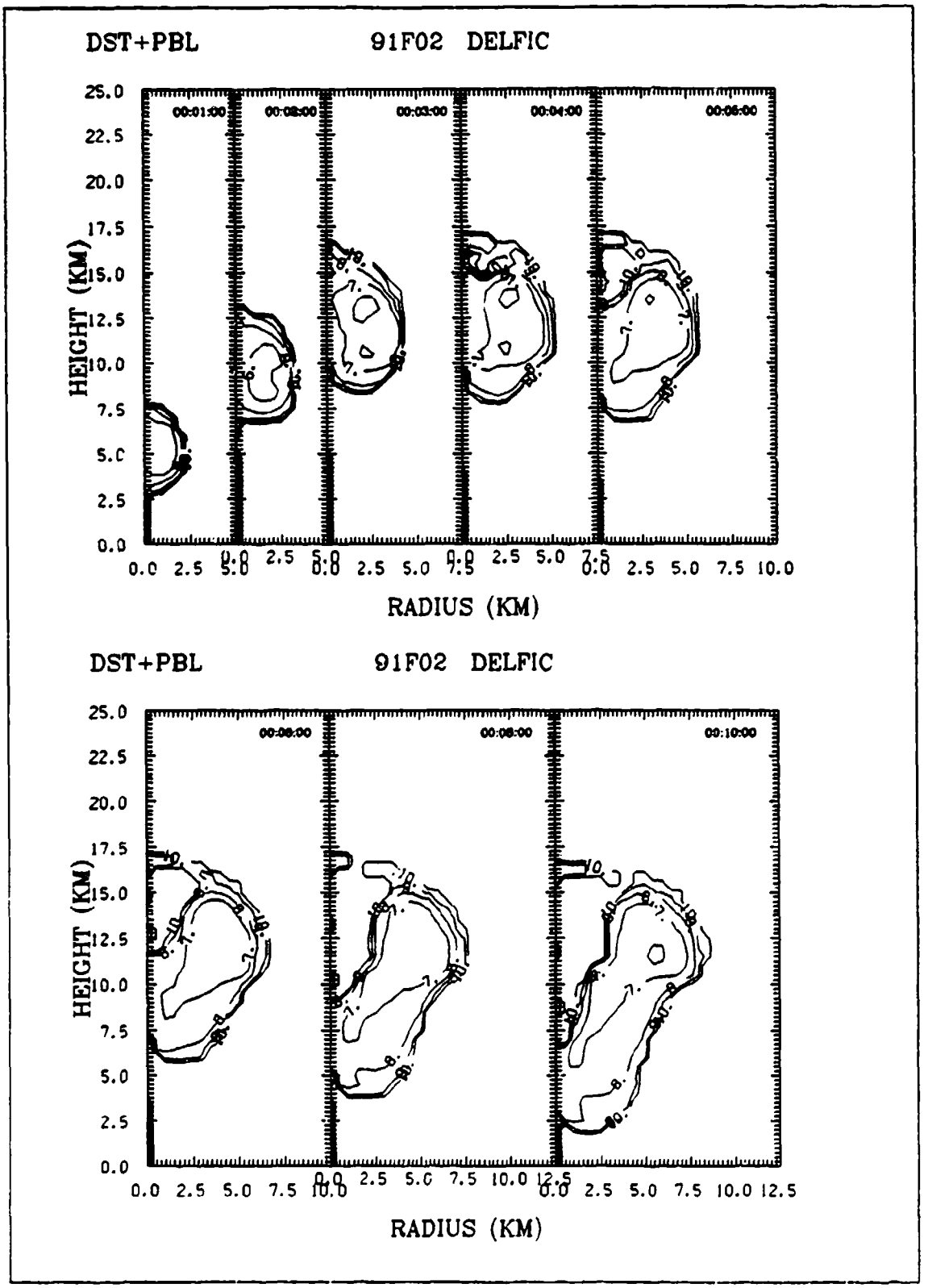

Figure 39: 91F02 (800 kt 50 SHOB) DELFIC Density Contours (10^{-x} g/cc)

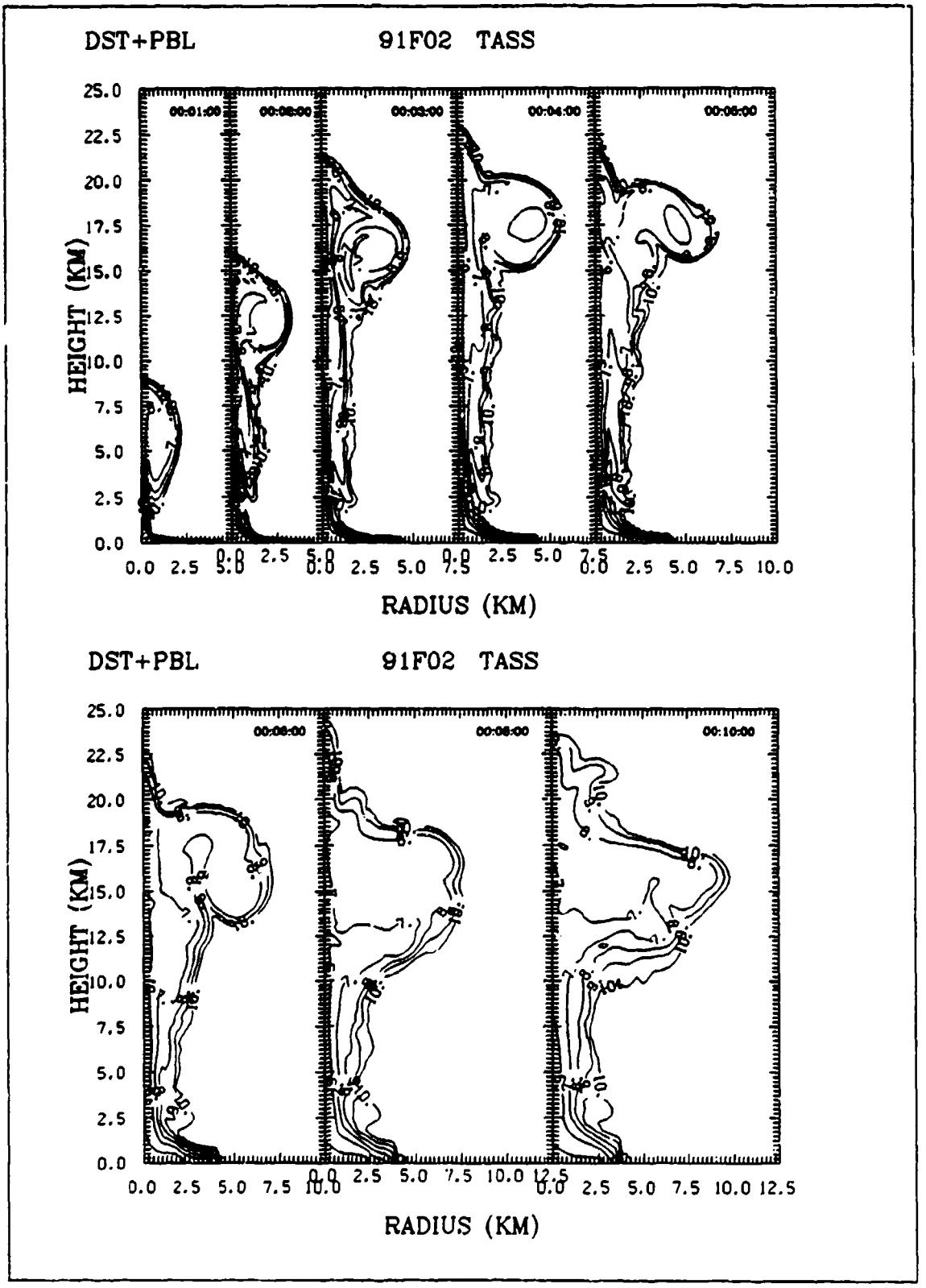

Figure 40: 91F02 (800 kt 50 SHOB) TASS Density Contours (10^{-x} g/cc)

A key difference again is that the TASS dust clouds represent both radioactive dust and nonradioactive dust alike. The hydrocodes also account for a time dependent, empirical loading of the dust cloud from two sources, ejecta and sweepup. The source of dust from the surface which originates at late times after the cloud has lifted off the ground, (i.e. sweepup), may account for the dust in the stem and close to the axis of the cloud. This dust may not enter the torus due to a reduced vortical intensity at late times. A partitioning of the radioactive dust within the main cloud may then result with the torus containing almost all of the radioactivity. There currently is no way of distinguishing radioactive dust from nonradioactive dust in the MAZ/TASS hydrocode results.

Vertical Distribution of Mass. The second set of comparisons to be made in this section is a comparison of the 1-D particle rise to the vortex flow method. The primary focus will be on the vertical distribution of different particle sizes. The radial distribution will also be discussed with implications on fallout contours mentioned.

Plots of mass as a function of altitude are shown for the 1979 test case (See Figure 41 on page 113). Results from both the old and new methods of particle rise are shown in each frame of the figure (DELFIC's 1-D on the left and vortex theory on the right). Values shown are the fractions of the total mass for the vertical height of the cloud layer shown in kilometers. The horizontal lines represent the CRM simulated cloud top and base altitudes. The first frame represents all sizes in the total cloud while the other frames are for specific particle sizes.

One-Dimensional Results. The CRM currently assumes the cloud starts off uniformly loaded at the beginning of its rise. The smaller groups, which have no appreciable settling velocity, are therefore still close to uniform in their vertical distribution at stabili-

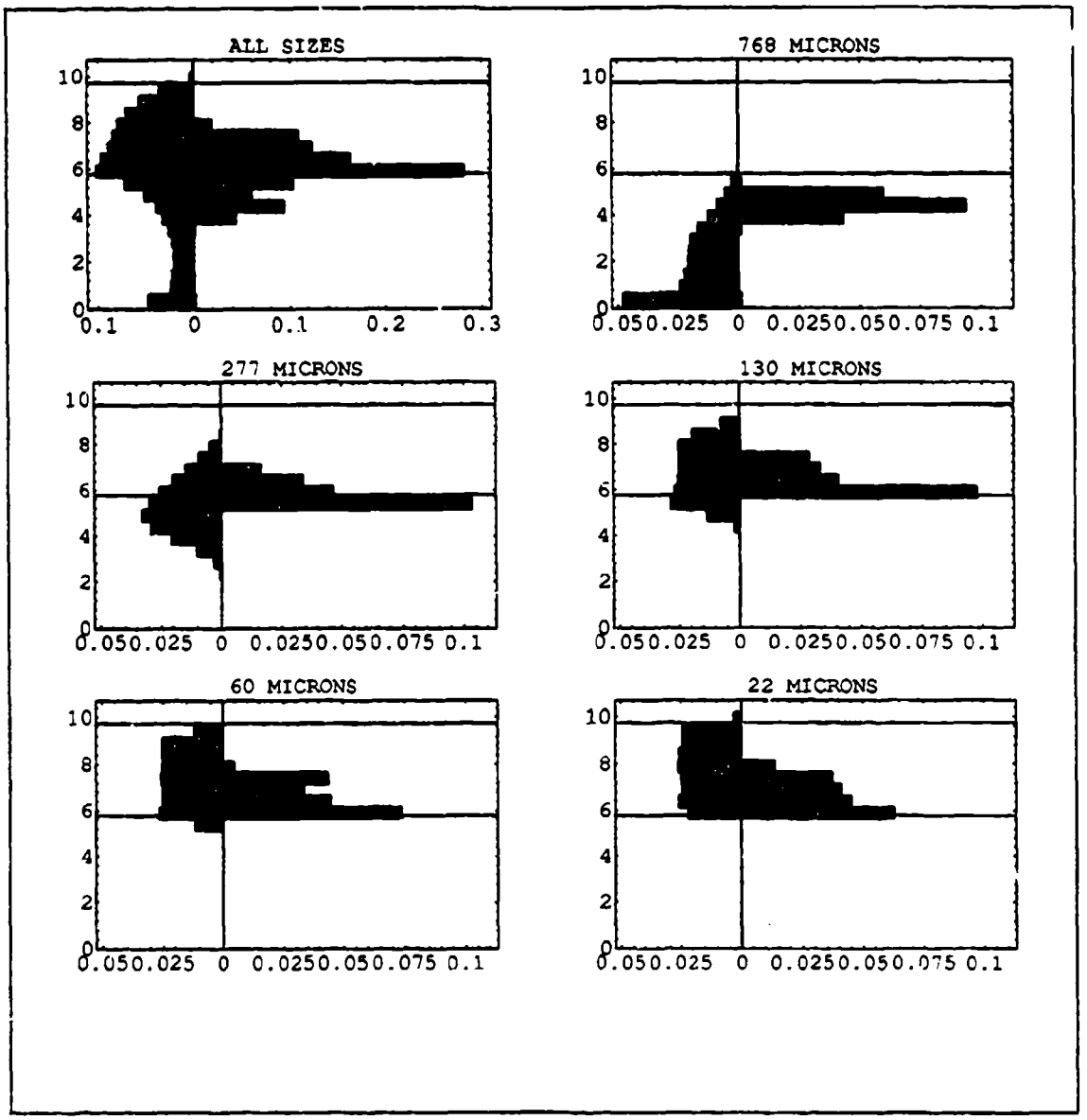

Figure 41: Stabilized Cloud Mass-Altitude Loading for 1979 Test Case (without vortex modeling on left and with vortex modeling on right for 5 particle sizes)

zation. The heavier groups do have a significant settling during the rise and help simulate a stabilized cloud stem.

DELFIC with Vortex. The results with vortex flow modeling show a drastically different stabilized cloud. There is less settling for large particles until the cloud has verti-

cally stabilized and the toroidal flow is turned off. The majority of the settling for the vortex modeling occurs after the cloud has vertically stabilized. This does allow for the larger particles to maintain a much higher distribution, with virtually nothing having settled to the surface by stabilization time. The smaller particles, on the other hand, do not stabilize as high in the cloud as they did in the 1-D modeling. This too is due to the vortex flow moving the particles about in a toroidal motion instead of just an updraft and gravity settling as in the current model.

Radial Distribution and Fallout Contours. To get an idea of the effect of the vortex flow field modeling on fallout contours, dose rate contours were generated and compared to the current modeling. The current DTM and OPM employ modeling which basically loses the radial definition of the 2-D stabilized cloud. An empirical radial distribution is superimposed on the grounded parcels. The difference in fallout contours, therefore, only show the effect of the change in the vertical distribution.

The results of this type of comparison for the 1979 test case are shown in Figure 42 on page 115. The one-hour dose rates are given for the fallout generated from both the 1-D stabilized cloud and the vortex flow field cloud. The main difference noted is that the 100 R/hr contour is extended over 10 kilometers farther downwind with the vortex stabilized cloud. Also, the hot spots for dose rates above 1000 R/hr are virtually eliminated. Both of these differences are due to the fact that the radioactivity associated with the larger particles is stabilizing at a higher altitude and therefore is spread over a larger area. This results in increased diffusion from the wind and a larger radius for the disks. A disk which starts transport with the main cloud's radius, as opposed to a disk which starts transport below the cloud with a stem radius, has its radioactivity spread over a larger surface area.

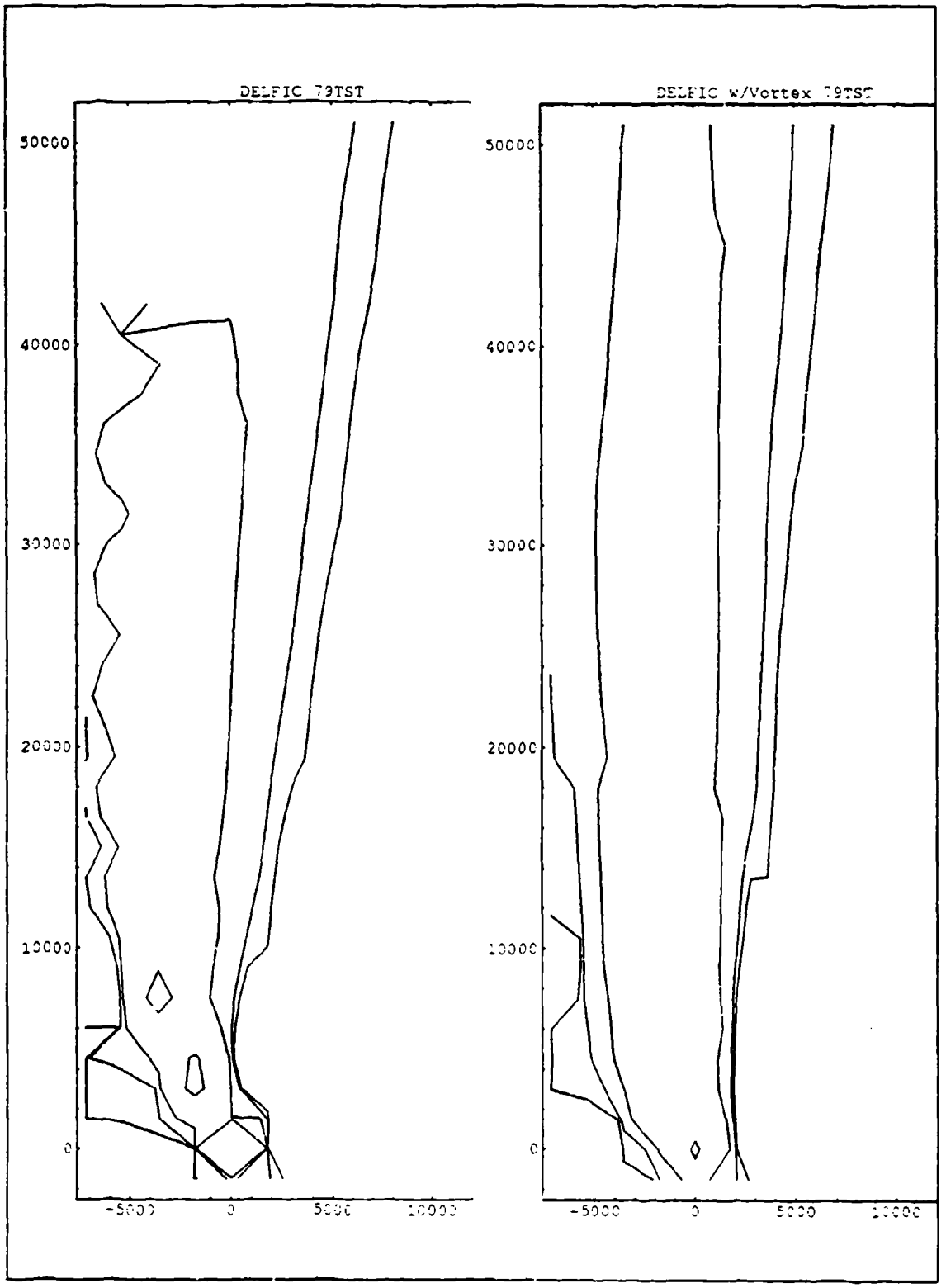

Figure 42: Fallout Contour Comparison for 1979 Test Case (contours represent 1, 10, 100, & 1000 R/hr Dose Rates at H+1 hr; distances are in meters)

V. Summary and Conclusions

This chapter presents a summary of the findings of the research into nuclear cloud rise and growth. The chapter contains sections for bubble rise simulation, particle rise simulation, and recommendations for future research into these areas.

Bubble Rise Simulations

The main conclusions on bubble rise concerns the performance of a single term entrainment equation and the use of constants for parameters which were previously yield dependent. It was shown that the single term entrainment equation (See Eqn (12)) could be used in a set of eight nonlinear ordinary differential equations to achieve an improved level of performance in predicting the heights of nuclear cloud tops. The values for the entrainment parameter and the eddy viscous drag parameter were changed to constant values in the predicting of nuclear cloud rise and growth.

The original CRM of DELFIC contained the single term form of the entrainment equation. It was based on the theory presented in the literature then, and still being used today. The revision in 1970 to a multiple term entrainment equation was based partly on modeling choices of the cloud shape. This change, and the change to yield dependent parameters, were attempts to match the observation of nuclear cloud tops by abandoning the accepted form of the equations. When the modeling choices used in the 1970 derivation were abandoned in 1977, the entrainment equation should have been returned to its single term form.

The entrainment and eddy viscous drag parameters are the two most important model parameters in the cloud rise equations. Each originated as constants in the 1967 version of

the CRM. Both, however, have been changed over the years to yield dependent parameters. This research confirmed that the increase with yield in the entrainment parameter was being offset by the decrease in the eddy viscous drag parameter. The suggested constant value for the entrainment parameter is 0.12 and the value for the eddy viscous drag parameter should be 0.10. These values are based on a minimization of the FRMS.

Both of the above conclusions were drawn after a careful validation using actual US atmospheric nuclear test observations. A set of 54 events with a wide range of yields and heights of bursts was used. These computer simulations, using recorded atmospheric inputs, showed that the improvements slightly increase the ability to match cloud tops.

As a preliminary step to making the above changes, corrections were made in the CRM subroutines. Inconsistencies with the stated theory in the 1979 documentation were removed. These corrections also made a slight increase in the performance of the model.

Particle Rise Simulations

The major conclusion drawn in the particle rise studies was that better agreement with hydrocodes in simulating the stabilized radioactive cloud can be achieved by using a 2-D flow field. The particle rise modeling of the CRM in 1-D was replaced with numerical simulation of an analytic flow field based on Hill's spherical vortex. As a result, the larger particles (>200 microns) in the fallout size distribution stabilize higher in the atmosphere. This is consistent with comparisons to full hydrocode simulations.

The new model accounts for circulation in a toroidal field within the rising bubble. This was accomplished by applying a known analytical solution of a rising bubble in a still atmosphere to nuclear cloud rise. This added information of the flow field was achieved

without resorting to a full hydrocode solution. The characteristics of the rising bubble needed for the solution of the flow field were provided by the bubble rise simulations discussed in the previous section.

By applying the above particle rise method to nuclear clouds, increased fidelity was achieved in determining the locations of the radioactive dust in the stabilized nuclear cloud. Previous studies showed that there was an inconsistency in the stabilized heights of larger fallout particles when compared to the dust loading produced by hydrocodes. The reason for the discrepancy was shown to be in the way the CRM simulates the particle rise in one dimension. By accounting for a spatially varying velocity field which includes circulation, these larger particles do achieve a higher altitude. The circulation in the cloud keeps the particles within the cloud longer, thereby allowing them to achieve a higher altitude.

Comparisons to hydrocode dust loading plots indicate that the radioactive debris in the nuclear cloud concentrates in a toroidal core within the rising bubble. This spatial partitioning of the debris which starts in the fireball from the dust which enters the cloud at later times is seen. When comparing dust density contours, the sweepup dust appears to form the bulk of the stem and fill in the void along the vertical axis. The dust that is swept up into the cloud at later times may not be as radioactive as the debris in the torus. The toroidal positioning of the radioactive dust in the new model is much different than the bivariate gaussian distribution assumed by the DTM and OPM modules of DELFIC.

Changes to the dose rate map from the change in vertical distribution of the radioactivity were noticed. The higher altitudes achieved by the larger particles help spread the associated activity over a larger area. This reduces the number of hot spots from the early

downing of the large particles but increases the range of the lower intensity contours. The difference in radial distribution may also alter the dose rate contours.

Recommendations

1. As hydrocodes become more useful and their output more trusted, they could be used to initialize the soil loading in the particle rise of DELFIC. A spatially varying description in the early seconds after detonation could replace the assumed uniform cylindrical distribution from cloud top to the surface.
2. A time dependent loading of the cloud should be investigated. The location of the vortex sphere at the time of soil loading is of utmost importance in determining if soil enters the toroidal core. Soil entering the cloud after the initial time may not be highly radioactive. It should be flagged and only passed onto the transport phase for dose rate calculations if it becomes collocated with the initial radioactive debris and thus acquire radioactivity by condensation or agglomeration.
3. The spheroidal vortex theory should be investigated to perfectly align the vortex region with the visible oblate bubble. This may raise the location of the stabilized dust even further by raising the vortex midplane to the center of the visible bubble.
4. A method for accounting for residual circulation in the vertically stabilized cloud should be added to better match reality. This may be possible by relating the circulation to the turbulent kinetic energy density, or a characteristic velocity, which are currently calculated in the bubble rise equations. Also, a method that allows for diffusive spreading of the particles back towards the void near the axis should be investigated.
5. A review of the cloud shape in the bubble rise equations should be done. A physical

mechanism for including the independent tracking of the cloud top and base after the cloud top has reached apogee is in order. The inclusion of oscillation for large yield clouds and a late time collapse would allow for a closer modeling of real nuclear clouds. Allowance for a changing cloud eccentricity should be made.

6. A more comprehensive validation of the bubble rise model should be done once a change to the cloud shape modeling has occurred. An increase in the number observed events can be accomplished now with the declassification of test data not available to researchers earlier. The gap in the yield range from 110 kt to 3.5 MT should be filled in along with more shots from the Pacific Proving Grounds.
7. The transport and output processor modules of DELFIC should be reviewed for inclusion of a 2-D description of the stabilized radioactive dust cloud. Once a 2-D cloud is accepted by a new DTM/OPM, the effects of both the revised vertical distribution and possible effects from the radial distribution on fallout contours may be found. A comparison to actual recorded fallout footprints from the US atmospheric nuclear tests would be in order.

Bibliography

1. Air Weather Service. *Accuracies of Radiosonde Data*. AWS-TR-105-133, Washington DC, September 1955. (AD 075 863)

2. Bacon, David P. et. al. *Single Burst Nuclear Cloud Database: Volume 1 - Cloud Rise and Stabilization Modeling*. Science Applications International Corporation, McLean, VA, 1 June 1991.

3. Batchelor, G. K. *An Introduction to Fluid Dynamics*. Cambridge: University Press, 1967.

4. Carnahan, Brice et. al. *Applied Numerical Methods*. New York: Wiley, 1969.

5. Carpenter, H. J. *Letter to E. Sevin, et al., DNA, on Dust Loading in the Stabilized Cloud from a Nuclear Burst*. R D Associates, Marina Del Rey, CA, 14 December 1982.

6. Cockayne, J. E. Personal communication. Science Applications International Corporation, McLean, VA.

7. Cockayne, J. E. et. al. *Theoretical/Empirical Predictions of Nuclear Dust Clouds*. Science Applications Inc., McLean, VA, 31 Dec 1979. (ADB 050 838)

8. DASIAC. Weather data for selected nuclear test shots. Compilation of extracts from unnamed reports including shot Johnnie Boy and the Hardtack-II series. DoD Nuclear Information and Analysis Center, Santa Barbara, CA, Spring 1993.

9. Dunn, Thomas J. and David P. Bacon. *Single Burst Nuclear Cloud Database: Volume 4 - Nuclear Cloud Particulate Environments (DRAFT)*. Science Applications International Corporation, McLean, VA, 5 November 1993.

10. Elliott, William P. and Dian J. Gaffen. *On the Utility of Radiosonde Humidity Archives for Climate Studies*. Bulletin American Meteorological Society, Vol. 72, No. 10:1507-1520, October 1991.

11. Fohl, T. and A. D. Zalay. *Vortex Ring Model of Single and Multiple Cloud Rise*. Mount Auburn Research Associates Inc., Newton Upper Falls, MA, Unpublished.

12. Galbaliy, I. E. et. al. *A Numerical Model of the Late (Ascending) Stage of a Nuclear Fireball*. Commonwealth Scientific and Industrial Research Organisation (Australia). Division of Atmospheric Research. (Series: Division of Atmospheric Research technical paper; no. 16), 1987.

13. Glasstone, Samuel and Philip J. Dolan. *The Effects of Nuclear Weapons, 3rd Edition.* US Department of Defense and the Energy Research and Development Administration, Washington DC, Government Printing Office, 1977.

14. Grossman, B., et. al. *Operation Teapot, Project 9.4, Atomic Cloud Growth Study, WT-1152.* Boston: Air Force Cambridge Research Center, October 1955. (AD 426 840)

15. Harvey, T. et. al. *KDFOC3: A Nuclear Fallout Assessment Capability (Draft).* UCRL-52338 Rev. 1. April 5, 1993.

16. Hawthorne, Howard A. *Compilation of Local Fallout Data From Test Detonations 1945-1962 Extracted From DASA 1251. Volume I - Continental US Tests.* General Electric Co., Santa Barbara, CA, DASIAC, 01 May 1979. (ADA 079 309)

17. Hawthorne, Howard A. *Compilation of Local Fallout Data From Test Detonations 1945-1962 Extracted From DASA 1251. Volume II - Pacific Tests.* General Electric Co., Santa Barbara, CA, DASIAC, 01 May 1979. (ADA 079 310)

18. Hawthorne, Howard A. *Fallout Hazard Prediction Inconsistencies.* General Electric Co., Santa Barbara, CA, DASIAC, 01 Oct 1979. (ADA 086 216)

19. Hill, M. J. M. *On a Spherical Vortex.* Philos. Trans. R. Soc. London Ser. A 185:213-45, 1894.

20. Huebsch, I. O. *The Development of a Water-Surface-Burst Fallout Model: The Rise and Expansion of the Atomic Cloud.* U.S. Naval Radiological Defense Laboratory, San Francisco, CA, USNRDL-TR-741, 23 April 1964. (AD 441 983)

21. Huebsch, I. O. *Turbulence, Toroidal Circulation and Dispersion of Fallout Particles From the Rising Nuclear Cloud.* U.S. Naval Radiological Defense Laboratory, San Francisco, CA, USNRDL-TR-1054, 24 October 1966. (AD 800 536)

22. Huebsch, I. O. et al. *Department of Defense Land Fallout Prediction System. Volume III - Cloud Rise.* Technical Operations, Inc., Burlington, MA, 19 May 1967. (AD 819 770 - withdrawn from DTIC but available through loan from DASIAC, Santa Barbara, CA)

23. Huebsch, I. O. *Wind Shear, Turbulence and Interface Criteria for Nuclear Explosion Cloud, Debris and Fallout Models.* Naval Radiological Defense Laboratory, San Francisco, CA, NRDL-TR-69-72, 8 August 1969. (AD 856 228)

24. Huebsch, Ian O. *Analysis and Revision of the Cloud Rise Module of the Department of Defense Land Fallout Prediction System (DELFIC).* Euclid Research Group, Berkeley, CA, Aug 1975. (ADB 007 607)

25. Jodoin, Vincent J. *Critique of DELFIC's Cloud Rise Module*. Air Force Institute of Technology, Wright-Patterson AFB, OH, May 1993. (ADA 265 587)

26. Joint Task Force Seven. *Operation Castle. Radiological Safety. Volume 2*. Washington D.C., 01 September 1985. (ADA 995 409)

27. Kaman Tempo. *Operation Redwing. Radiological Safety*. Kaman Tempo, Santa Barbara, CA, 01 July 1983. (ADA 995 182)

28. Klemm, W. Jeffrey and Joseph C. Maloney. *Department of Defense Land Fallout Prediction System: Adaption for Extremely Low-Yield Detonations*. USA Ballistic Research Laboratories, Aberdeen Proving Ground, MD, March 1975. (ADB 003 037)

29. Lamb, Sir Horace. *Hydrodynamics, Sixth Edition*. New York: Dover Publications, 1945.

30. Levine, Joseph. *Spherical Vortex Theory of Bubble-Like Motion in Cumulus Clouds*. Journal of Meteorology, Volume 16:653-662, December 1959.

31. Maloney, Joseph C. *Department of Defense Land Fallout Prediction System (DELFIC) - Conversion to FORTRAN 77 and User's Guide*. U.S. Army Ballistic Research Laboratory, Aberdeen Proving Ground, MD, September 1988. (ADB 126 610)

32. Mazzola, Thomas Andrew. *The Interaction of Multiple Buoyant Clouds*. MS Thesis, University of Southern California, School of Engineering, May 1985.

33. McGahan, Joseph T. Briefing charts. Science Applications International Corporation, McLean, VA.

34. McGahan, Joseph T. Personal communication. Science Applications International Corporation, McLean, VA.

35. McGahan, Joseph T. et. al. *The Modeling of Nuclear Clouds*. General Research Corp., Arlington, VA. Unpublished.

36. McGahan, Joseph T. et. al. *Sensitivity of Fallout Predictions to Initial Conditions and Model Assumptions*. Science Applications, Inc., McLean, VA, December 1974. (ADA 002 464)

37. Milne-Thompson, L. M. *Theoretical Hydrodynamics, 5th Edition*. New York: The Macmillan Company, 1968.

38. Minor, Bryan M. *The Effect of Water Content on the Predictions of the Cloud Rise Module of DELFIC*. MS Thesis, Air Force Institute of Technology, School of Engineering, March 1988. (ADA 194 618)

39. Mitchell, Lloyd V. *Radiosonde Dew-Point Accuracies 40° C to -40° C.* AWS-TR-198, August 1967. (AD 659 760)

40. Morgan, Dewitt N. et. al. *Air Weather Service Participation. Report on Operation Upshot-Knothole, Nevada Proving Grounds, Mar-Jun 53. AEC-WT-703.* Air Force Special Weapons Center, Kirtland AFB, NM, Jun 1953. (ADA 077 506)

41. Norment, H. G. *Department of Defense Land Fallout Prediction System, Volume I. System Description.* Technical Operations Research, TO-B 66-40, DASA 1800-I, 27 June 1966. (AD 483 897)

42. Norment, H. G. et. al. *Department of Defense Land Fallout Prediction System, Volume II. Initial Conditions.* Technical Operations Research, TO-B 66-44, DASA 1800-II, 30 September 1966. (AD 803 144)

43. Norment, H. G. et. al. *Department of Defense Land Fallout Prediction System, Volume IV. Atmospheric Transport.* Technical Operations Research, TO-B 66-46, DASA 1800-IV, 2 February 1967. (AD 815 263)

44. Norment, H. G. *Department of Defense Land Fallout Prediction System. Volume II. Initial Conditions. Supplement.* DNA 1800-II (Supplement), October 1972. (AD 753 842)

45. Norment, H. G. and S. Woolf. *Department of Defense Land Fallout Prediction System. Volume III. Cloud Rise. Revised.* ARCON Corporation, Wakefield, MA, 1 September 1970. (AD 879 890)

46. Norment, Hillyer G. *Validation and Refinement of the DELFIC Cloud Rise Module.* Atmospheric Science Associates, Bedford, MA, 15 Jan 1977. (ADA 047 372)

47. Norment, Hillyer G. *DELFIC: Department of Defense Fallout Prediction System. Volume I - Fundamentals.* Atmospheric Science Associates, Bedford, MA, 31 December 1979. (ADA 088 367)

48. Norment, Hillyer G. *DELFIC: Department of Defense Fallout Prediction System. Volume II - User's Guide.* Atmospheric Science Associates, Bedford, MA, 31 December 1979. (ADA 088 512)

49. O'Brien, V. *Steady Spheroidal Vortices - More Exact Solutions to the Navier-Stokes Equations.* Q. Appl. Math. 19:163-168, 1961.

50. OL-A, USAFETAC/GCOO. Microfilm (2 reels) of upper air data for Yucca Flats Test Site, NV for April through October 7, 1957. Environmental Technical Applications Center (AWS), Asheville, NC, 12 August 1993.

51. Pozrikidis, C. *The Non-linear Instability of Hill's Vortex.* J. Fluid Mech. 168:337-367, 1986.

52. Press, William H. *Numerical Recipes in FORTRAN: the art of scientific computing, 2nd ed.* Cambridge: University Press, 1992.

53. Sabersky, Rolf H. et. al. *Fluid Flow, a first course in fluid mechanics, second edition.* New York: Macmillan, 1971.

54. Sanchez, Odon et. al. *The Development of Thermals From Rest.* Journal of the Atmospheric Sciences, Volume 46 No.14: 2280-2292, 15 July 1989.

55. Schwenke, T. W. and P. Flusser. *Department of Defense Land Fallout Prediction System, Volume VI. Output Processor.* TO-B 66-48, DASA-1800-VI, 20 February 1967. (AD 814 055)

56. Shannon, John. *Vortex Dust Model for Rising Nuclear Clouds.* Science Applications Inc., Arlington, VA, Unpublished.

57. Shariff, Karim and Anthony Leonard. *Vortex Rings.* Annu. Rev. Fluid Mech. 24:235-279, 1992.

58. Taylor, G. I. *Dynamics of a Mass of Hot Gas Rising in Air.* US Atomic Energy Commission, MDDC-919, LA Report 236, 16 March 1945.

59. Tompkins, R. C. *Department of Defense Land Fallout Prediction System, Volume V. Particle Activity.* NDL-TR-102, DASA-1800-V, February 1968. (AD 832 239)

60. Turner, J. S. *The Flow into an Expanding Spherical Vortex.* J. Fluid Mech. 18:195-208, 1963.

61. Willis, Jay C. *The History of Fallout Prediction.* Report prepared for Nuclear Effects 699 (Fallout Modeling), Air Force Institute of Technology, 1 June 1977. (ADA 079 560)

62. Winegardner, D. K. *Department of Defense Land Fallout Prediction System, Volume VII. Operators' Manual.* NDL-TR-104, DASA-1800-VII, April 1968. (AD 836 871)

63. Wolfram, S. *Mathematica. A System for Doing Mathematics by Computer, Second Edition.* Redwood City, CA: Addison-Wesley, 1991.

64. Zimmerman, E. E. and William R. Seebaugh. *Nuclear Dust Cloud Environments.* DNA 4509F, Science Applications, Inc., McLean, VA, 31 January 1978. (ADC 015 972)

65. Zimmerman, E. E. *Conversion of the VORDUM System for AWRE/UK Operation.* DNA-TR-86-117, Science Applications, Inc., McLean, VA, 20 December 1985. (ADB 113 731)

Appendix A: Cloud Tops

The cloud tops of the Single Burst Nuclear Cloud Database (SBNCD) 91 Series of simulations are discussed in this appendix. In particular, the cloud tops computed in the MAZ/TASS simulations are compared to the cloud tops computed with the Cloud Rise Module (CRM) of DELFIC. The values used for the MAZ/TASS hydrocode simulations are the 10^{-8} g/cc (i.e. approximate visible density) DST+PBL soil mass contours (9). Two different values are used for the CRM simulations: bubble rise visible cloud tops, and particle rise 10^{-8} g/cc soil mass contours.

All cases were run with the same atmospheric sounding used in the MAZ/TASS simulations. These atmospheric properties included temperature, pressure, humidity, and winds for various altitudes. The comparisons made in this study use only soil mass for the density contours. It must be remembered that the addition of condensed water mass to the density contours would only *increase* the predicted cloud top values by raising the 10^{-8} g/cc contour. The bubble rise cloud top, on the other hand, would not change, as it is based on the rise of the entire visible bubble.

Shown in Table 12 on page 128 are the computed cloud tops for the 9 near surface bursts compared in Chapter IV. The comparison shows that the MAZ/TASS cloud tops overpredict the CRM bubble rise values for 7 of the 9 cases. The difference between MAZ/TASS and the CRM increases with SHOB for those yields with multiple SHOBs.

The CRM particle rise results show that the visible contour is always below the bubble rise cloud top value. This is due to the modeling choice of matching the visible bubble

cloud top to the vortex sphere top. This ensures that all particles in the vortex region will be below the validated bubble rise cloud top value. This also implies that even if the condensed water contribution to density contours were added to the soil density, the visible contour would not exceed the bubble rise cloud top.

Since the bubble rise cloud top predictions are validated against US atmospheric nuclear test observations, the conclusion is that MAZ/TASS cloud top predictions are too high. This is especially true for larger SHOBs.

Table 12: MAZ/TASS vs. DELFIC Cloud Tops

Case	Yield (kt)	SHOB (ft/kt1/3)	TASS Cloud Top (km)	Bubble Rise Cloud Top (km)	Particle Rise Cloud Top (km)
91H01	20	0	11.5	8.0	6.5
91B01	100	0	12.5	13.5	11.0
91B02	100	50	15.5	13.7	11.0
91B03	100	120	17.5	13.8	10.5
91A01	300	0	17.5	15.6	13.0
91A02	300	50	17.8	15.7	14.0
91A03	300	120	20.3	15.9	12.5
91F01	800	0	18.0	18.0	15.5
91F02	800	50	23.0	18.3	16.5

Appendix B: Latent Heat

The energy in the buoyantly rising bubble is affected by the release of latent heat during its rise to lower temperatures and pressures. The amount of latent heat released in the DELFIC Cloud Rise Module (CRM) simulations of the Single Burst Nuclear Cloud Database 91 Series cases is discussed. The values are compared to the much larger values of the MAZ/TASS hydrocode simulations.

To begin, the cloud gets its initial buoyant energy from the nuclear detonation. In the CRM of DELFIC this is modeled as 45% of the total device yield. In MAZ/TASS 32.5% of the yield is used initially (9). In addition, as the cloud cools to condensation temperature for the vapor in the cloud an additional amount of energy is released. This latent heat is determined in the CRM simulations by the ratio of condensed water in the cloud to that of air. By determining the amount of air, the mass of condensed water in the cloud is determined. The latent heat released to produce this amount of condensed water is then found.

Table 13 on page 130 shows the latent heat values calculated with the two codes on the 91 Series cases. The values listed for the CRM are the maximum value seen during the cloud rise and growth phase of development. The values for TASS were provided by Dunn (9). All simulations used the same atmospheric sounding as input.

The CRM values indicate a trend of increasing latent heat released with increasing yield and decreasing SHOB. The TASS values do not show such a trend. The TASS simulations also show a much larger release of latent heat by a factor from almost 3 to over 10. This larger latent heat release is somewhat offset in the total effective buoyant energy by the CRM's use of a larger fraction of the initial device yield. However, the TASS simula-

tions still calculate a much larger effective buoyant energy for all cases by up to 50%.

The reason for this difference may lie in the basic assumption of the single cell approach to DELFIC bubble rise modeling. By allowing only a single temperature for the whole cloud, the entire cloud will cool and condense at the same time. In a hydrocode approach to the solution, the cloud is allowed to keep certain cells in the multicell cloud hot while a majority of the cells can cool to much lower temperatures. In addition to allowing for hot spots in the cloud, the hydrocode solution allows for local concentrations of water vapor and therefore condensation. These two differences may allow the TASS simulations to condense more of the water vapor present in the particular atmosphere used.

Table 13: MAZ/TASS vs. CRM Latent Heat and Effective Buoyant Energy

Case	SHOB ($ft./kt^{1/3}$)	Yield (kt)	TASS Latent Heat (kt)	Tass Effective Buoyant Energy (kt)	CRM Latent Heat (kt)	CRM Effective Buoyant Energy (kt)
91H01	0	20	18	24	7	16
91B01	0	100	68	100	19	64
91B02	50	100	50	82	18	63
91B03	120	100	64	97	17	62
91B05	400	100	42	74	13	58
91A01	0	300	76	174	23	158
91A02	50	300	120	218	21	156
91A03	120	300	134	231	18	153
91A05	400	300	100	197	12	147
91F01	0	800	175	435	25	385
91F02	50	800	263	523	23	383

Vita

Vincent J. Jodoin was born on 3 July 1963 in Leominster, Massachusetts to Joseph and Carole Jodoin. Upon graduation from North Attleboro High School, MA, in 1981, Vince entered college on a four-year Reserve Officer Training Corps scholarship. He graduated from Rensselaer Polytechnic Institute in 1985 with a Bachelor of Science in Nuclear Engineering and a commission in the United States Air Force. The same weekend, he was married to Carol Ann Pagano of Troy, New York.

His first assignment was with the 31st Test and Evaluation Squadron (SAC) at Edwards Air Force Base, California. There he worked as an Aircraft Systems Test Engineer in testing the weapon delivery capabilities of the B-52, B-1B, and B-2. His next assignment was in the Graduate Nuclear Engineering program at the Air Force Institute of Technology, where he earned a Master of Science in Nuclear Engineering. While at AFIT, Lt. Jodoin completed his work towards an MS in Electrical Engineering with Distinction from the California State University at Fresno. He was then assigned to the Air Force Technical Applications Center, Patrick AFB, Florida, where he served as a Nuclear Science and Technology Analyst for the US nuclear treaty monitoring program. Capt. Jodoin was then selected for the Doctoral Science program in the Engineering Physics Department at AFIT.

Capt. Jodoin's decorations include the Air Force Meritorious Service Medal and the Air Force Commendation Medal. He has three beautiful daughters, Jenna, Danielle, and Christina. In July of 1994, Capt. Jodoin will be starting his next assignment at the United States Air Force Academy, Colorado, as an Instructor of Physics.

Permanent Address: 167 Cliff Dr
North Attleboro, MA 02760

REPORT DOCUMENTATION PAGE

Form Approved
OMB No 0704-0188

1. AGENCY USE ONLY (Leave blank)	2. REPORT DATE	3. REPORT TYPE AND DATES COVERED
	June 1994	Ph.D. Dissertation

4. TITLE AND SUBTITLE
Nuclear Cloud Rise and Growth

5. FUNDING NUMBERS

6. AUTHOR(S)
Vincent J. Jodoin, Capt., USAF

7. PERFORMING ORGANIZATION NAME(S) AND ADDRESS(ES)
Air Force Institute of Technology
WPAFB OH 45433

8. PERFORMING ORGANIZATION REPORT NUMBER
AFIT/DS/ENP/94J-2

9. SPONSORING/MONITORING AGENCY NAME(S) AND ADDRESS(ES)
HQ Defense Nuclear Agency
ATTN: LTC Byers/SPWE
6801 Telegraph Rd.
Alexandria, VA 22310

10. SPONSORING/MONITORING AGENCY REPORT NUMBER

11. SUPPLEMENTARY NOTES

12a. DISTRIBUTION/AVAILABILITY STATEMENT
Approved for public release; distribution unlimited

12b. DISTRIBUTION CODE

13. ABSTRACT (Maximum 200 words)

Nuclear cloud rise and growth to stabilization is investigated. The Cloud Rise Module of the Defense Land Fallout Interpretive Code (DELFIC) is reviewed and improved. Both the modeling of bubble rise dynamics and particle rise dynamics are addressed. Improvements are made in predicting the stabilized particulate cloud for nuclear fallout purposes. The results are compared to US atmospheric nuclear weapons tests and to the output of MAZ/TASS hydrocode simulations.

The improvements to the bubble rise dynamics include using a single term entrainment equation and constants for the entrainment and eddy viscous drag parameters. The validation showed a slight improvement was obtained with the improved model in predicting the cloud top values for 54 US near-surface bursts.

The improvement to the particle rise model consisted of replacing the 1-D particle rise with a 2-D analytical flow field model. The model was based on Hill's spherical vortex. This improvement provided a radial distribution to the radioactive dust cloud. The larger fallout particles (>200 microns) achieved a higher altitude due to simulating the circulation within the cloud. Dose rate contours for some cases will be altered due to this change in vertical distribution from the 1-D model.

14. SUBJECT TERMS	15. NUMBER OF PAGES
NUCLEAR CLOUD RISE, NUCLEAR WEAPON EFFECTS, FIREBALL RISE, DELFIC, FALLOUT, ATMOSPHERIC PHYSICS, DISSERTATION	145
	16. PRICE CODE

17. SECURITY CLASSIFICATION OF REPORT	18. SECURITY CLASSIFICATION OF THIS PAGE	19. SECURITY CLASSIFICATION OF ABSTRACT	20. LIMITATION OF ABSTRACT
UNCLASSIFIED	UNCLASSIFIED	UNCLASSIFIED	UL